FOREWORD

This research was performed to evaluate theoretically the feasibility of various techniques of reducing heat transfer to windows of advanced Air Force vehicles. The work was performed from June 1962 to October 1963 and from April 1964 to December 1964 by Stephen J. Lis, Ronald G. Barile, and Gilbert Engholm of the MRD Division, General American Transportation Corporation, Niles, Illinois. The work was sponsored by the Air Force Flight Dynamics Laboratory, Research and Technology Division, Wright-Patterson Air Force Base, under Contract No. AF 33(657)-9138, Project No. 1368, "Design Technologies and Structural Configuration Concepts for Aerospace Vehicles", Task No. 136802, "Transparent Installation Design".

Mr. Kennerly H. Digges and Lt. Michael Mann, USAF, of the Air Force Flight Dynamics Laboratory were each project engineer during the first and second contract periods respectively.

Acknowledgement is hereby given to the following individuals for their counsel and assistance: Mr. R. A. Bambenek, Group Leader, and Mr. R. J. Baschiere, Research Engineer, GATC, MRD Division; Dr. S. Raynor, Consultant and Professor of Mechanical Engineering, Northwestern University; Dr. Y. S. Touloukian, Consultant and Professor of Mechanical Engineering, Purdue University. The excellent cooperation and assistance of Mr. Jon Hilgeman of the RTD Open Shop Computer Facility is gratefully acknowledged for expediting the computer programs.

Publication of this report does not constitute Air Force approval of the report's findings or conclusions. It is published only for the exchange and stimulation of ideas.

HOLLAND B. LOWNDES, JR.
Acting Chief
Structures Division

ABSTRACT

A basic investigation was performed to describe the heat transfer and temperature distribution in semi-transparent window materials subjected to simultaneous convective and radiative heat input. The mechanism of heat transfer within the window is treated by separated conductive and radiative modes. Results derived from IBM 7090 digital computer programs are presented for single glaze windows subjected to a hypersonic skip glide trajectory, a supersonic flight and a circular earth orbit. The conditions where radiative interchange is important are studied. Initial results considering the effects of a thin transparent film on a single glazing are presented.

TABLE OF CONTENTS

LIST OF ILLUSTRATIONS

LIST OF ILLUSTRATIONS (Cont'd)

LIST OF ILLUSTRATIONS (Cont'd)

LIST OF ILLUSTRATIONS (Cont'd)

LIST OF TABLES

INTRODUCTION

One of the basic requirements of manned aerospace vehicles is that the crew must be able to make visual observations during ascent, maneuvers, and descent. For this purpose a viewing port or window has proved the most effective and desirable means. To permit adequate observation by the crew, the material of such a window must be reasonably transparent to visible light rays. However, such a material is usually transparent to other radiations emanating from the outside environment and within the window which can be detrimental and which affect the mechanisms of heat transfer through and within the window. Thus, the need for direct observation gives rise to such problems as thermal stress, excessive interior temperature, and thermal energy transmitted into the cabin due to exposure to aerodynamic heating as well as thermal radiation during any prescribed mission.

A basic investigation was undertaken to describe theoretically the mechanisms involved in heat transfer to, within, and from window materials when exposed to an environment of combined convective and radiative heating. These heat transfer mechanisms were programed for an IBM 7090 computer to obtain insights to the transient temperature distributions that would develop and to evaluate the effects of glass properties, thicknesses and coatings.

Manuscript released by authors December 1964 for publication as an RTD Technical Documentary Report.

SECTION 1

SUMMARY OF RESULTS

A detailed analysis of the combined effects of conduction and radiation heat transfer through single-glaze windows has been made. The analysis was programmed for solution on a digital computer. Instantaneous temperature profiles were computed by an opaque and by a transparent analysis for three trajectories with different heating rates. The results indicate that the temperature predicted based upon conduction effects alone (opaque analysis) are greater than those predicted based upon conduction plus radiant effects. These temperature differences may be as large as 150°K for some glasses. In every case considered the maximum temperature gradient predicted within the glass is less for the transparent analysis than it is for the opaque analysis. The higher the temperatures developed within the glass the greater are the effects of the radiant heat transfer. For temperatures above about 1000°K it is necessary to consider the radiant transfer if the surface temperatures are to be estimated to better than ±150°K.

The assumptions made in the analysis are as follows:

1. Unidirectional unsteady-state heat flow in a plane, parallel, optically smooth, homogeneous, and isotropic glass was assumed.
2. Absorption coefficients are considered constant within finite spectral bands. Above a certain wavelength the material is considered perfectly opaque.
3. The materials are considered to be non-dispersive.
4. Thermal properties are not considered as temperature dependent.
5. Any external radiant source is considered perfectly diffuse and initially unpolarized.
6. Radiative attenuation within the material is considered to be described by the Lambert-Bouguer law and the propagation is that of a plane electromagnetic wave.
7. Emission from within the body is described by a derived volume emissive power.
8. Internal emission is perfectly diffuse and initially unpolarized.
9. Aerodynamic heating in hypersonic flight is considered as a fraction of stagnation point heat transfer. Gas cap radiation to the window is considered as emitting from a plane parallel graybody source, at a uniform temperature behind a normal shock, and the gas cap thickness is treated as equal to the stand-off distance at the stagnation point.
10. Aerodynamic heating in supersonic flight is given by the heat transfer to a flat plate traveling at zero angle of attack. External radiation is neglected during supersonic flight.
11. Direct solar radiation with a 6000°K black body spectral distribution and a form factor based upon the solar constant is used for the window heat input during the orbital mission.
12. The effects of thin transparent films on a transparency substrate are assumed to produce superpositions according to "thin" or "thick" film theory.

13. External (gas cap) radiation is assumed to be from incoherent sources.

14. Internal emitted radiation is assumed to be from coherent sources.

During the initial phase of the contract two digital computer programs were written for: (1) single-glaze unfilmed transparency, and (2) a multiple-glaze transparency with first order effects of a film on the emergent faces. An extension to the contract authorized the revision of the single-glaze computer program to include higher order effect of films (of the order 0.2 μ thick) on either or both faces of a single glazing and to provide for the computation of the emission from the semi-transparent glazing. The revised program (SIGTRAN) was written and run at the RTD IBM 7094 computer facility for a limited number of cases.

Initial results for filmed transparencies were obtained. These results indicate that the gross two-wavelength-band approximation for the optical properties of film materials as well as substrate materials does not adequately describe gold film properties and fused silica and plexiglas data. Tin oxide film properties and soda-lime and alumino-silicate data are fairly well approximated. In view of these limiting approximations, the results show that a tin oxide-coated glazing develops slightly higher temperatures within the glazing as compared to an unfilmed transparency exposed to the same hypersonic skip-glide trajectory. Consequently, the total radiant flux emitted into the cabin from a tin oxide-coated glazing is equal to or greater than that from an unfilmed transparency during the trajectory. Gold filmed results show that the highest temperature levels are obtained with a 0.2 μ gold filmed transparency which developed only about 1% of the cabin heat flux radiated by the unfilmed window.

Obviously the accuracy of the gold filmed results are limited by the gross wavelength band approximations to the gold data and the relatively large thickness of this film. Furthermore, fused silica (a material which is highly transparent in the visible and near infrared and highly absorbent in the far infrared) represents a case approaching the two bounds of the semitransparent domain. Consequently, the temperature predictions for fused silica are greatly affected by truncation errors encountered in the numerical computer solution to the extent that surface temperatures computed by the transparent analysis exceed the opaque analysis. Remedial action to correct these limitations were not authorized within the scope of the present study.

SECTION 2

DISCUSSION OF BASIC PHENOMENA

2.1 Heat Transfer Within Windows

A partially transparent material can transfer heat by both conduction and radiation. Other investigators have considered a "radiative conductivity" to describe the radiative mode. This approach has shortcomings since the "radiative conductivity" is not a true property of the material but is also a function of its dimensions. This study has separated the two mechanisms, treating the conduction as "true" (phonon) conduction and the radiative interchange separately as parallel mechanisms of heat transfer. In the following sections the mechanisms of heat transfer are discussed as they affect the window.

2.1.1 Radiation

Radiant exchange between the surfaces of opaque bodies is a relatively straightforward phenomenon. Usually the radiation is considered to traverse a non-absorbing medium between the opaque surfaces and a net balance of energies provides a sufficient description of the heat transfer. In contrast, partially transparent materials absorb radiation as it passes through the material and absorption takes place throughout the depth of the material. A window must be evaluated by considering its absorption and emission characteristics in addition to its transmission properties since the window itself can become a significant emitter at high temperatures. Furthermore, the radiation absorbed by a portion of the window could come from an external source as well as from within the window itself. Thus a window exhibits simultaneous interaction of absorption and emission of radiation throughout its volume.

The ability of a window material to absorb radiation is characterized by its absorption coefficient, γ_λ defined by the Lambert-Bouguer law:

$$I_{\lambda x} = I_{\lambda o} e^{-\gamma_\lambda x \sec \alpha} \qquad (1)$$

which states that within a partially transparent medium the intensity of monochromatic radiation, $I_{\lambda x}$ at a position x from an incident intensity, $I_{\lambda o}$ is reduced exponentially as its path length, x sec α, where α is the angle of incidence with the normal direction x. The absorption coefficient, γ_λ, is a function of the wavelength. Recent measurements by European workers (summarized in Reference 1) have shown that γ_λ is dependent upon the temperature. Typical absorption coefficient data for window glass (soda-lime) are shown in Figure 1.

The emission of radiation by a window material is a bulk phenomenon and is characterized by its spectral volume emissive power. This is a measure of the monochromatic power radiated at a given wavelength and solid angle by a unit volume of material at a given temperature. This radiation is diffuse and proceeds uniformly in all directions. Gardon (Reference 2) equated the calculated hemispherical emissive power of a semi-infinite partially-transparent radiator to the hemispherical emissive power of a comparable opaque radiator and

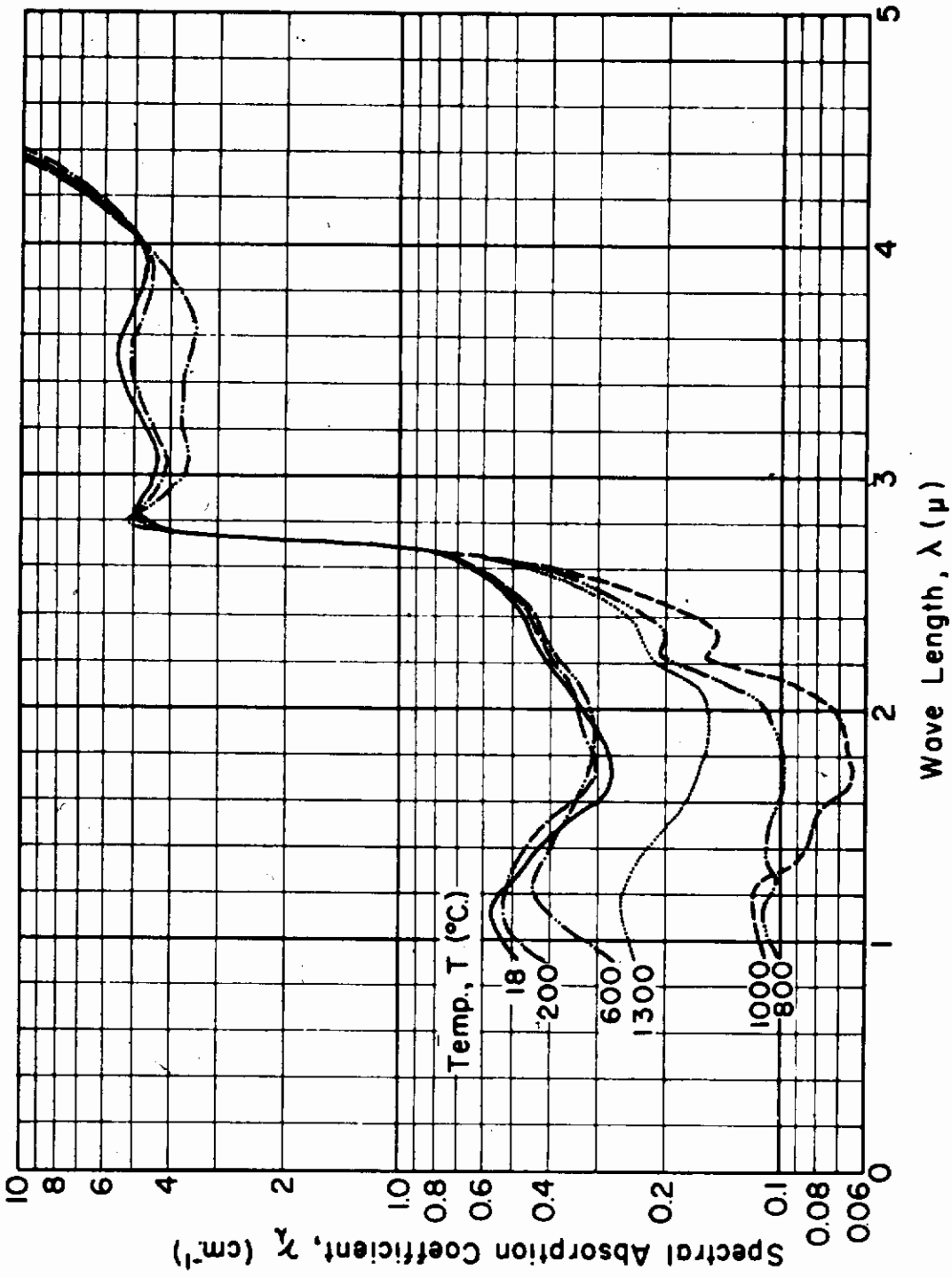

Figure 1 SPECTRAL ABSORPTION COEFFICIENT OF WINDOW GLASS

obtained the "spectral volume emissive power" of a partially-transparent material as:

$$j_\lambda = \frac{\gamma_\lambda n^2 W_{B\lambda}}{\pi} \qquad (2)$$

where j_λ = the spectral volume emissive power

γ_λ = the spectral absorption coefficient

n = the ratio of indices of refraction of the emitting medium to the emergent medium

$W_{B\lambda}$ = hemispherical spectral emissive power of an ideal (blackbody) radiator

With the spectral volume emissive power known, the rate of emission from the surface of a partially transparent body can be determined as a function of its size and temperature distribution by integrating the rates of emission of each elemental volume. The integration must include the effects of attenuation of the radiations as they travel toward the surface of the body and reflections and refractions at the surfaces. The basic mechanism of radiant interchange within a window material is embodied in the concepts of its absorption and emission. The complications that arise are due to a complete accounting of all radiations resulting from inter-reflections and multiple passages through the window.

A diffuse radiation source emits in all directions from its surface. Consider all the beams from the source that are incident on the window at an angle β, measured from the normal to the window. Of all these parallel beams, only those shown in Figure 2 will reach the elemental volume δV. As can be seen, the first beam is refracted at the exposed surface and then propagates through the window material which further reduces its intensity by absorption, until the beam reaches δV. In passing through the elemental volume, another fraction of the beam is again absorbed. Other beams reach the elemental volume by reflections from either or both of the window surfaces. The beams are attenuated as they pass through the window. Thus, many beams from many points on the radiating source are incident upon the window at an angle β and reach the elemental volume δV. These beams are incoherent with respect to one another, hence the superposition of these beams results in a summation of the individual beams and no interference occurs. An integration of all the beams from the radiation source that reach the window provides the total intensity reaching the elemental volume δV. A summation of the absorptions of each beam passing through the elemental volume yields the total absorption of external radiations.

In order to complete the radiant energy balance it is necessary to consider radiations emitted within the window itself. Once the temperature distribution within the window is known, the volume emissive power determines the emission from any elemental volume within the material. Since self-emission takes place in all directions, each elemental volume will emit toward both boundaries. These beams will reflect and will reach every other elemental volume of the window. The self-emitted beams will be reflected and refracted giving rise to multiple reflections in both directions. The summation of absorptions due to the passage of self-emitted radiations from each elemental

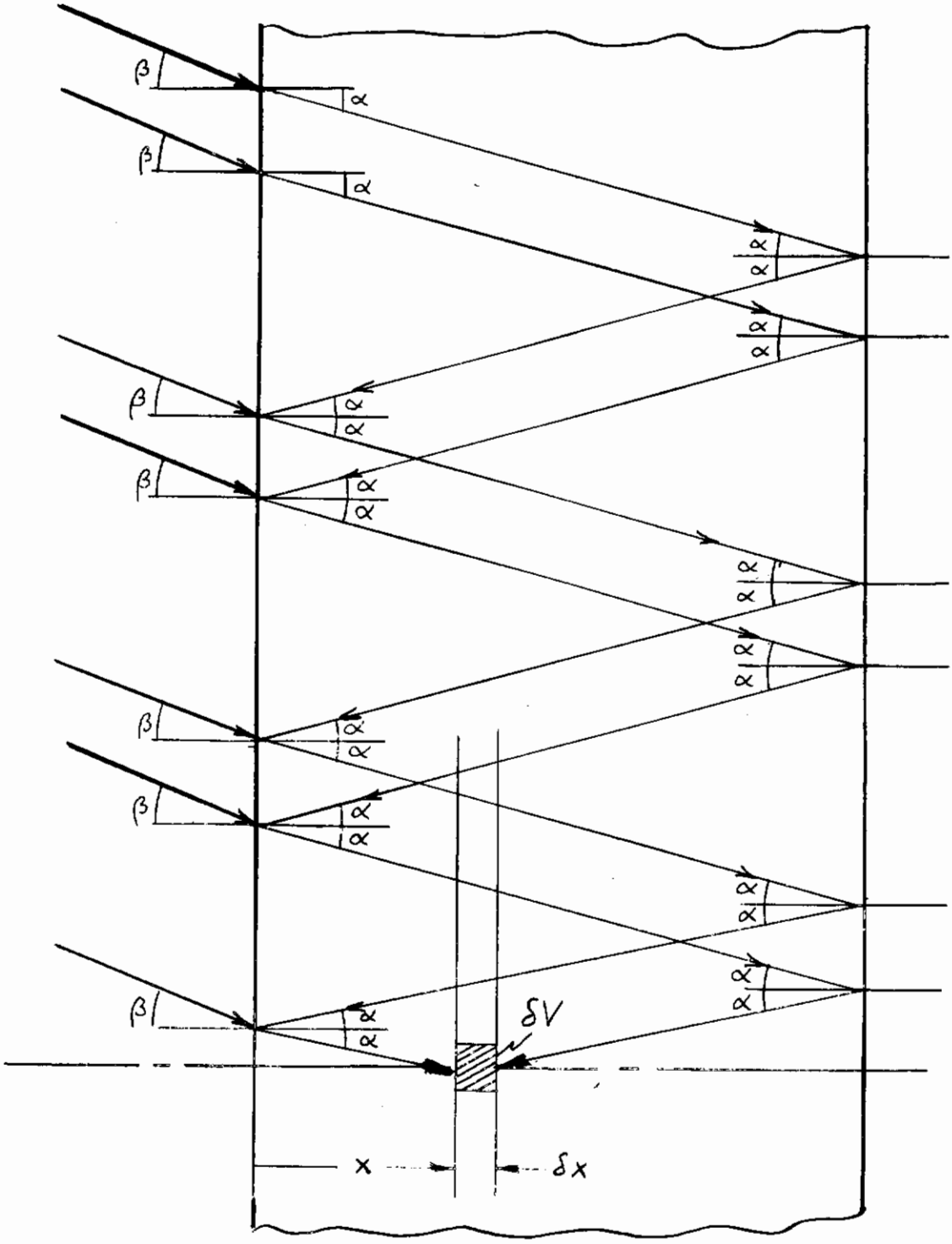

Figure 2 RADIATION FROM EXTERNAL SOURCES

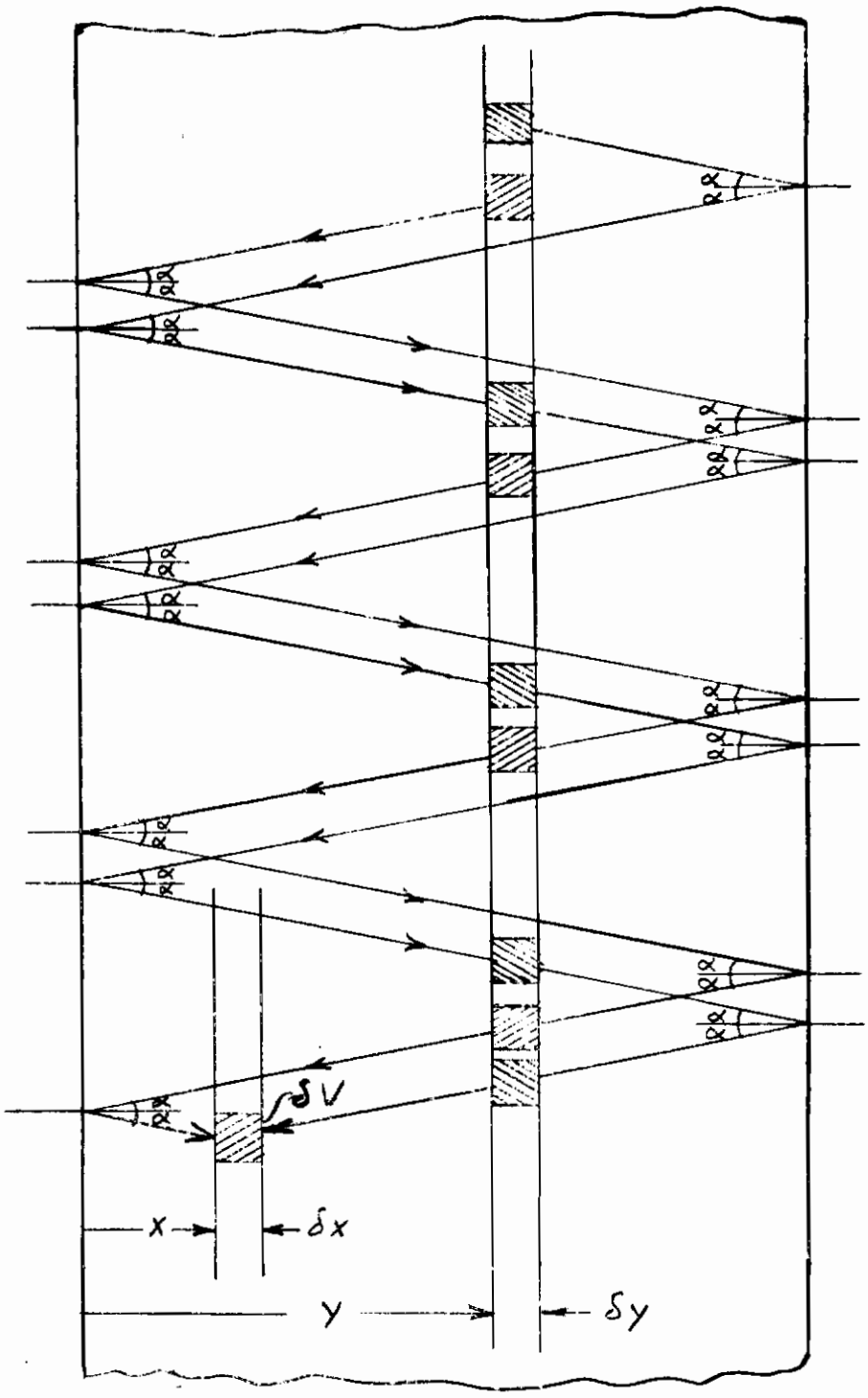

Figure 3 RADIATION FROM INTERNAL SOURCES

volume yields the re-absorption of internally emitted radiation from these volumes.

Thus, an energy balance of absorption due to external radiation, self emission, and re-absorption from other elemental volumes produces the net absorption of spectral energy at each position within a partially transparent window. Integration of these monochromatic energies over the transparent spectrum of the window yields the total energy absorbed at each position or layer in the window.

At the surface of the window, radiations in the opaque portion of the spectrum are partially absorbed and the remainder reflected. The window also emits in this wavelength band. With the exception of spectral considerations, these opaque radiations are analyzed as any opaque surface which requires no further specializations.

2.1.2 Conduction

The thermal conductivity of a partially transparent window material is a very important property in determining its temperature gradients. The transfer of energy in dielectric solids can occur by acoustical energy waves and/or by optical energy waves. Energy transfer can be viewed as the propagation of anharmonic lattice waves through the material or as the interaction between quanta of vibrational thermal energy or phonons. In this respect, the concept of molecular mean free path is introduced in direct analogy to the kinetic theory of gases, so that the phonon or "true" conductivity of a dielectric solid may be defined by (Reference 3):

$$k_c = \frac{1}{3} c_v v \ell \qquad (3)$$

where: k_c = the phonon (true) conductivity

c_v = the heat capacity per unit volume

v = the average sound velocity

The volumetric heat capacity and average sound velocity may be determined from reliable data, but the difficulty arises in a measure of the molecular mean free path, ℓ. Thus equation (3) really defines the molecular mean free path from measured phonon conductivity.

In addition to heat-energy transfer by vibrational modes, heat may be transferred through partially transparent window materials by absorption and reradiation of electromagnetic energy. Thus, in addition to phonon conductivity an analogous photon conductivity can be considered. Instead of molecules or phonons the waves are considered as being composed of photons. A significant difference exists since photons may propagate in a vacuum. A radiative or photon conductivity arises from close analogy between the kinetic theory or heat conduction of gases and dielectric solids and heat transfer by radiation and absorption. An expression for the photon conductivity is (Reference 4)

$$k_r = \frac{16}{3} \sigma n^2 T^3 \ell \qquad (4)$$

where σ = the Stefan-Boltzman constant

n = the index of refraction

T = the absolute temperature

ℓ = the molecular mean free path

However, it has been shown (Reference 5) that a theoretical treatment of steady state requires that the concept of radiation conductivity be applied only at distances greater than $5/\gamma_\lambda$ from any boundary, where γ_λ is an effective high temperature absorption coefficient. Hence, if γ_λ is about 0.5 cm^{-1}, the radiation conductivity analysis is not valid within 10 cm from any bounding surface. Thus for windows of practical thicknesses, the application of the photon or radiation conductivity is not valid.

In opaque materials, conduction is the only mechanism by which heat is redistributed within the interior of the material. The laws which describe conduction are well known and require no further explanation. In a partially transparent window material the radiative mechanism increases the rate of heat transfer within the material. Conduction, therefore, must be carefully separated from the radiant interchange that occurs within the partially transparent medium. The laws of conduction will be applied to "true conduction" utilizing the "true" thermal conductivity rather than an "apparent" thermal conductivity which has been determined by considering both mechanisms of heat transfer. Therefore, it is extremely important to select the appropriate thermal conductivity data for the window materials.

Unlike apparent conductivities involving both "true" and "radiation" conductivities, the "true" conductivity of glass is a weak function of temperature (Reference 6). At room temperatures radiative effects do not contribute significantly to the heat transfer mechanism. Therefore, conductivities measured at near room temperature may be ragarded as "true" conductivity values.

2.1.3 Convection

Just as conduction and radiation are the mechanisms by which heat is exchanged within the window material, convection serves as one of the primary mechanisms by which heat is transferred to and away from the surfaces of the window. In the absence of experimental data or the results of any detailed analysis, it will be necessary to estimate an aerodynamic heating rate based upon an idealized model trajectory. In the present report, hypersonic trajectories are used to compute convective input to the exposed surface of the window as a fraction of stagnation point heat transfer rate. A supersonic transport trajectory is used to estimate local heat transfer coefficients from correlations based upon flat plates at zero angle of attack. Thus, the local convective heat input at the window is determined on the basis of these heat transfer coefficients and the difference between the recovery (or adiabatic wall) temperature and the window surface temperature.

At the interior surface of the window, a convective heat transfer coefficient of 1.5 $Btu/ft^2hr^\circ F$ was chosen as representative (Reference 7). The convective heat transfer rate to the cabin thus depends upon the window interior surface temperature and an assumed cabin air temperature.

Material in Section 2.2 and 2.3 establish the boundary conditions for the partial differential equation (Eq. 11, p. 19), the solution of which is the main objective of this program.

The convective heat transfer in this subsection will be discussed in more detail in Section 2.2. The radiative input will be discussed in Section 2.3.

2.2 Window Heating Rates

The following three missions were selected to illustrate typical applications of the analysis and computer program developed:

1. Hypersonic re-entry into the earth's atmosphere
2. Supersonic flight in the earth's atmosphere
3. Orbiting flight about the earth.

2.2.1 Hypersonic Re-entry

The hypersonic re-entry imposes the highest heating rates that the window system of an aerospace vehicle will experience. For lift-type vehicles a possible re-entry trajectory is one which follows the equilibrium glide line of the vehicle, i.e., a combination of velocity, altitude and lift such that all vertical forces of weight, lift, and centrifugal force are in equilibrium.

An idealized re-entry vehicle with a vehicle wing load W/S = 25PSF and an initial velocity of 26,000 fps at 400,000 ft orbit, the skip-glide, hypersonic trajectory at the maximum re-entry angle of 7° shown in Figure 4 has been chosen to estimate window heating rates (Reference 8).

At hypersonic velocities, the aerodynamic heat transfer rates at the assumed window location are highly dependent upon the vehicle configuration and effects of shock interactions. A general treatment applicable to all vehicles is impossible. The heat transfer coefficients at the window location are assumed to be a fixed fraction of stagnation point heat transfer. A local heat transfer rate of 10% of the stagnation point value was assumed for the computations performed during this study.

2.2.2 Supersonic Flight

A typical supersonic transport would be designed to cruise at Mach 3 and to carry 100 passengers and a crew of 6 (see Reference 9). A New York to Paris flight plan (Figure 5) consists of a linear ascent to Mach 1 at 22,000 feet, a parabolic acceleration to Mach 3 at 65,000 feet, and a cruise at Mach 3 until the descent. The deceleration is assumed linear from Mach 3 to Mach 0.8 and held constant. With the assumed flight plan the trajectory can be determined (Figure 6).

The window was considered to be a flat plate traveling at zero angle of attack. A correlation for the heat transfer coefficient based upon free stream conditions is used (see Appendix I). Thus, the aerodynamic heating rate is computed as a function of the free stream conditions, adiabatic wall temperature and wall temperature. Radiation from the external surroundings are considered negligible.

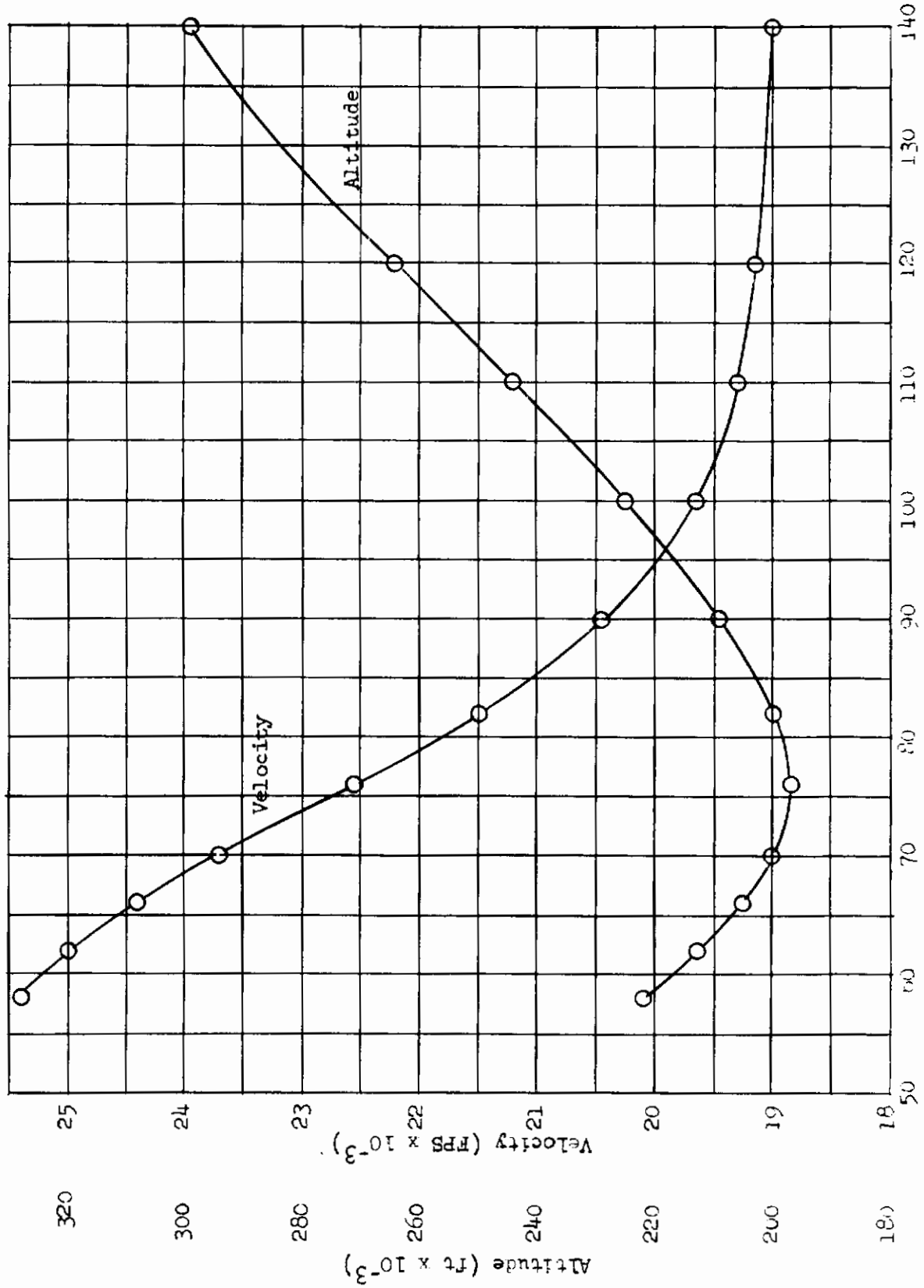

Figure 4 HYPERSONIC SKIP-GLIDE RE-ENTRY TRAJECTORY

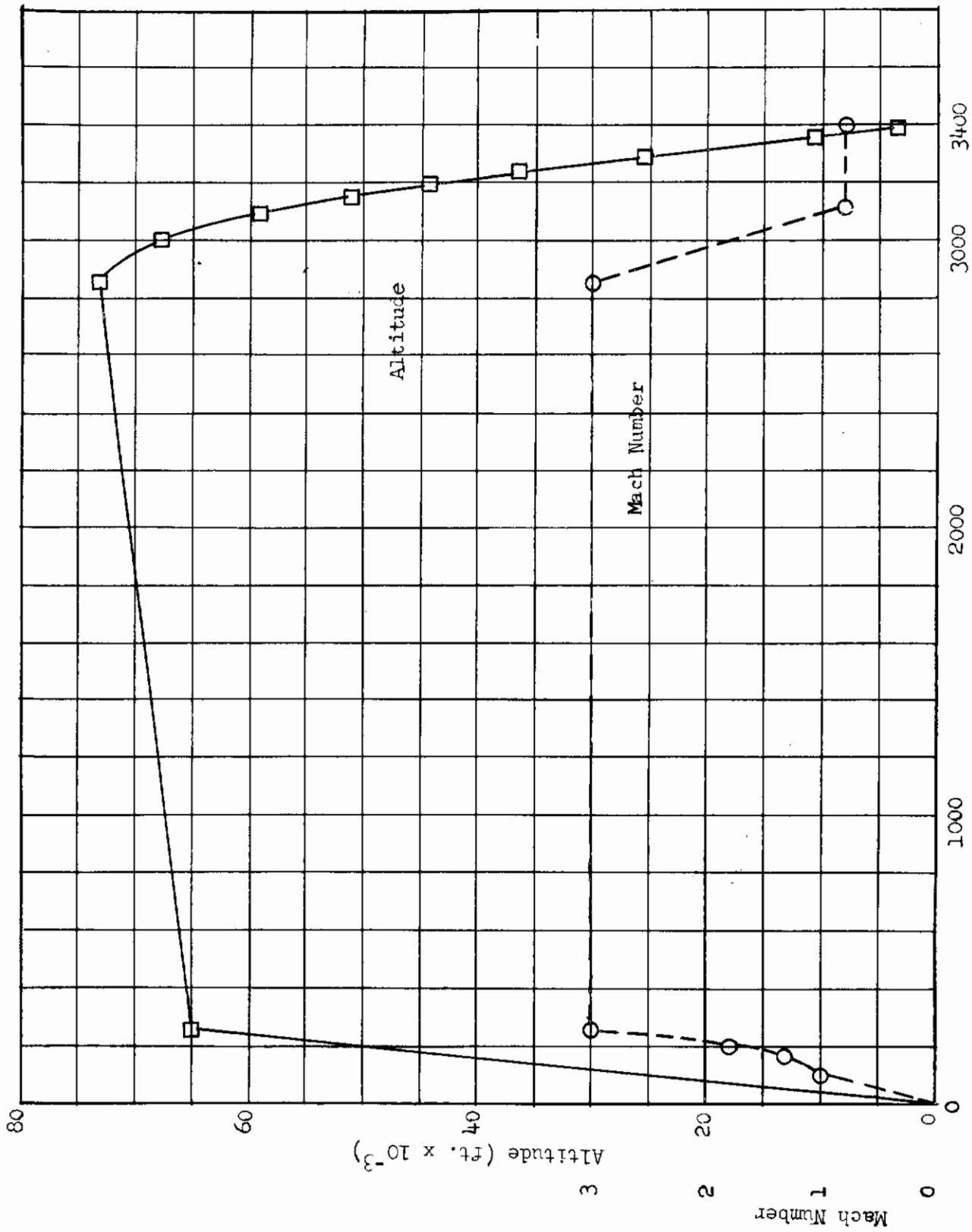

Figure 5 SUPERSONIC TRANSPORT FLIGHT PLAN

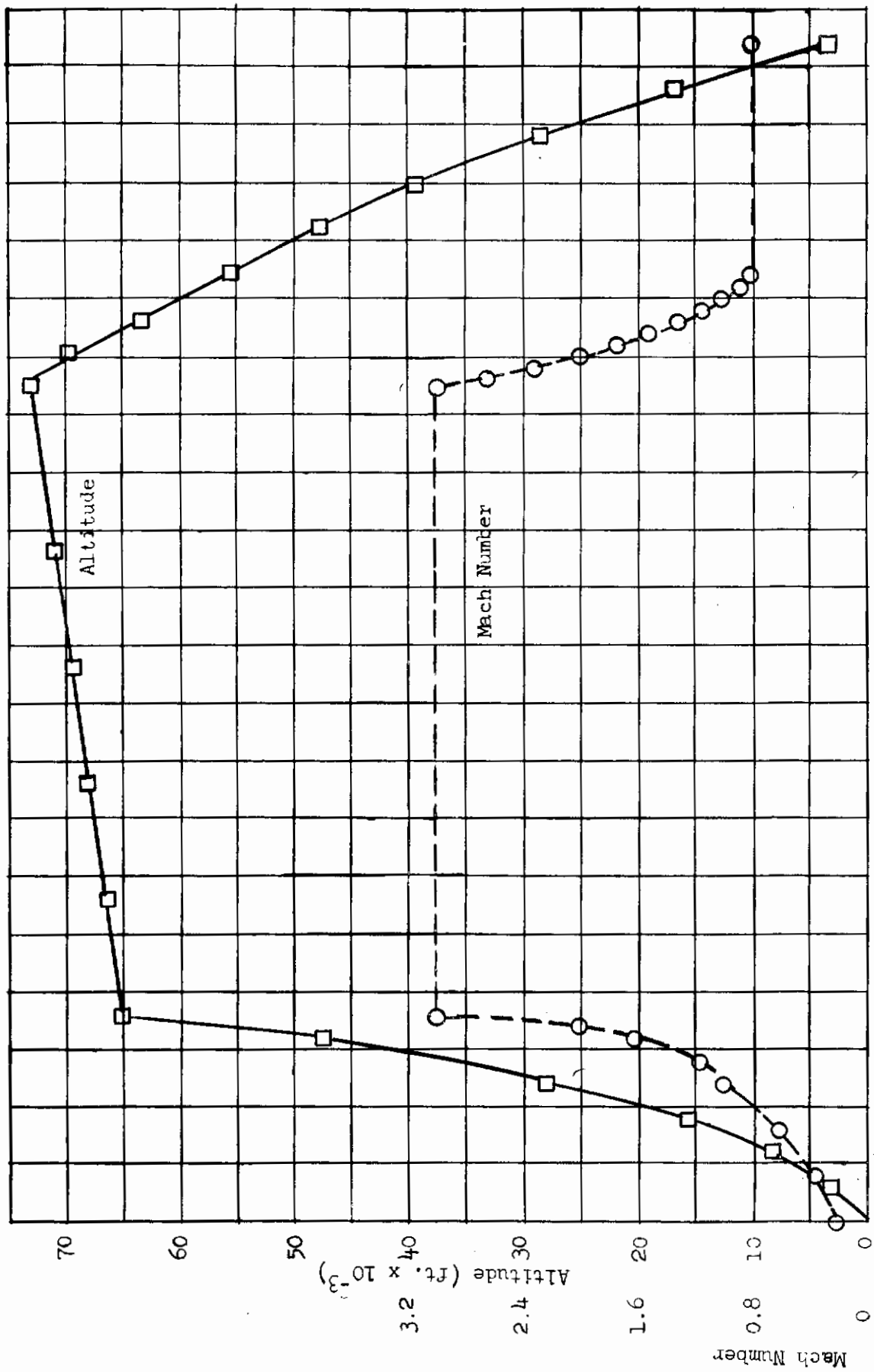

Figure 6 MACH 3 SUPERSONIC TRANSPORT TRAJECTORY

2.2.3 Earth Orbit

Analysis of the sources of radiations to an earth orbiting vehicle show that practically all of the heat input is direct solar radiation. The solar constant above the earth's atmosphere describes the input from direct solar radiation and the ratio of the solar constant to the blackbody emissive power of a 6000°K source (the apparent temperature of the sun) produces a "form factor", lumping orientation and attenuations from the solar source to the orbiting vehicle. Thus applying the form factor to the blackbody spectral distribution of the sun, the input to the window is adequately described.

2.3 Gas Cap Radiation

At re-entry speeds the hot gases around the vehicle can develop significant radiant heating effects. A complete description of the flow about such a vehicle includes knowledge of the reactions of molecules, atoms, ions, and electrons and the corresponding energy transport processes. Effects such as diffusion, recombination in the boundary layer, non-equilibrium flow and catalytic properties of walls must also be considered (References 10-12).

Convective heating to the stagnation region of a hypersonic vehicle is relatively well understood, but an accurate estimate of radiation from the hot gases to the vehicle is more difficult. To make such an estimate it is necessary to know in detail the complete flow field behind the shock including local temperature, density, pressure, and velocity profiles. Shock tube investigations have furnished some radiation data (References 13-15) but prominent researchers do not agree on the magnitude of the radiation from hot air. They agree roughly in methods of calculation but the main source of divergence lies in the value used for the oscillator strength or electronic f number.

Experimental and calculated results are presented in various forms such as spectral intensity, integrated intensity, spectrally dependent absorption coefficients, and integrated emissivities, all of which are temperature and density dependent. Two different physical models are used to estimate radiant heating rates: (1) a planar radiating layer and (2) a hemispherical radiating layer. The models may be further subdivided to: absorbing or non-absorbing media, isothermal or non-isothermal, isobaric or non-isobaric, etc. The hemispherical model is considered more correct (References 16 and 17) while the non-isothermal effects have been shown to be small (Reference 16).

The independent parameters used to determine the radiation field are the velocity, altitude, and body configuration (nose radius for stagnation point). A method for determining hot air radiation may be approached rigorously by defining the spectral intensity of emitting gases which are in direct view of the window. Keck (Reference 14) has made experimental measurement of spectral intensities in shock heated air. From these data f numbers were calculated for the principal species that radiate, i.e., NO_β, NO_γ, N_2 (2+), O_2, etc. The average spectral intensity over a small wavelength band is calculated and measured in the range of 2000 to 10,000 Å in the temperature range of 4000 to 9000°K and densities from 0.01 to 10 times standard atmospheric density. Keck's work is inadequate for the present application due to the limited range of temperature and density.

A more complete presentation is given by Myerott (Reference 15) in which absorption coefficients of air are calculated for the conditions: wavelength, 0.1167 to 1.9837 microns; temperature 1000 to 12000°K and; density 10^{-6} to 10 times standard atmospheric density. The fraction of blackbody radiations can be determined using the absorption coefficient given by:

$$I_\lambda = W_{B\lambda} \left[1 - e^{-\hat{\gamma}_\lambda \delta^*}\right] \qquad (5)$$

where: I_λ = intensity at wavelength λ

$W_{B\lambda}$ = blackbody intensity at wavelength λ

$\hat{\gamma}_\lambda$ = mean absorption coefficient

the mean absorption coefficient is given by;

$$\hat{\gamma}_\lambda = \hat{\gamma}_\lambda \left[1 - e^{-h/kT}\right] \qquad (6)$$

where: $\hat{\gamma}_\lambda$ = gas absorption coefficient at wavelength λ

h = Planck constant

k = Boltzman constant

It is seen that $\hat{\gamma}_\lambda$ is temperature, density, and wavelength dependent. Though numerical values of $I_\lambda / W_{B\lambda}$ are available (c.f. Reference 18) it was found that the spectral dependence is too complicated to be used effectively.

The work of Kivel and Bailey (Reference 13) was finally chosen as the best applicable source for supplying radiative inputs from shock heated air. The spectral volumetric intensity is integrated over all wavelengths and is presented in graphical form as a function of air temperature and density. From the volumetric intensity, curves are given for the graybody emissivity of shock heated air per unit thickness as a function of air temperature and density. These curves have been fitted by a logarithmic polynomial expansion of the form:

$$\log \epsilon/\delta^* = a_0 + a_1 \log T + a_2 \log^2 T + a_3 \log^3 T + a_4 \log^4 T \qquad (7)$$

where ϵ/δ^* = graybody emissivity per unit thickness (cm^{-1})

$a_0 \ldots a_4$ = constants determined from the polynomial fit

log = logarithm to the base 10

T = absolute temperature (°K)

A least-squares analysis was used to determine the constants $a_0 \ldots a_4$. The resulting values for the constants are shown in Tables 1 and 2. As may be noted, one set of constants is applicable in the range $1000 \leq T < 8000$°K and the second set of constants is applicable in the range $8000 \leq T \leq 18{,}000$°K. To determine intermediate values, double logarithmic interpolation is performed between temperature and density values on both sides of the values required.

TABLE 1
COEFFICIENT FOR THE LEAST-SQUARES FIT
LOW TEMPERATURE: $1000 \leq T < 8000°K$

Density ratio ρ/ρ_o*	a_0	a_1	a_2	a_3	a_4
10^{-6}	-6.925307	2.8251600	-2.5936484	0.19645656	0.063094980
10^{-5}	-3.7398826	-2.4643677	-0.78233130	0.29189669	0.000000000
10^{-4}	-16.4635100	5.3745600	-1.8453232	0.28489560	0.000000000
10^{-3}	-64.254100	34.832836	-3.9048150	-1.1711824	0.22468464
10^{-2}	-21.239832	7.3043176	-1.3141154	0.14599265	0.000000000
10^{-1}	-75.888910	43.790509	-5.1229970	-1.4008835	0.27386482
10^{0}	49.092640	-42.948052	7.1221220	1.1666329	-0.26152723
10^{1}	104.74205	-79.760151	11.775116	2.3571684	-0.48591030

* ρ_o is air density at sea level

TABLE 2
COEFFICIENTS FOR THE LEAST-SQUARES FIT
HIGH TEMPERATURE: $8000 \leq T \leq 18000°K$

Density ratio ρ/ρ_o*	a_0	a_1	a_2	a_3	a_4
10^{-6}	-42.329078	3.3773731	0.38418980	1.1454587	-0.23198607
10^{-5}	-56.086180	-4.0042870	2.6224950	2.0830205	-0.43381861
10^{-4}	-60.699710	-4.5744890	2.9574360	2.3487883	-0.48580387
10^{-3}	-87.580695	7.8681740	0.49151000	2.9433819	-0.56388439
10^{-2}	-38.483046	-3.1711910	1.5607300	1.4969915	-0.28388548
10^{-1}	-11.1572062	-0.34727720	-0.23287300	0.32303328	-0.024583496
10^{0}	0.1892374	-1.3357925	-0.31752664	-0.05693168	0.051322102
10^{1}	4.7243840	-1.6747281	-0.14927570	-0.19923154	0.069056794

* ρ_o is the density at sea level

A simplified equation for the shock detachment distance (δ^*) has resulted from an attempt to improve gas dynamic calculations based on the Newtonian theory of impact. Following the scheme used by Prandtl for the reduction of the hydrodynamic equations for large Reynolds Numbers, the gas dynamic equations were simplified in the limit where M, the free stream Mach Number, is large, and γ (the ratio of specific heats) approaches unity. For high speed

design, the results seem to be satisfactory. To transform the equation for finite M, the formal substitution is made: $(\gamma - 1)/2 \longrightarrow 1/K$ where K is the ratio of normal shock to free stream density. Then δ^* takes the form

$$\delta^* = \frac{2R}{3K} \tag{8}$$

R = nose or body radius

In this form the equation applies to high K (high M) only. If (K - 1) is substituted for K, a surprising agreement with experiment is also obtained for low supersonic speeds. Thus, the final form of δ^* is (Reference 18):

$$\delta^* = \frac{2R}{3(K - 1)} \tag{9}$$

Equation (7) is used to compute the graybody emissivity per unit thickness, ϵ/δ^* for a given temperature, T_H behind a normal shock and corresponding density, ρ, behind the shock. For a given nose radius (assumed to be 6 inches in this study) and free stream density, the shock detachment distance may be computed by equation (9). Thus, the product of ϵ/δ^* and shock detachment distance yields the graybody emissivity of the gas cap radiation, ϵ. However, the graybody emissivity is scaled according to the exponential (Reference 16)

$$\epsilon_g = \frac{q''_r}{\sigma T_H^4} = 1 - e^{-\epsilon} \tag{10}$$

where
- ϵ_g = graybody hot gas emissivity
- q''_r = radiative flux
- σ = Stefan Boltzman constant
- T_H = hot gas absolute temperature
- ϵ = emissivity defined by equation (7)

Equation (10) yields an effective emissivity of the shock heated air accurate to within 20% of the exact solution as presented in Reference 20. The basic assumptions leading to equation (10) are that the radiating layer is planar (normal shock) of thickness δ^* which is divided into infinitesimal slabs having an absorptivity per unit thickness equal to their emissivity per unit thickness. The results given are then integrated over the width of the slab.

The foregoing steps have been used to estimate the bow shock radiation incident upon a hypersonic re-entry vehicle. The shock is assumed to be normal and the radiation to come from a graybody whose emissivity is dependent on density, temperature and standoff distance.

SECTION 3

ANALYSIS AND RESULTS

3.1 Thermal Analysis

The analytical solutions for the transient temperature distribution of windows subjected to aerodynamic heating and/or external radiations are contained in Appendix I. The following expression relates the rate of change of temperature of any point to the sum of the net rates of energy reaching the point by conduction and by radiation.

$$\rho c \frac{\partial T_i}{\partial t} = \sum_j q_i'''(T_j) + k \frac{\partial^2 T_i}{\partial x_i} \qquad (11)$$

The radiant interchange term emphasizes that the radiant mechanism is treated separately from the conductive mechanism of heat transfer. The radiant interchange term is made up of the net absorption from external sources, Q_A, emission of its own radiation, Q_E, and reabsorption of radiations emitted from the surrounding medium, Q_R, thus:

$$\sum_j q_i'''(T_j) = Q_A(x_i) - Q_E(x_i) + Q_R(x_i) \qquad (12)$$

The evaluation of the radiant interchange term leads to integrals which can not be solved in closed form and must be solved numerically. Differential equation (11) also requires numerical solution. Therefore, the analysis for temperature distributions within the partially transparent window material involves the solution of an integro-differential equation with appropriate boundary and initial conditions.

The boundary conditions are determined from the trajectory and the cabin conditions. For the single-glaze problem, where only one pane is considered, the thermal effects due to a hypersonic skip-glide re-entry trajectory, supersonic transport trajectory, and a circular earth orbit have been computed (see Section 2.2). For all these computations a 1/2" thickness of glass has been assumed. Four different window materials were considered. Fused silica (Corning 7940), Soda-lime (Corning 0080) and Alumino-silicate (Corning 1723) were exposed to the hypersonic and supersonic trajectories while Soda-lime and Plexiglas were used for the orbiting missions. The thermal and optical properties of these materials are summarized in Table 3.

3.1.1 Material Properties

Both thermal and optical properties of the window materials are required for the thermal analysis. The thermal properties consist of the thermal conductivity and volumetric specific heat. The thermal conductivity, as discussed previously (see Section 2.2.2), is the "true" thermal conductivity of the material. Thus, in the absence of other data which reliably separate the radiation effects from measured thermal conductivities, the value at room temperature is taken as the "true" conductivity and is assumed to be invarient with temperature. The volumetric specific heat, though available as temperature dependent quantities is taken as the mean value over the temperature range (References 21 and 22).

TABLE 3

THERMAL PROPERTIES AND OPTICAL PROPERTIES OF TRANSPARENT MATERIALS

		Fused Silica (Corning 7940)	Soda-lime (Corning 0080)	Alumino-Silicate (Corning 1723)	Plexiglas 55
	k Thermal Conductivity (watt/cm°K)	1.339×10^{-2}	8.370×10^{-3}	1.246×10^{-2}	1.730×10^{-3}
	c Specific Heat (cal/gm°K)	0.17		0.22	0.35
	ρc Volumetric Spec.Ht. (watt-sec/cm^3°K)	1.566	2.511	2.444	1.744
	κ Thermal Diffusicity (cm^2/sec)	8.550×10^{-3}	3.333×10^{-3}	5.098×10^{-3}	0.992×10^{-3}
	n Refractive Index	1.459	1.512	1.547	1.50
1st Wavelength Band	λ_1 Wavelength-Cutoff (microns)	2.0	2.75	2.5	1.25
1st Wavelength Band	γ_1 Absorption Coeff. (cm^{-1})	0.02	Temperature Dependent (See Fig. 10)	0.024	0.1
2nd Wavelength Band	λ_2 Wavelength-Cutoff (microns)	3.75	4.5	4.5	2.0
2nd Wavelength Band	γ_2 Absorption Coeff. (cm^{-1})	0.4	Temperature Dependent (See Fig. 10)	6.0	0.7

The optical properties generally available for transparent materials are refractive index, and apparent transmissivity at normal incidence. The required absorption coefficient can be obtained from these data by reference to the work of McMahon (Reference 23). The resulting absorption coefficients are shown in Figures 7 through 10.

It is possible to fit step-function approximations through these data to facilitate computations. These approximations are also shown in Figures 7 to 10. As can be seen, the simplification is a rough approximation to the fused silica data (Figure 7) and Plexiglas data (Figure 9), but is a good approximation to the alumino-silicate and soda-lime data. The soda-lime data are shown with temperature variation for absorption coefficients (see References 2 and 6). Some temperature dependent data for apparent transmissivity have been given for fused silica in Reference 21, however, these data are practically the same as the room temperature data.

3.2 Computer Program

The single-glaze computer program was written to accept the hypersonic, supersonic and orbiting missions input, and with the option of computing the temperature distribution by considering radiant interchange and conduction or by considering conduction alone. The first section of the program computes the radiant interchange field associated with the initial temperature field. These computations are numerical integration of the functions shown in Appendix I using Simpson's rule (see Reference 24). With the radiant interchange field computed for the initial temperature field the new temperature field is computed for the next time interval. Since the temperature field requires the solutions of simultaneous linear equations, Crout's method (Reference 25) is utilized. An iterative computation is performed to assure convergence of the temperature computations to within 0.1%. The finite time increment is reduced until prescribed convergence is obtained.

The computer running times are shown in Table 4. As can be seen, hypersonic trajectores of one minute duration real time required about 2 to 3 minutes of computer time. Supersonic trajectories of 167 minutes duration real time required about 4 to 5 minutes of computer time. This extreme variation in computer time illustrates that rapidly changing inputs (hypersonic) require that smaller time increments be used in each calculation thus requiring longer running times.

During the second phase of the contract, computer program revisions were performed on the single-glaze computer program. The new program SIGTRAN is a computer program for the solution of the temperature distribution and heat flux of a single-glaze, filmed transparency subjected to hypersonic, supersonic and orbiting missions. Provisions are included to treat a thin transparent film on one or both surfaces. The total integrated flux into the cabin is also computed. With this revised computer program several limited cases were run with thin gold and tin oxide films on an alumino-silicate substrate and subjected to hypersonic skip-glide trajectory described in Section 2.2.1. The computation time was roughly doubled because of the increase in computations necessary to determine the flux emitted into the cabin.

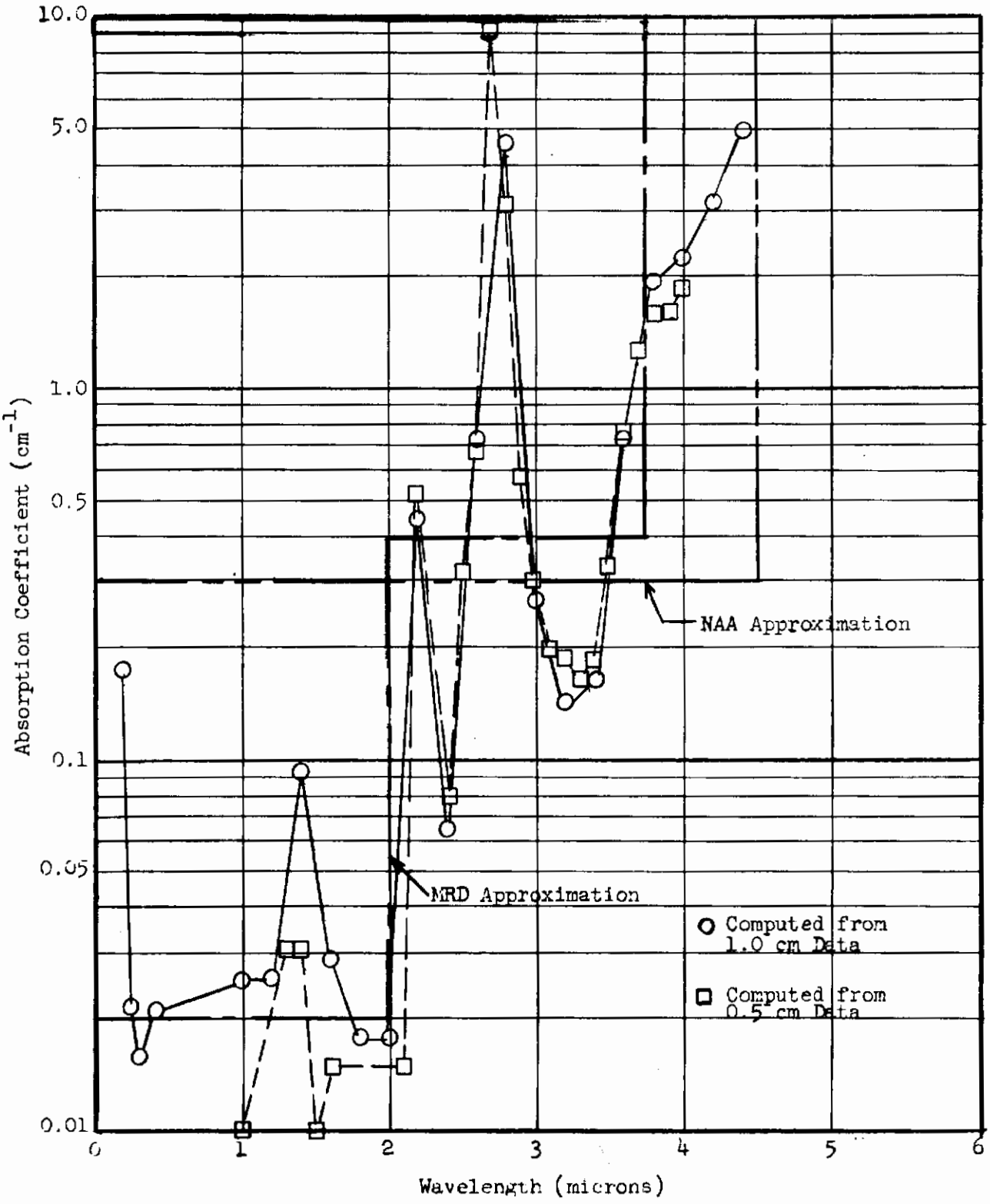

Figure 7 SPECTRAL ABSORPTION COEFFICIENT FOR FUSED SILICA GLASS

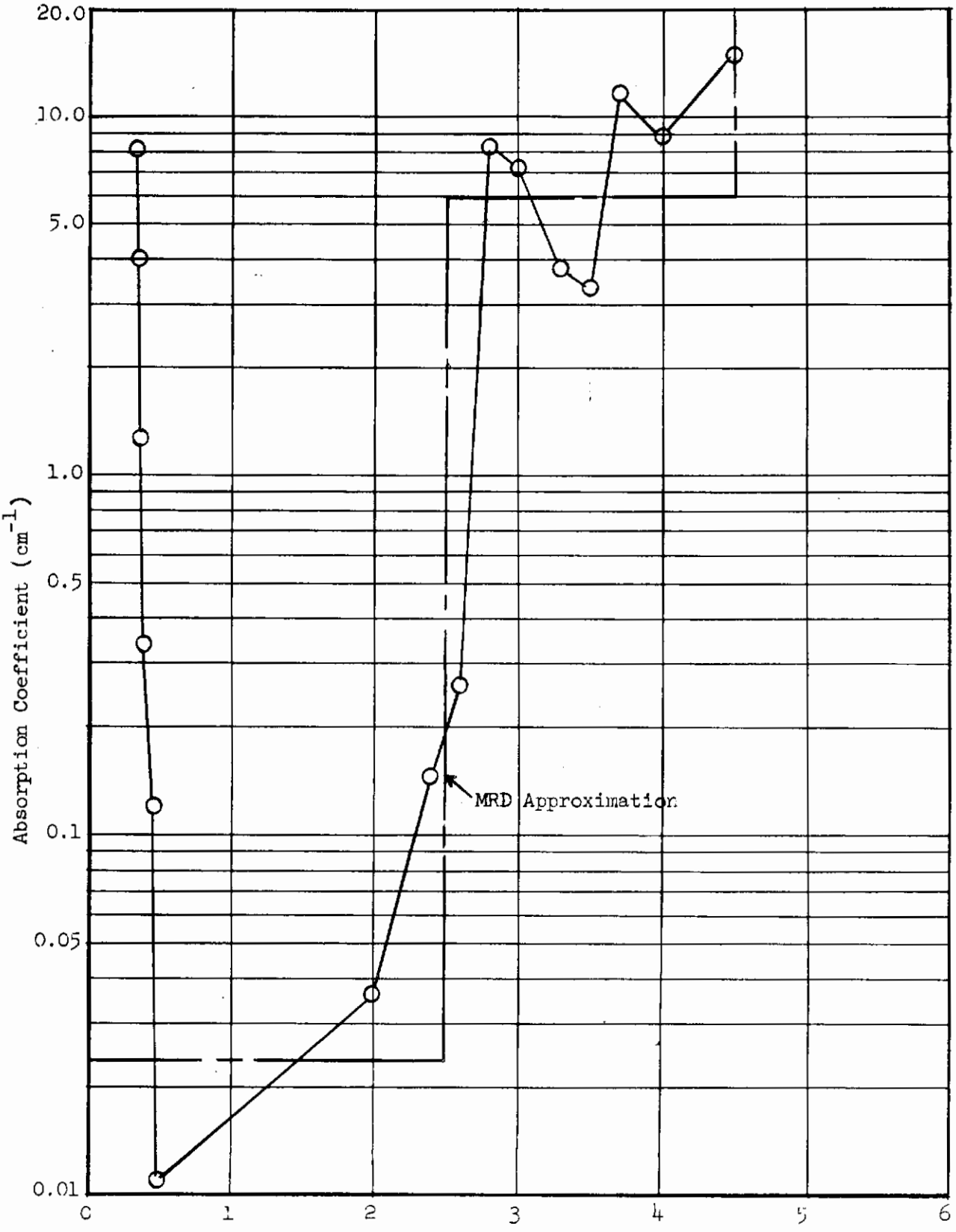

Figure 8 SPECTRAL ABSORPTION COEFFICIENT FOR ALUMINO-SILICATE GLASS

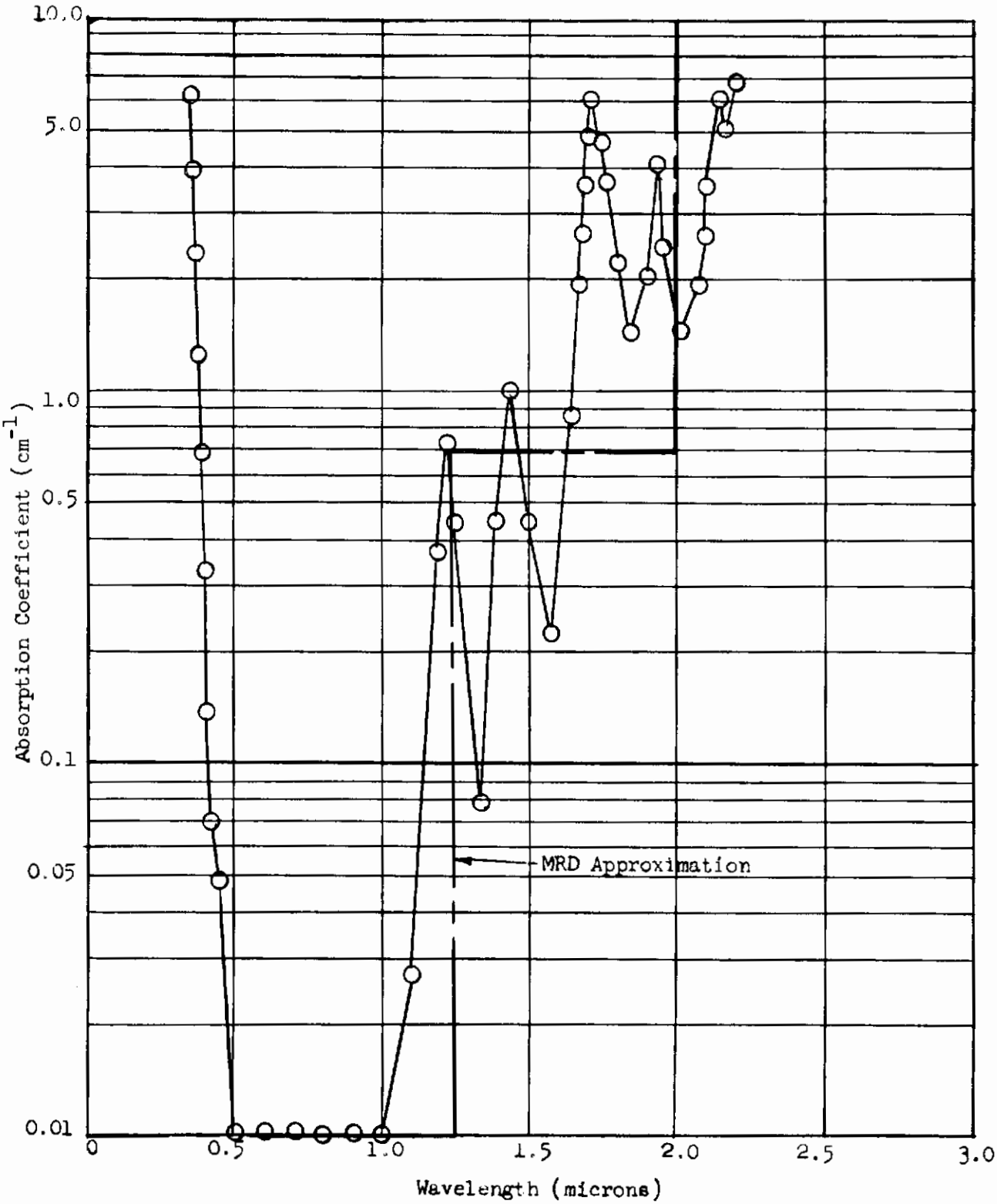

Figure 9 SPECTRAL ABSORPTION COEFFICIENT FOR PLEXIGLAS

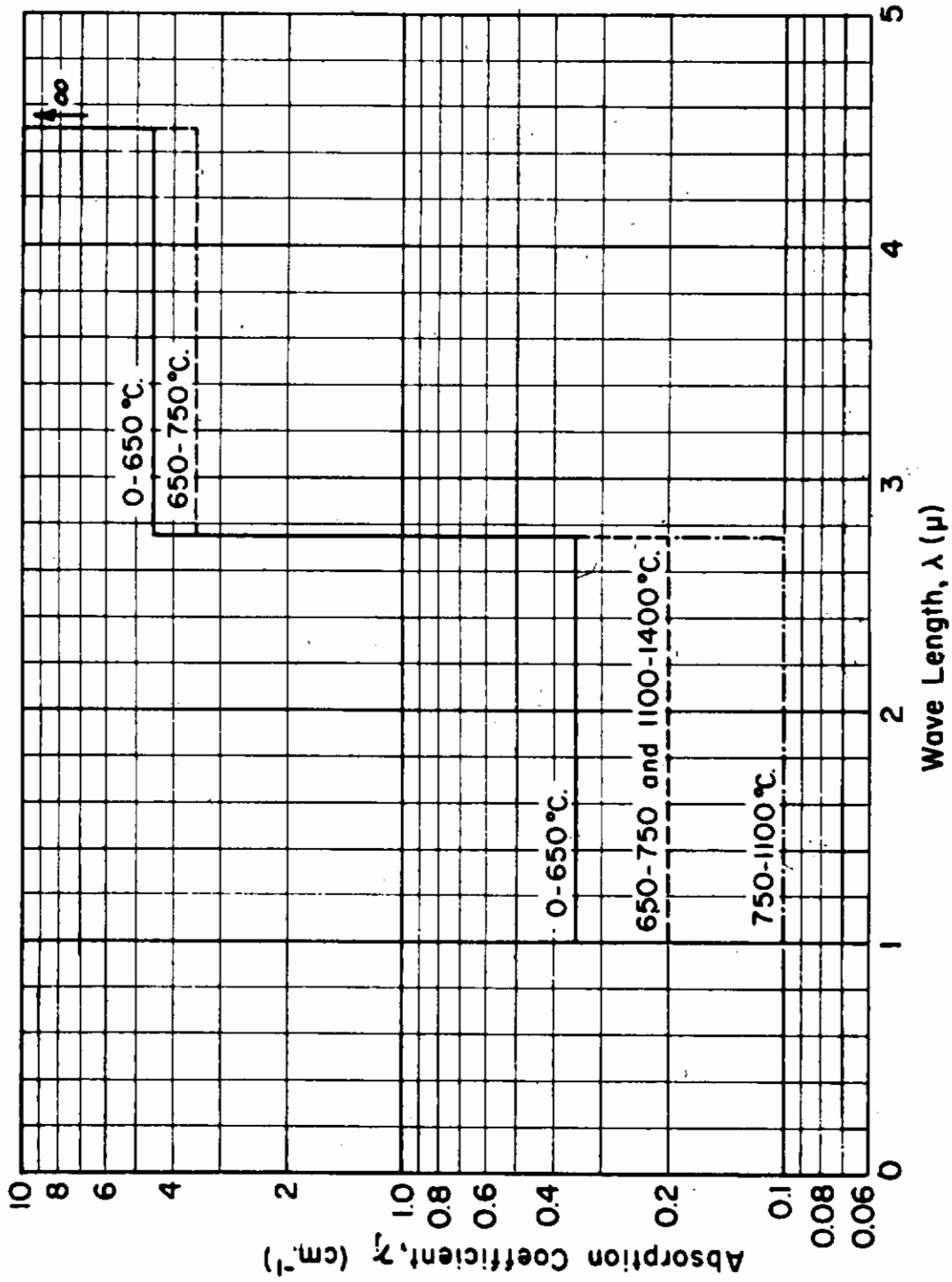

Figure 10 STEP FUNCTION APPROXIMATIONS TO SPECTRAL ABSORPTION COEFFICIENTS FOR SODA-LIMA GLASS

TABLE 4

COMPUTER RUNNING TIME

Trajectory	Computation Theory	Window	Total Computation Time (min.)	Number of Calculations	Calc/min	Duration of Traj., Sec.
Hypersonic	Transparent	Soda-lime	2.97	101	33.7	60
Hypersonic	Transparent	Fused Silica	2.40	116	34.2	60
Hypersonic	Transparent	Alumino-Silicate	2.23	111	49.7	60
Supersonic	Transparent	Soda-lime	4.80	238	49.6	10,000
Supersonic	Transparent	Fused Silica	4.32	215	49.8	10,000
Supersonic	Transparent	Alumino-Silicate	4.43	221	49.8	10,000
Orbit	Transparent	Soda-lime	2.03	101	49.6	100
Orbit	Transparent	Plexiglas	2.03	101	49.6	100
Hypersonic	Opaque	Soda-lime	2.60	108	47.2	60
Hypersonic	Opaque	Fused Silica	2.48	117	47.2	60
Hypersonic	Opaque	Alumino-Silicate	3.30	111	47.2	60
Supersonic	Opaque	Soda-lime	1.47	240	163.2	10,000
Supersonic	Opaque	Fused Silica	1.31	213	163.1	10,000
Supersonic	Opaque	Alumino-Silicate	1.38	224	162.3	10,000
Orbit	Opaque	Soda-lime	0.62	101	162.9	100
Orbit	Opaque	Plexiglas	0.62	101	162.9	100

3.3 Results for the Single-Glaze Window Without Films

3.3.1 Hypersonic Skip-Glide Trajectory

The surface temperatures predicted for the single-glaze window are shown in Figures 11 and 12. As can be seen from Figure 11, the transparent analysis including radiant interchange as a mechanism for heat transfer, produces the highest surface temperature in the fused silica window and the lowest in the alumino-silicate window. The opaque calculations (Figure 12) show the same trend though somewhat lower in value with the interesting result that the soda-lime surface temperature is brought very close to the fused silica surface temperature. These results may be further studied by observing the temperature gradients within the glasses for successive times during the trajectory (Figures 13 to 22).

3.3.1.1 Discussion of Opaque Results - Consider the opaque profiles shown in Figure 19. Soda-lime glass exhibits the steepest surface temperature gradient while fused silica and alumino-silicate glasses have approximately equal temperature gradients (the alumino-silicate gradient is slightly steeper than that for fused silica). These calculations consider conduction as the only mechanism of heat transfer within the window. Thus, soda-lime glass with the lowest thermal conductivity of the three materials naturally has the highest temperature gradient at the surface. Likewise, fused silica and alumino-silicate glasses with almost equal thermal conductivities (both greater than that for soda-lime glass) develop temperature gradients that are almost equal (but lower than that for soda-lime glass).

To illustrate the relationship between the surface temperatures of the three materials consider a constant heat flux as incident on the window. This is not the case in the actual problem since the input to the window is dependent upon both window surface temperature and external conditions which are variable, but the simplification can be used to illustrate trends in the results. A window, initially at uniform temperature, subjected to a constant heat flux, F_o, at the boundary X = L, and perfectly insulated at the boundary X = 0, will develop a temperature excess over the initial temperature given by: (Reference 26)

$$\theta = \frac{F_o t}{\rho c L} + \frac{F_o L}{k}\left\{\frac{3X^2 - L^2}{6L^2} - \frac{2}{\pi}\sum_{n=1}^{\infty}\frac{(-1)^n}{n^2} e^{-\kappa^2 n^2 \pi^2 t/L^2} \cos\frac{n\pi X}{L}\right\} \qquad (13)$$

where

θ	=	temperature excess over the initial temperature, °K
F_o	=	constant flux at X - L, watt/cm^2
ρc	=	volumetric specific heat, watt-sec/cm^3°K
X	=	spacial coordinate, cm
L	=	thickness = 1.27 cm
κ	=	thermal diffusivity, cm^2/sec
t	=	time, sec
n	=	dummy index for the summation

Figure 11 SURFACE TEMPERATURES COMPUTED FOR HYPERSONIC SKIP-GLIDE RE-ENTRY BASED UPON RADIATION AND CONDUCTION

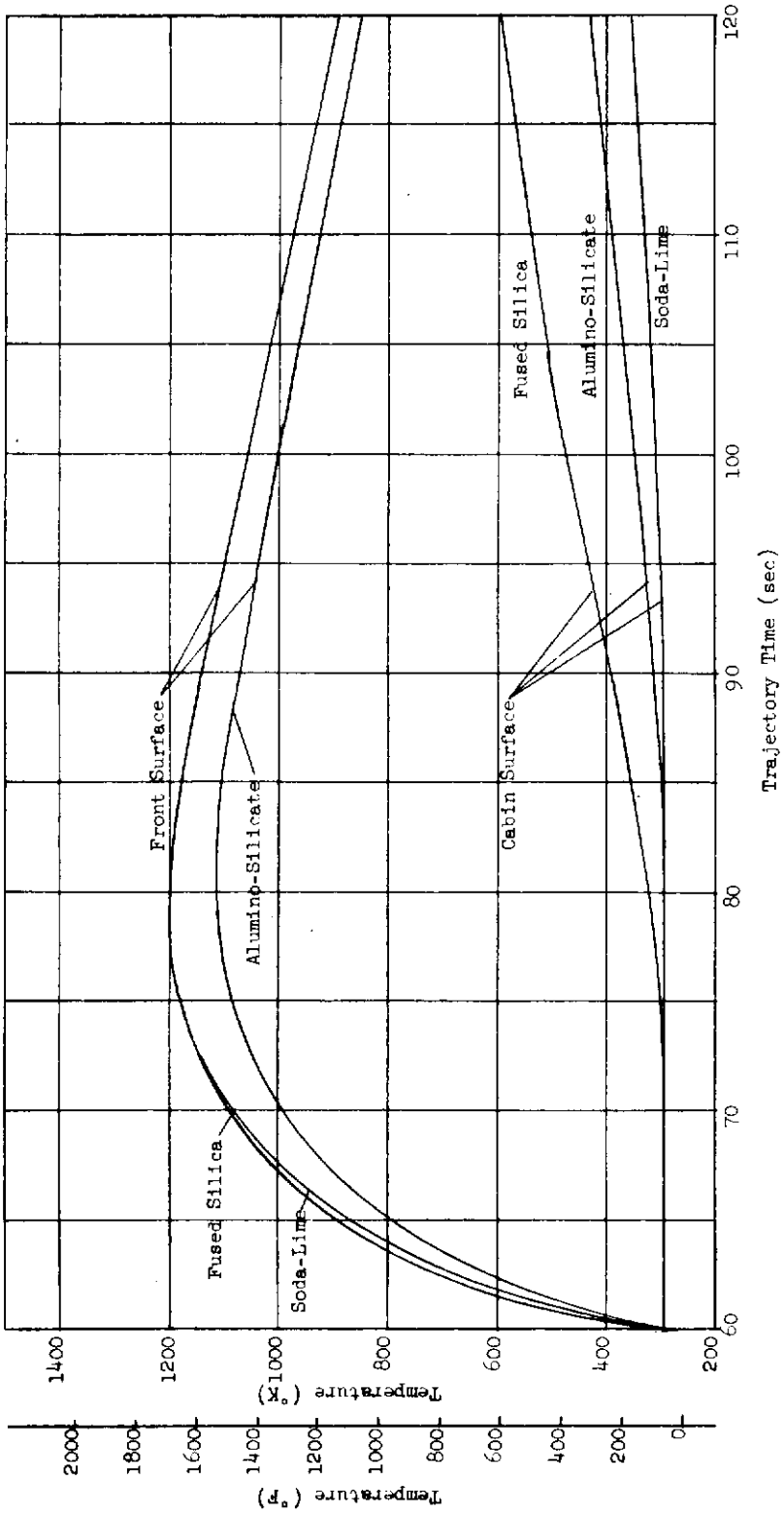

Figure 12 SURFACE TEMPERATURES COMPUTED FOR HYPERSONIC SKIP-GLIDE RE-ENTRY BASED UPON CONDUCTION ALONE

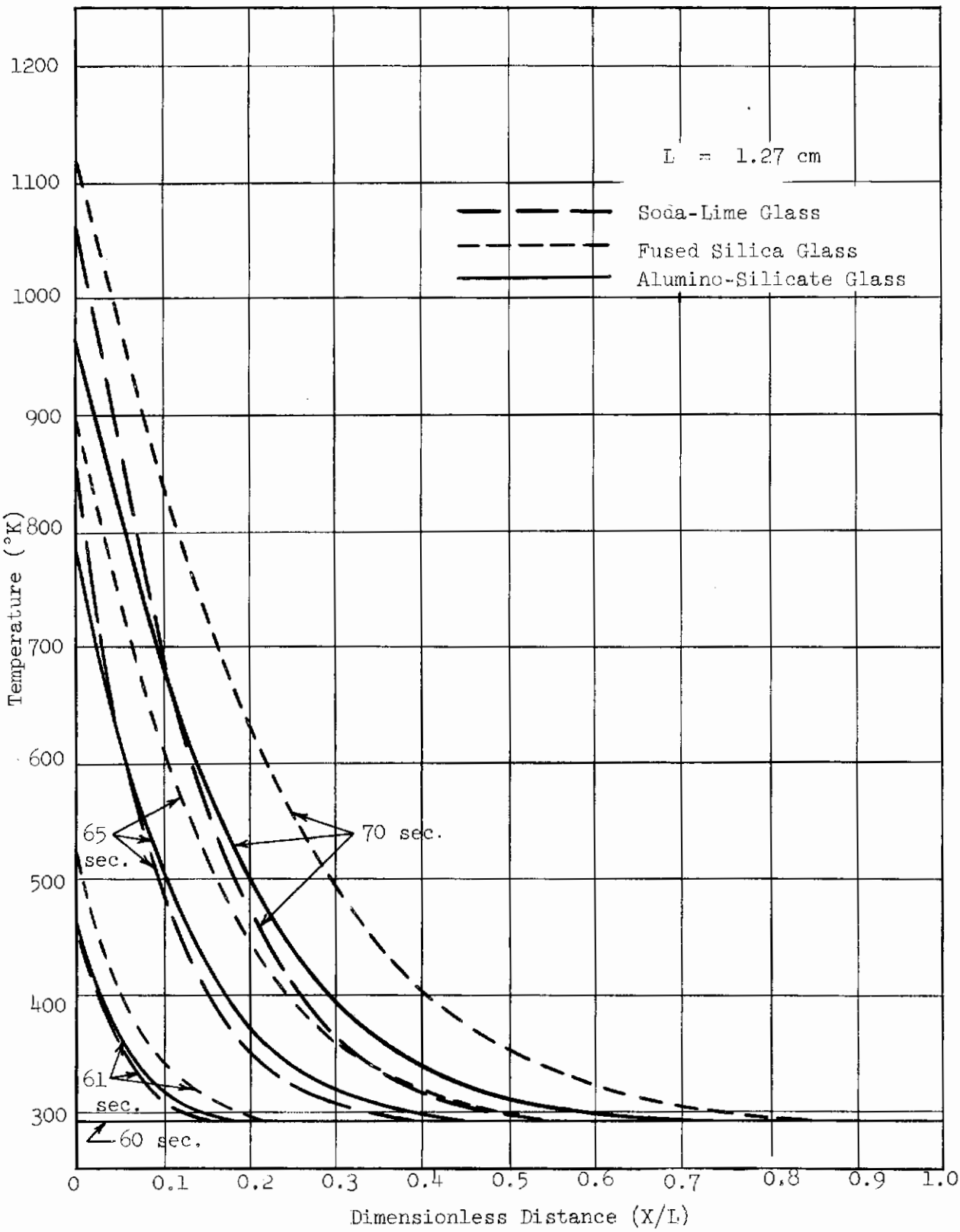

Figure 13 TRANSPARENT TEMPERATURE PROFILES AT BEGINNING OF HYPERSONIC SKIP-GLIDE TRAJECTORY

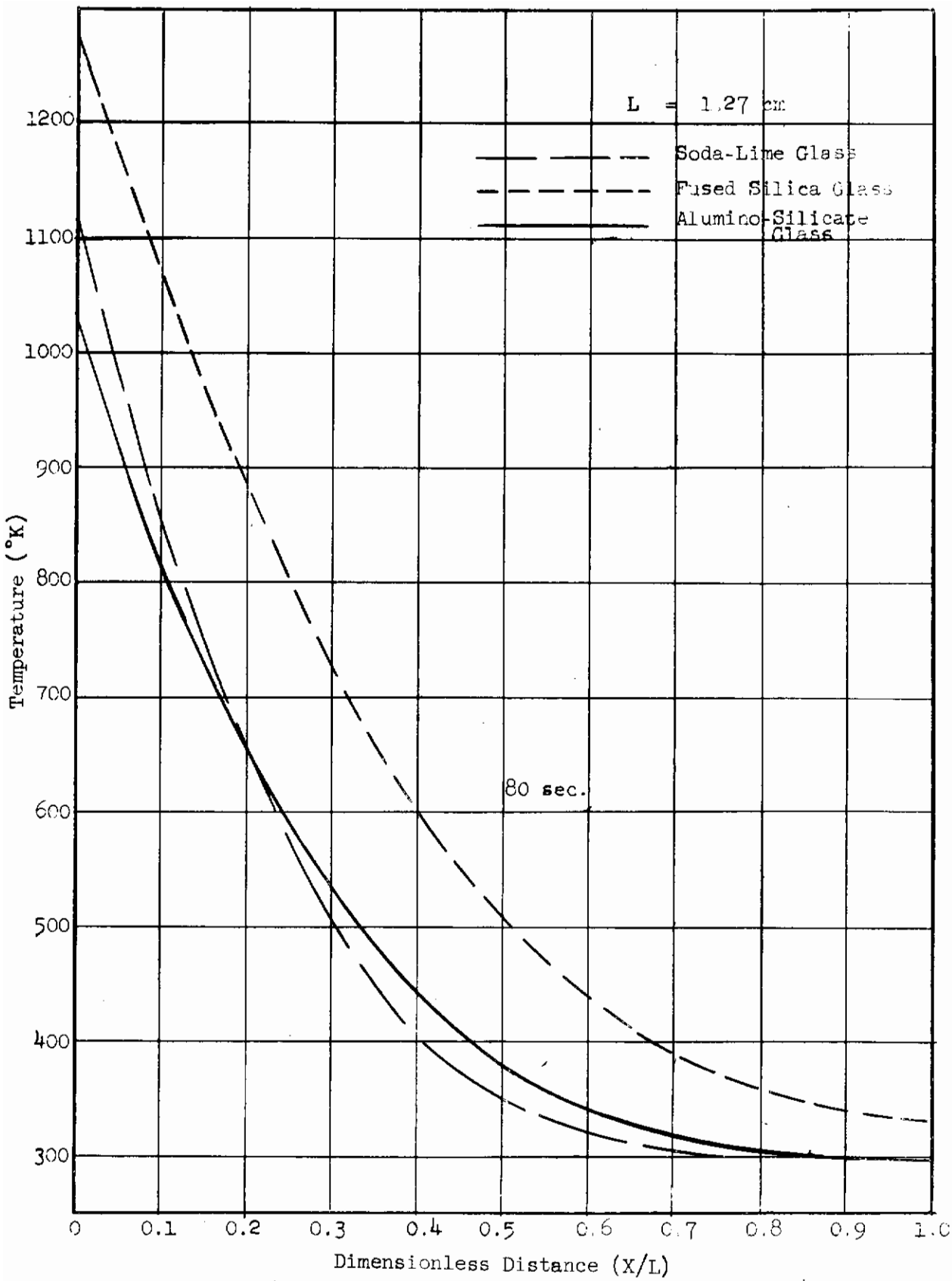

Figure 14 TRANSPARENT TEMPERATURE PROFILES AFTER 80 SECONDS OF HYPERSONIC SKIP-GLIDE TRAJECTORY

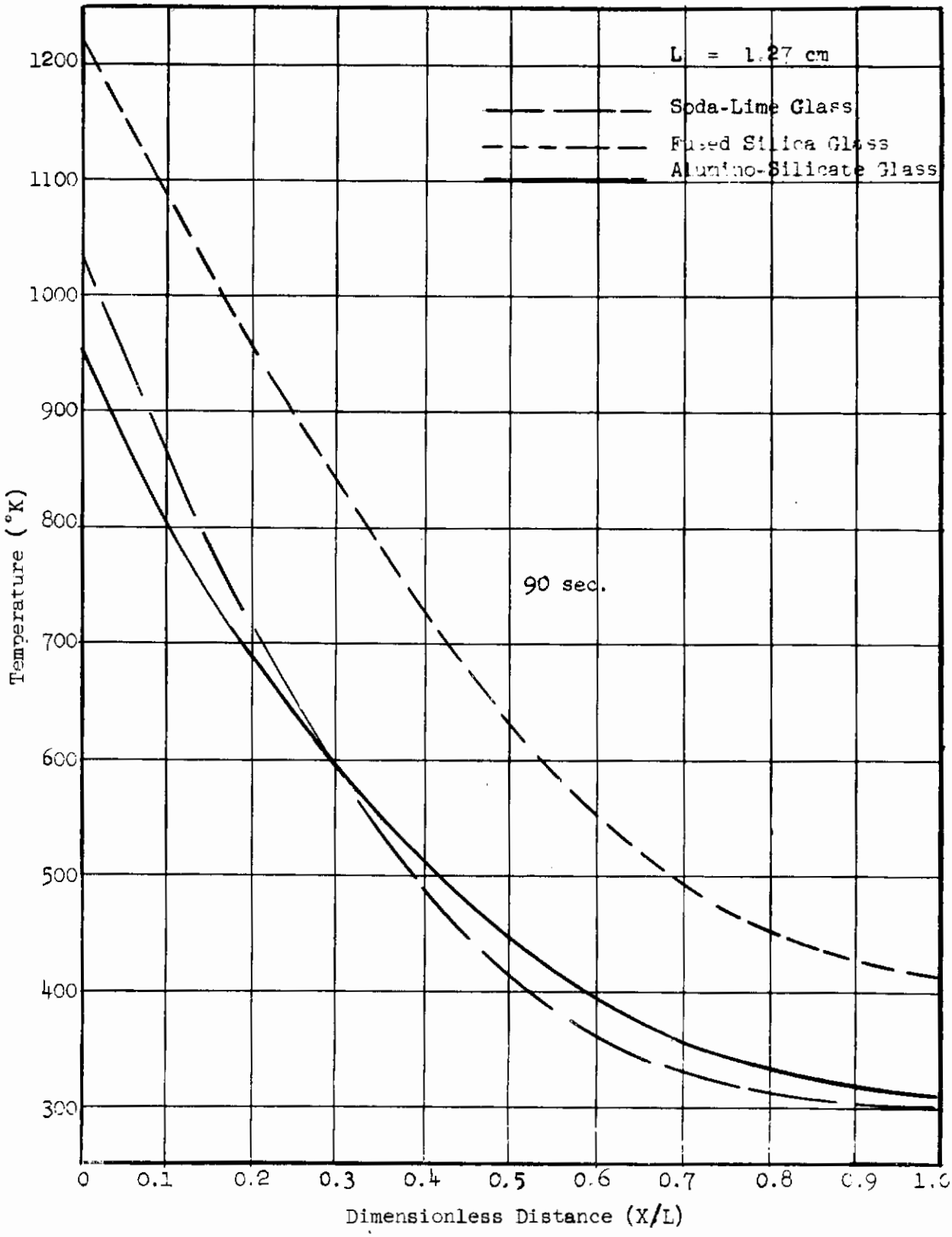

Figure 15 TRANSPARENT TEMPERATURE PROFILES AFTER 90 SECONDS OF HYPERSONIC SKIP-GLIDE TRAJECTORY

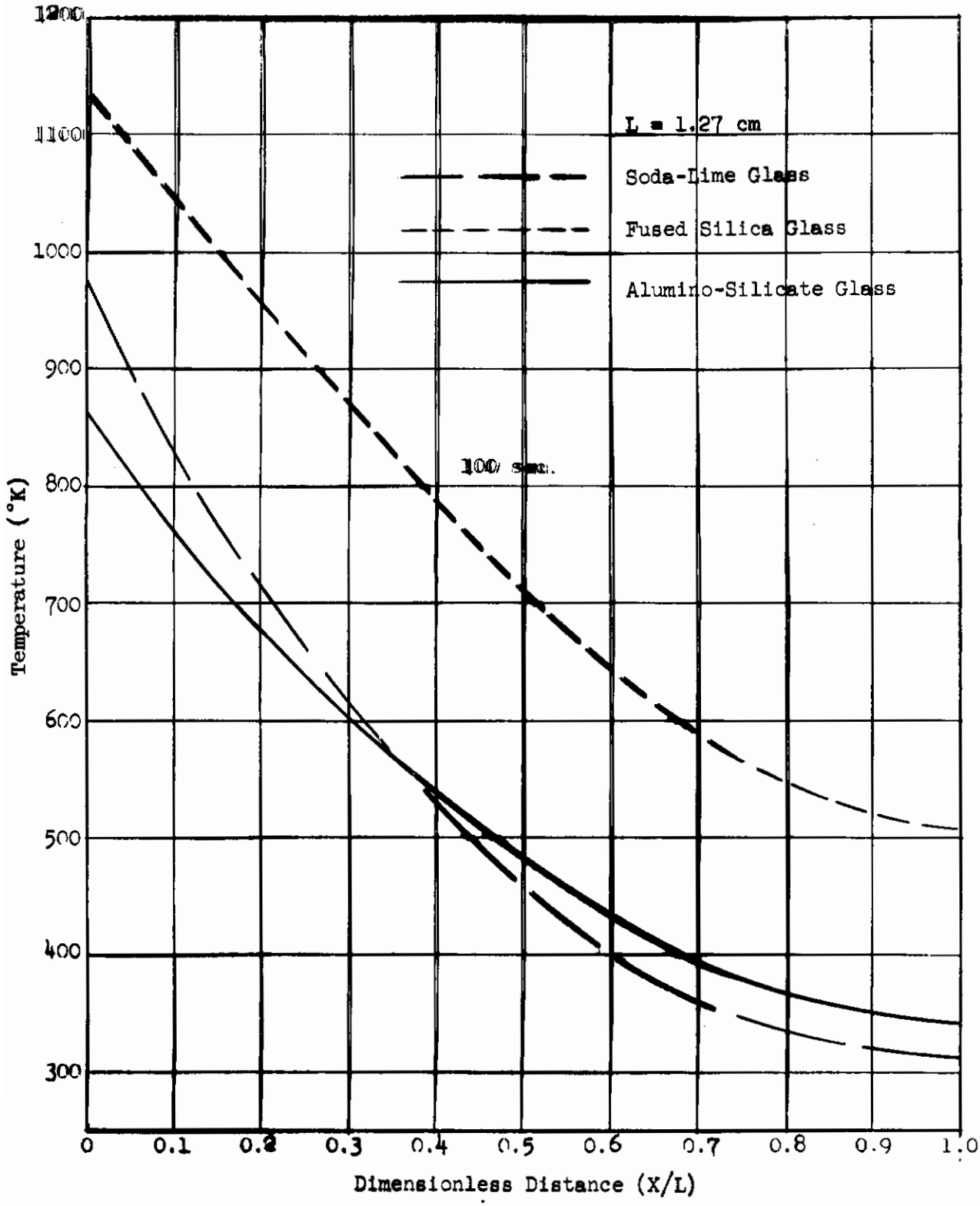

Figure 16 TRANSPARENT TEMPERATURE PROFILES AFTER 100 SECONDS OF HYPERSONIC SKIP-GLIDE TRAJECTORY

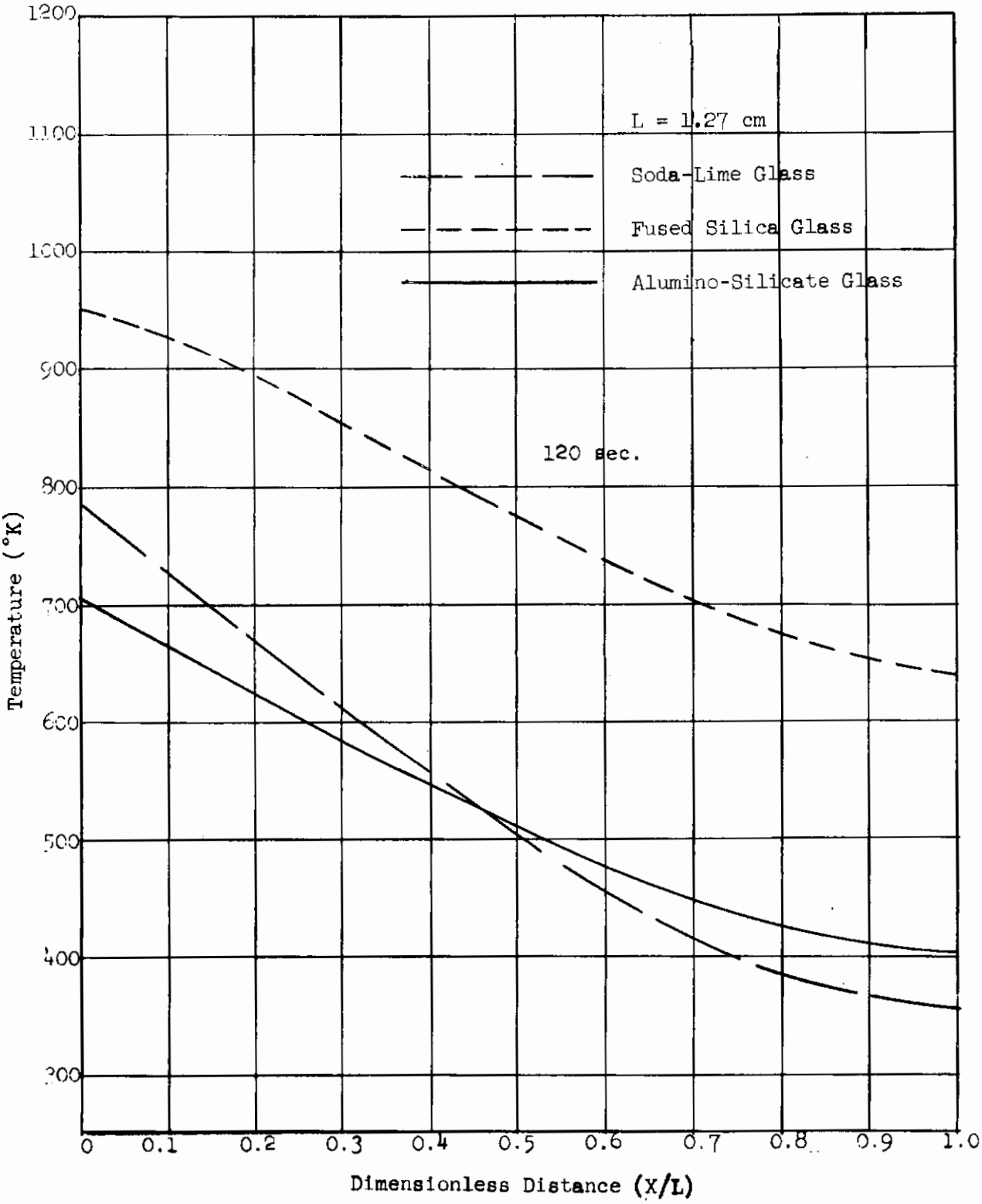

Figure 17 TRANSPARENT TEMPERATURE PROFILES AFTER 120 SECONDS OF HYPERSONIC SKIP-GLIDE TRAJECTORY

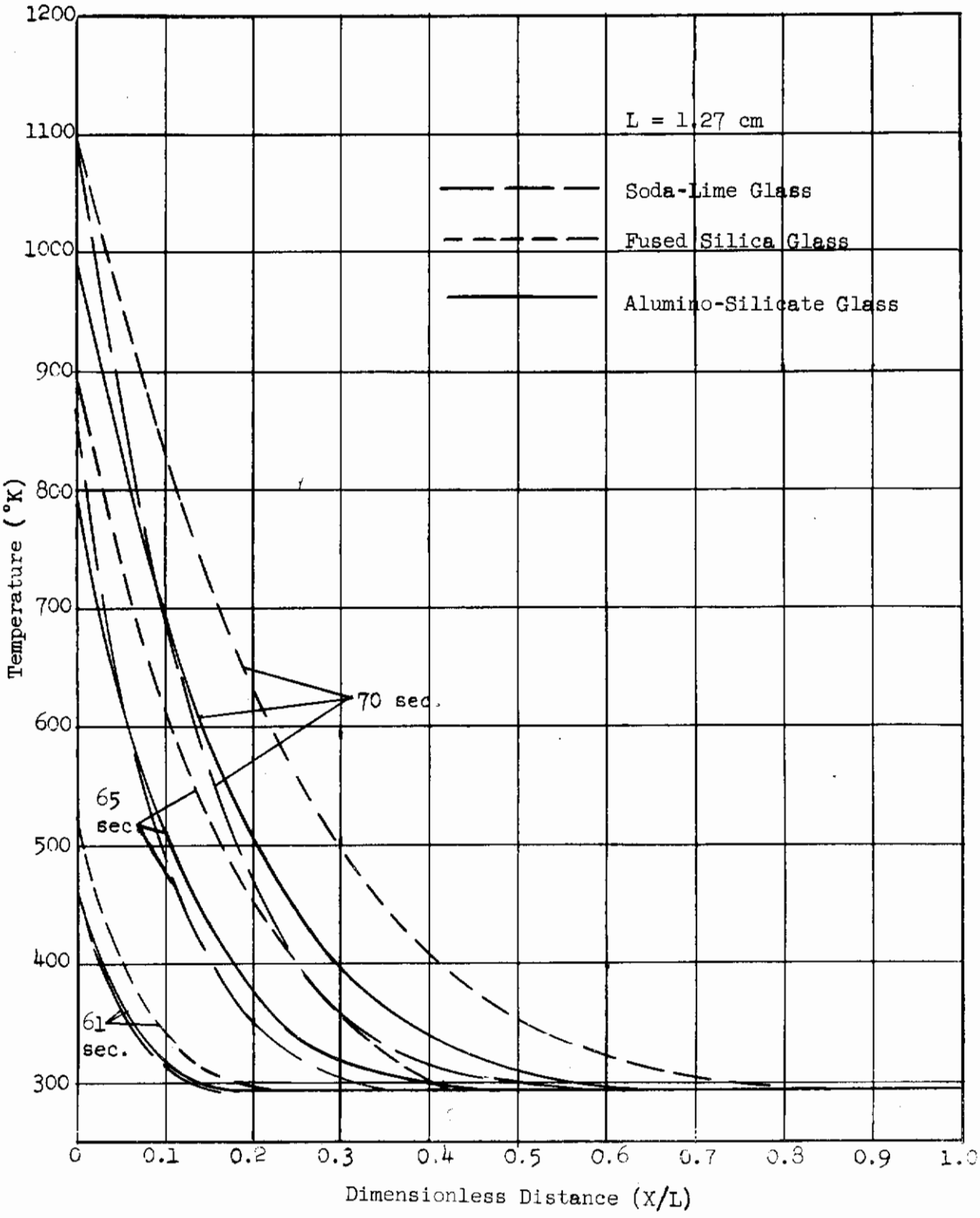

Figure 18 OPAQUE TEMPERATURE PROFILES AT BEGINNING OF HYPERSONIC SKIP-GLIDE TRAJECTORY

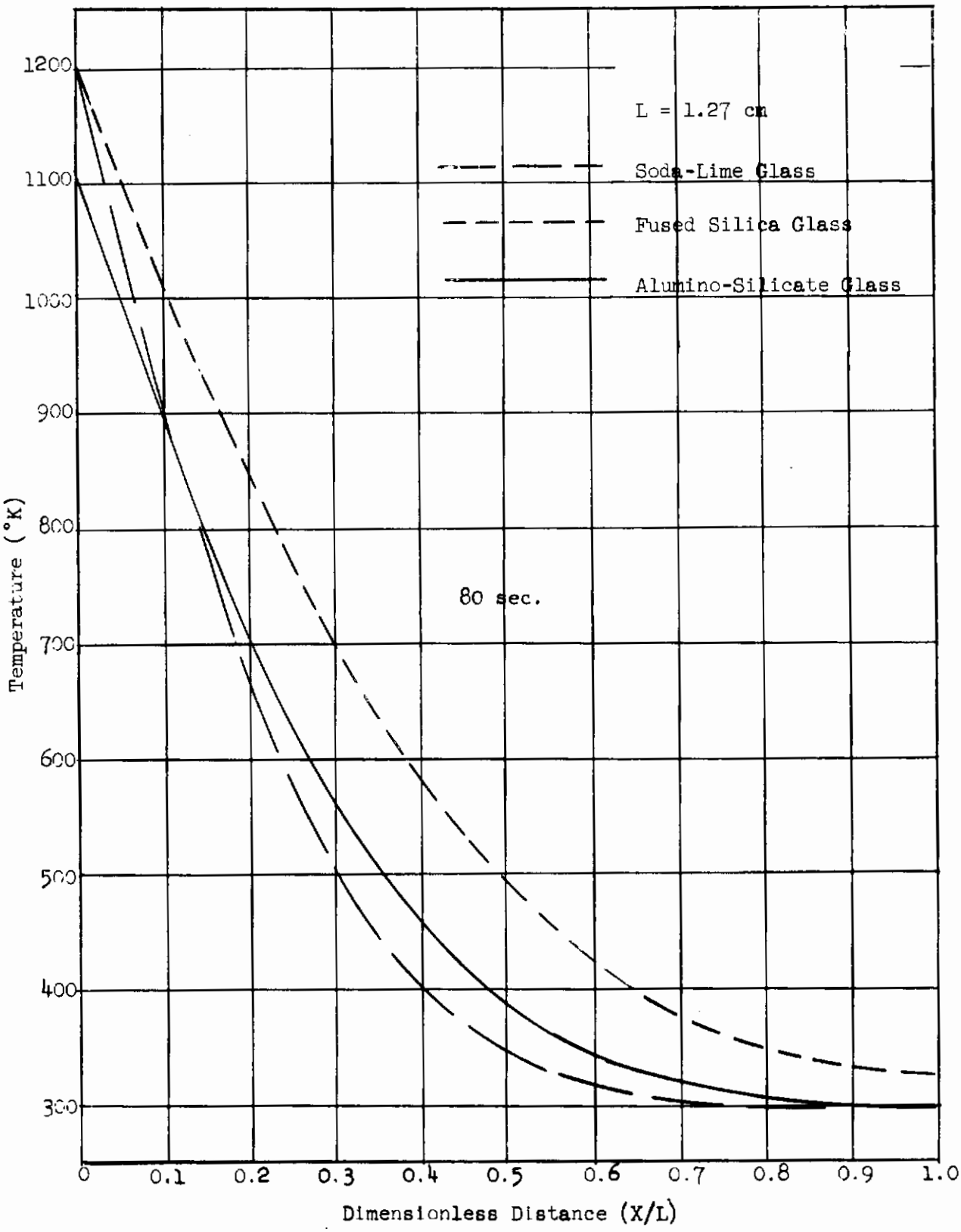

Figure 19 OPAQUE TEMPERATURE PROFILES AFTER 80 SECONDS OF HYPERSONIC SKIP-GLIDE TRAJECTORY

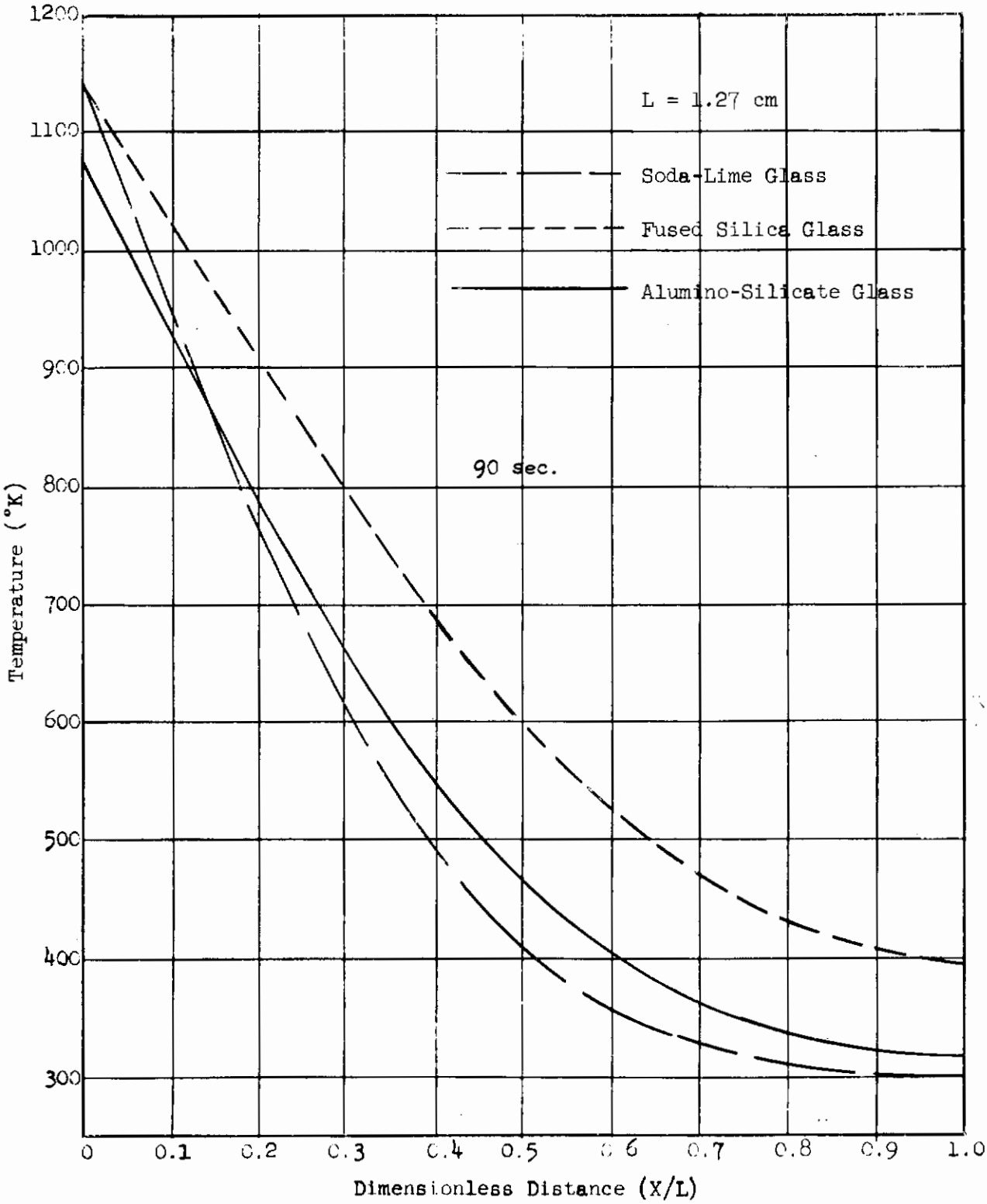

Figure 20 OPAQUE TEMPERATURE PROFILES AFTER 90 SECONDS OF HYPERSONIC SKIP-GLIDE TRAJECTORY

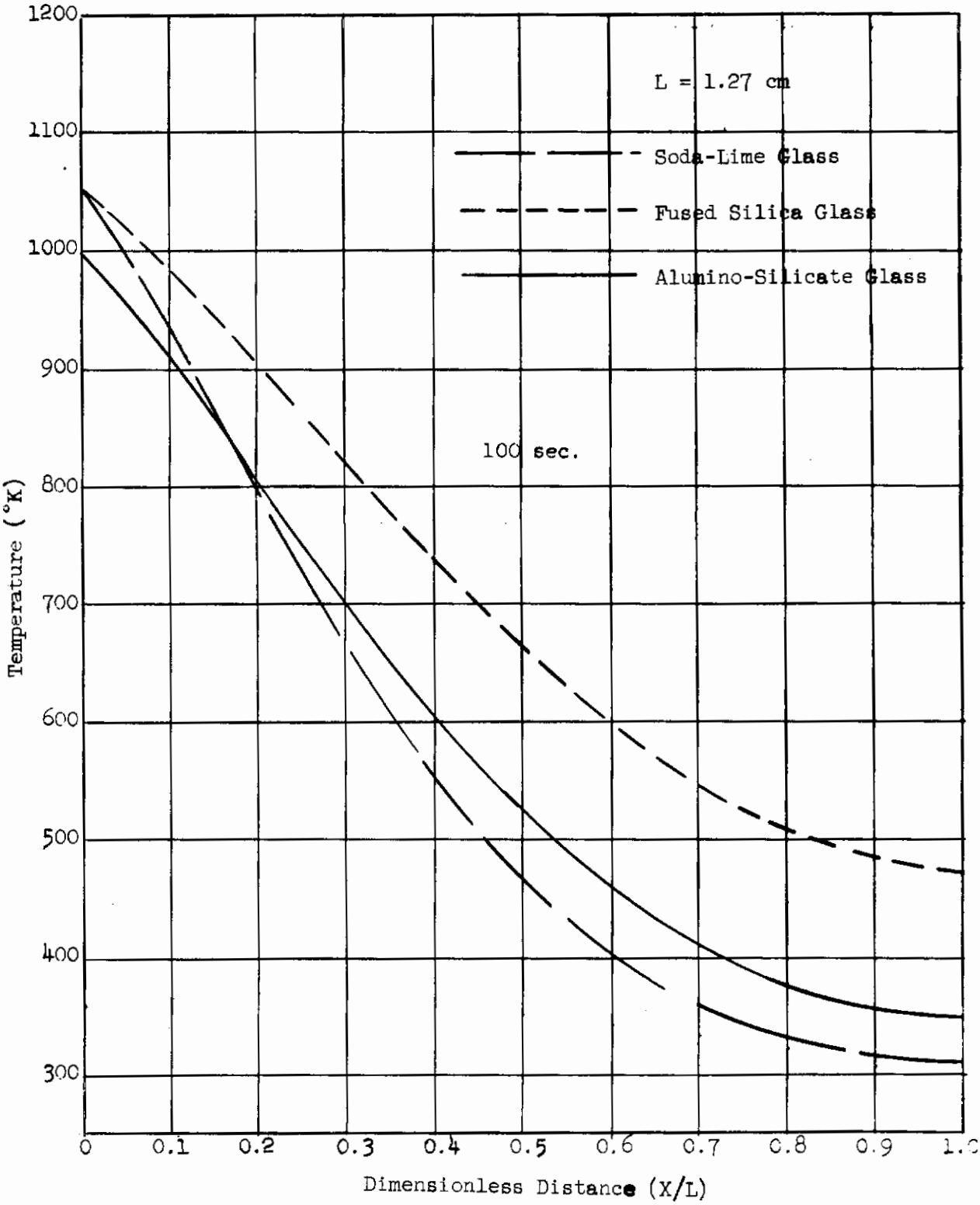

Figure 21 OPAQUE TEMPERATURE PROFILES AFTER 100 SECONDS OF HYPERSONIC SKIP-GLIDE TRAJECTORY

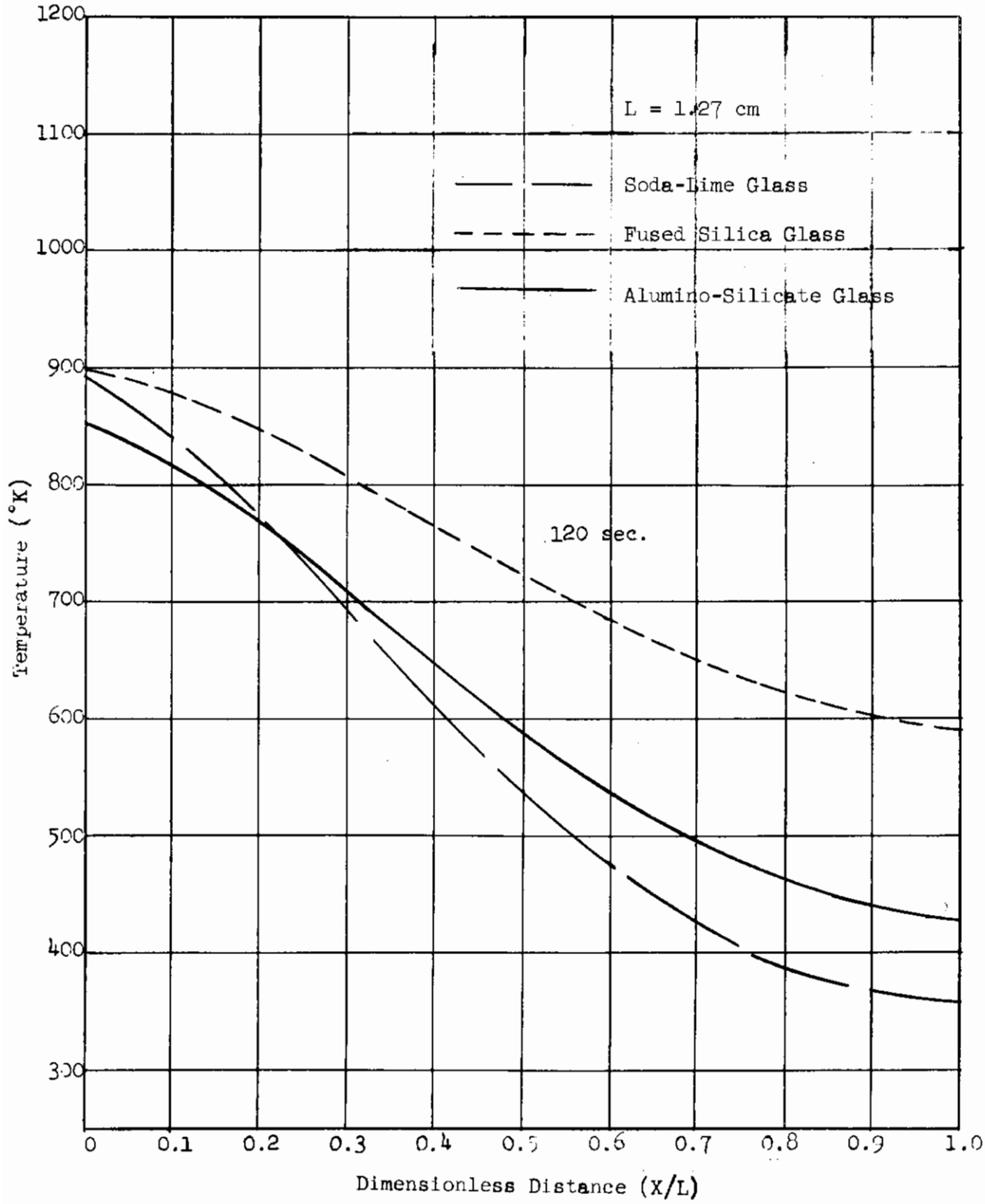

Figure 22 OPAQUE TEMPERATURE PROFILES AFTER 120 SECONDS OF HYPERSONIC SKIP-GLIDE TRAJECTORY

The solution of equation (13) for the exposed surface after 10 seconds of heating yields:

$\theta = 27.2\ F_o$ for fused silica glass

$\theta = 24.6\ F_o$ for alumino-silicate glass

$\theta = 26.1\ F_o$ for soda-lime glass

From these results it may be observed that fused silica would experience the highest temperature excess at the exposed surface followed closely by soda-lime glass and the lowest surface temperature excess would be experienced by the alumino-silicate glass. The temperature excess is a function of thermal conductivity, volumetric specific heat, and the thermal diffusivity as given in equation (13) and the trend of the temperatures are dependent upon all of these thermal properties.

The trends predicted from the illustrative example are the same as computed for the opaque computations shown in Figures 18 to 22. At various times during the trajectory, the fused silica and soda-lime glass have nearly the same surface temperature while alumino-silicate glass exhibits a somewhat lower surface temperature in all cases.

3.3.1.2 Discussion of Transparent Results - With the introduction of the radiative mode of heat transfer the absorption coefficient becomes the material property that greatly influences the window temperatures. The corresponding temperature profiles for the transparent analysis which considers both the radiative and conductive modes show that the relationship between temperature gradients of the three glasses remains the same as observed for the opaque calculations. Fused silica surface temperatures increased while soda-lime and alumino-silicate decreased relative to the opaque calculations.

The spectral absorption coefficient plays a dual role; (1) it affects the attenuation of external and internal radiations, and (2) it affects the self-emission. The absorption is governed by the exponential law:

$$a_\lambda = 1 - e^{-\gamma_\lambda X} \tag{14}$$

where a_λ = fraction of monochromatic energy absorbed

γ_λ = spectral absorption coefficient

X = path traversed.

The spectral rate of internal emission per unit volume at any position X is given by (see Appendix I)

$$Q_{E\lambda}(X) = 4n^2 \gamma_\lambda W_{B\lambda}(X) \tag{15}$$

where $Q_{E\lambda}(X)$ = spectral rate of internal emission at positions X

n = ratio of refractive indices of the emitting medium to the emergent medium

γ_λ = spectral absorption coefficient

$W_{B\lambda}(X)$ = blackbody emissive power at position X

The effects of including radiant interchange in the computations is best studied by considering the temperature profiles of the glasses. The computer results for fused silica and alumino-silicate glasses in hypersonic skip-glide trajectory are used to illustrate the trends. For this purpose consider the time when both of these glasses have nearly equal temperature profiles. These computer results are shown in Table 5 for the transparent and for the opaque model computations.

Since the hypersonic skip-glide trajectory develops its maximum heat flux at approximately 70 seconds, the transparent temperature profile for fused silica at 67.25 seconds and the transparent profile for alumino-silicate at 73.437 seconds occur during a relatively constant heat flux period. The radiant interchange distribution within the glass, as shown in Table 5, may be broken down further to an energy absorbed distribution (from external source and re-absorbed from the interior) and to an energy emitted distribution (as determined by applying equation (15) throughout the material). These separated distributions are shown in Figure 23.

Fused silica and alumino-silicate glass have the same absorption coefficient in the first spectral band, i.e., for all wavelengths up to the first cut-off λ_1 (see Table 3). However, in the second wavelength band, i.e., for wavelengths between the first cut-off wavelength, λ_1, and the second cut-off wavelength, λ_2, the absorption coefficient of fused silica is much less than it is for alumino silicate. It is seen that more long wavelength radiation is permitted to reach all points in the fused silica (low γ_λ) relatively undisturbed (low attenuation). Conversely, in alumino-silicate glass, long wavelength radiations are absorbed much more readily and greatly attenuated within relatively short distances. Thus the radiations are more uniformly distributed in fused silica than they are in alumino-silicate. Near the exposed surface more radiation is absorbed by both materials than at the interior due to attenuation of an external radiating source. Alumino-silicate glass absorbs the external energy more readily than does fused silica but the available radiation decreases more rapidly through the material.

Self-emission at the long wavelength associated with the relatively low glass temperature is greatest for the alumino-silicate glass. At the exposed surface and within the alumino-silicate glass the self-emission always remains significantly large compared to the absorption (as is shown in Figure 23). This is not true of fused silica where self-emission (which occurs primarily at long wavelengths) soon becomes negligible compared to the absorption. Thus, alumino-silicate absorbs more but also emits much more than does the fused silica. The fused silica absorbs less but tends to retain what it has absorbed. Thus, fused silica distributes both the radiant energies and the conducted energies more readily than does the alumino-silicate and therefore attains a higher temperature level, whereas the alumino-silicate glass develops a lower temperature level.

3.3.1.3 Comparison of Opaque and Transparent Results - Gardon (Reference 6) computed temperature profiles for opaque and transparent soda-lime glass and observed that the transparent profile was below that of the opaque profile. A comparison of the thermal and optical properties show soda-lime has the lowest diffusivity of the three materials and thus should (and does) have the steepest temperature profile of the three glasses when treated as opaque materials. The temperature excess computation (equation 13) for

TABLE 5

TEMPERATURE PROFILES AND RADIATIVE INTERCHANGE FACTORS

	Fused Silica			Alumino-Silicate		
	Transparent (@ 67.250 sec)		Opaque (@ 67.5 sec)	Transparent (@ 73.437 sec)		Opaque (@ 73.437 sec)
	Temp. (°K)	Σ q (watt/cm^3)	Temp. (°K)	Temp. (°K)	Σ q (watt/cm^3)	Temp. (°K)
Station Frnt.Face						
1	1018.504	-7.513	1013.893	1018.569	-98.487	1063.859
2	734.162	-0.428	738.809	757.321	-20.013	790.031
3	541.195	0.391	547.638	573.529	- 2.326	587.366
4	422.214	0.431	427.518	449.876	1.375	453.786
5	355.473	0.402	358.889	373.659	0.672	374.311
6	321.237	0.370	323.016	331.343	0.260	331.203
7	305.056	0.344	305.736	309.924	0.121	309.703
8	297.930	0.324	297.986	299.887	0.043	299.747
9	294.931	0.310	394.685	295.464	0.015	295.396
10	293.644	0.302	293.291	293.585	0.009	293.552
11 Back Face	293.023	0.149	292.694	292.884	0.017	292.815

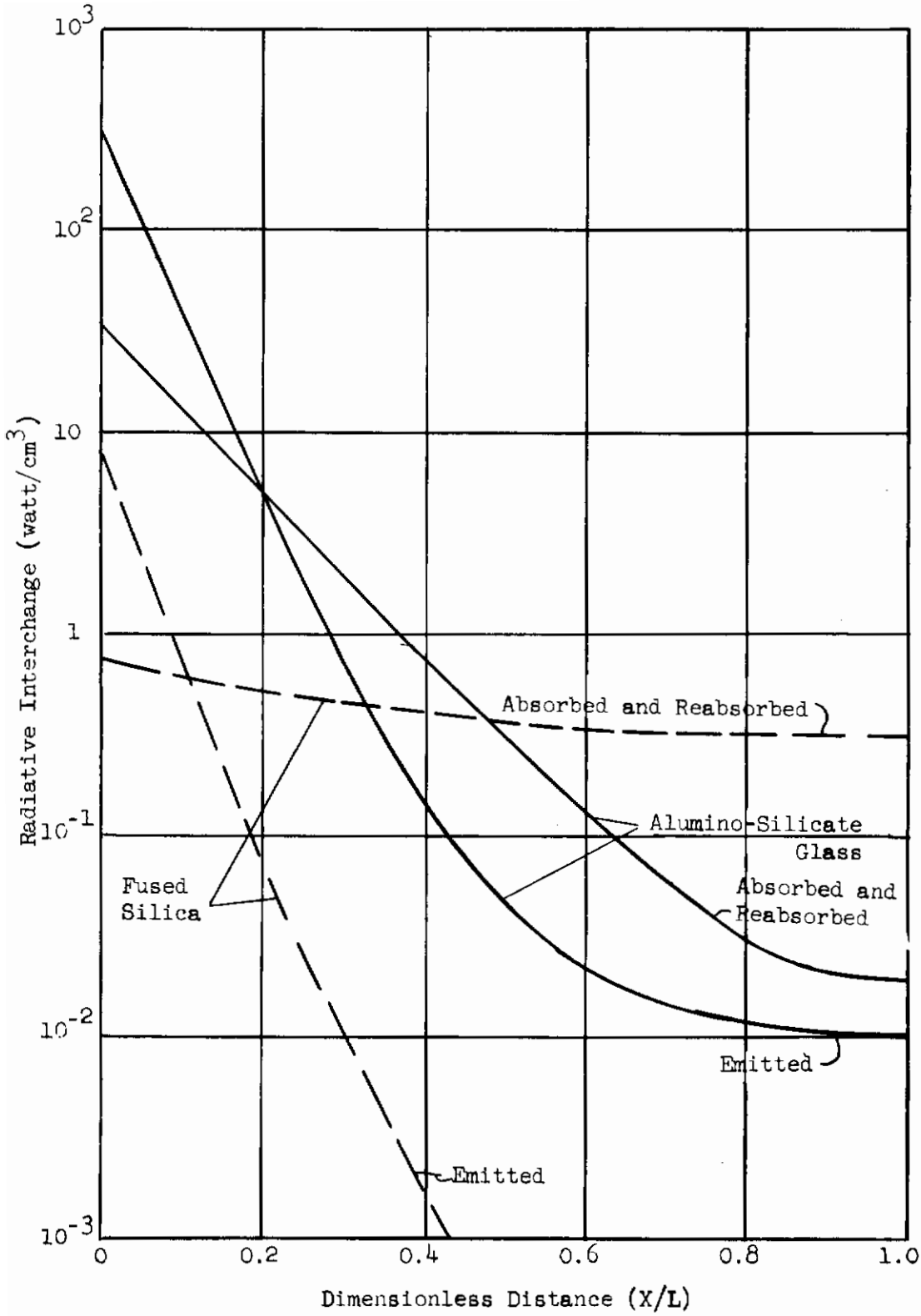

Figure 23 RADIATIVE INTERCHANGE DISTRIBUTIONS OF HYPERSONIC SKIP-GLIDE TRAJECTORY

constant heat flux shows that fused silica and soda-lime should have approximately the same surface temperature for the opaque calculation. This has been observed in the results of the single-glaze computer program. The absorption coefficient of soda-lime is similar to alumino-silicate and therefore soda-lime develops a transparent temperature profile below that of its opaque profile. Thus, the trend of alumino silicate glass agrees with Gardon's results for soda-lime glass due to the similarity of optical properties.

The significance of the transparent analysis is further illustrated by Figures 24 to 26. The surface temperature rise is overestimated by 20% (alumino-silicate glass surface temperature at 120 sec) if it is computed on an opaque (Fourier) analysis.

Both the transparent and opaque calculations show that the maximum surface temperature occurs at 80 seconds, that is,10 seconds after the maximum convective heating rate occurred. Therefore,it may be concluded that up to about 80 seconds the heat transfer within the glass increase as the glass becomes hotter and at 80 seconds the glass heat transfer rate near its exposed surface exceeds the net rate at which the window surface was heated.

The domain of the partially transparent heat transfer analysis lies between two prescribed limits. When the material considered has no transparency it is opaque and is treated in terms of pure conductive heat transfer. On the other hand, when the material is perfectly transparent, radiant interchange does not effect the heat transfer within the material and again the material is treated in terms of pure conductive heat transfer. All semi-transparent materials fall between these limits. Fused silica is easily distinguished from the other glasses considered in that it approaches almost perfect transparency. Consequently, the radiant interchange terms computed for fused silica are always much lower than those computed for alumino-silicate and soda-lime glasses. The effects of computational accuracy of numerical integration leading to the radiant interchange term becomes most pronounced for fused silica. It is the radiant interchange term alone that makes the temperature profile in the transparent analysis different from the temperature profile in the opaque analysis. The temperatures near the surface computed from conduction and radiation effects should be lower than corresponding temperatures computed from conduction effects alone. Therefore, the transparent profiles for fused silica are in error to the extent that they exceed the opaque profiles as shown in Figure 25 at positions near the exposed surface.

3.3.2 Additional Hypersonic Runs by RTD

Personnel at RTD made several runs using the single-glaze computer program. The trajectory for one of the runs is given in Figure 27. The results of this run (see Figures 28 to 30) were forwarded to MRD for comment since the transparent computations for fused silica showed slightly higher temperatures than the opaque computations while alumino-silicate glass showed the opposite effects. These results have, in general, been the same as previously discussed in Section 3.3.1.3.

3.3.3 Supersonic Transport Trajectory

The temperature predicted for single-glaze windows exposed to the supersonic transport trajectory (discussed in Section 2.2.2) are given in Figures

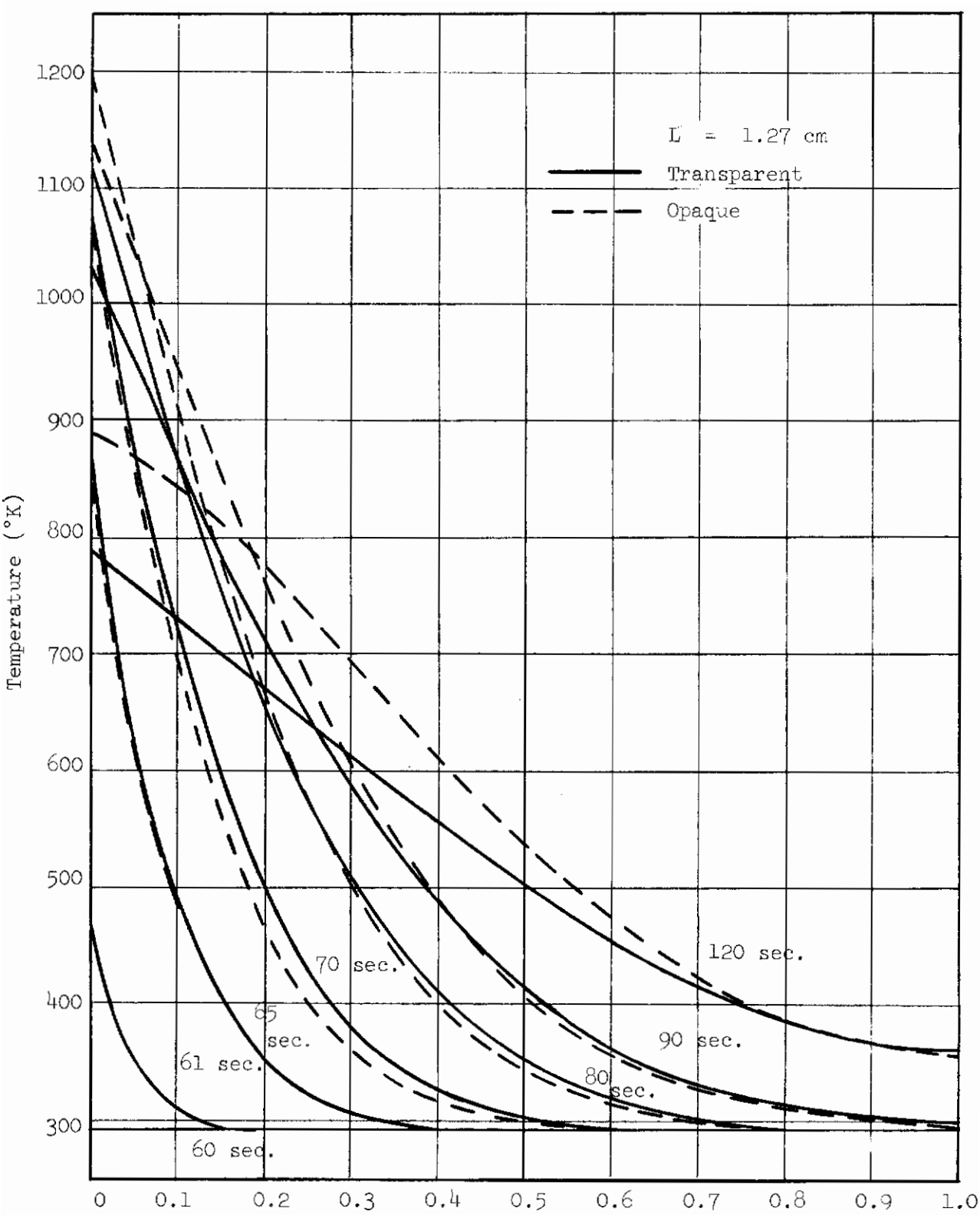

Figure 24 COMPARISON OF TEMPERATURE PROFILES OF HYPERSONIC TRAJECTORY FOR SODA-LIME GLASS

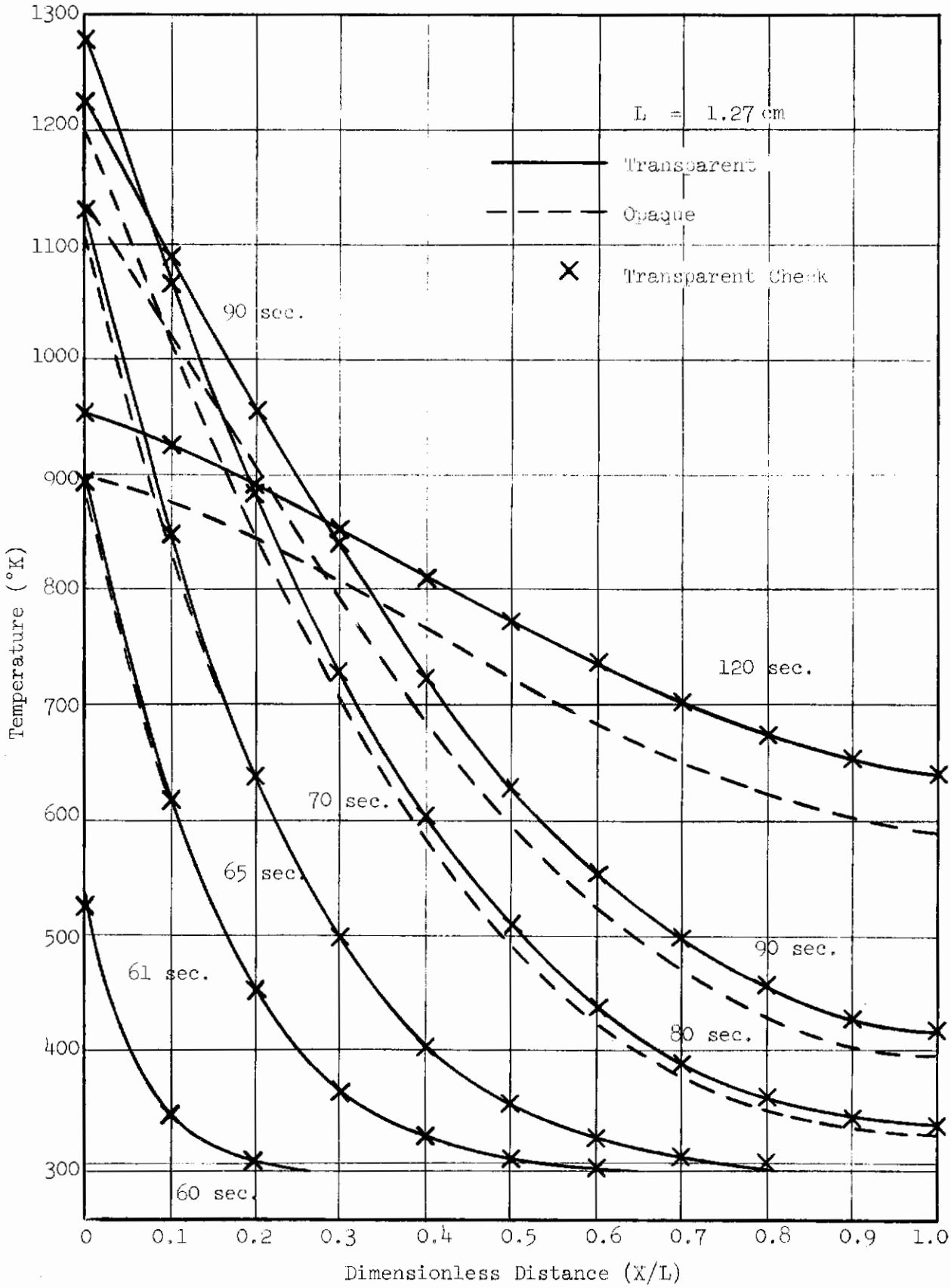

Figure 25 COMPARISON OF TEMPERATURE PROFILES OF HYPERSONIC SKIP-GLIDE TRAJECTORY FOR FUSED SILICA GLASS

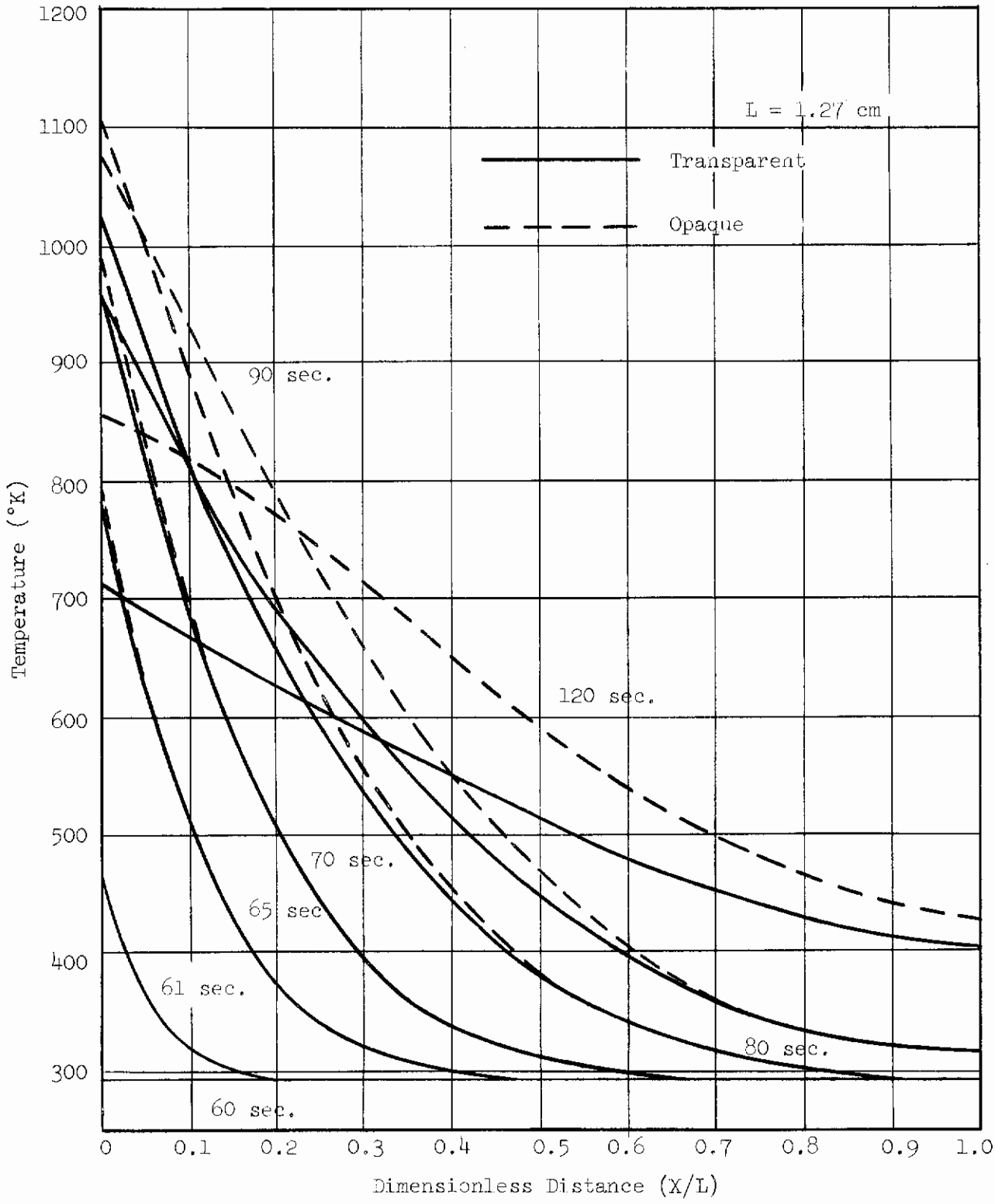

Figure 26 COMPARISON OF TEMPERATURE PROFILES OF HYPERSONIC SKIP-GLIDE TRAJECTORY FOR ALUMINO-SILICATE GLASS

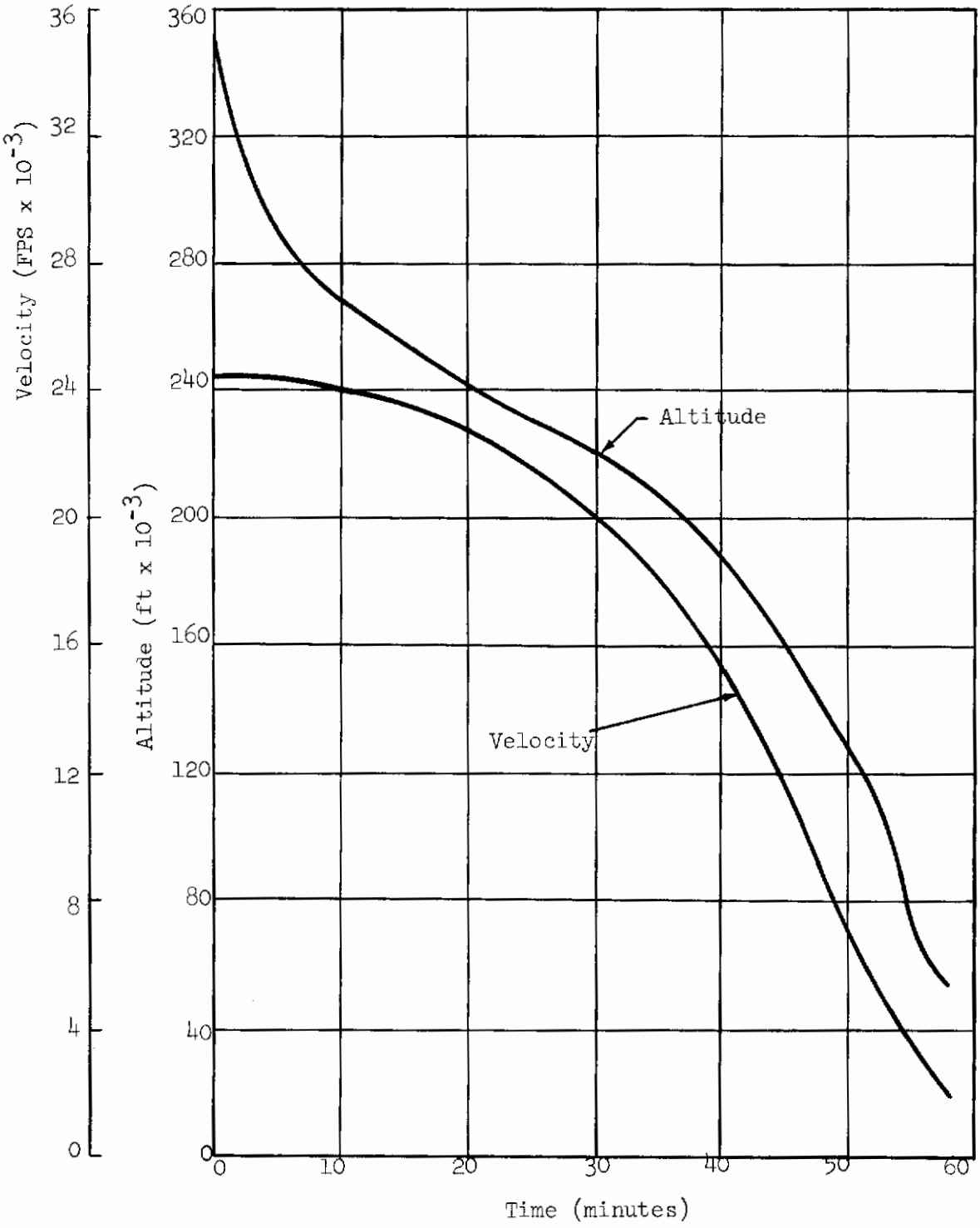

Figure 27 RTD FLIGHT PLAN,
HYPERSONIC SKIP-GLIDE

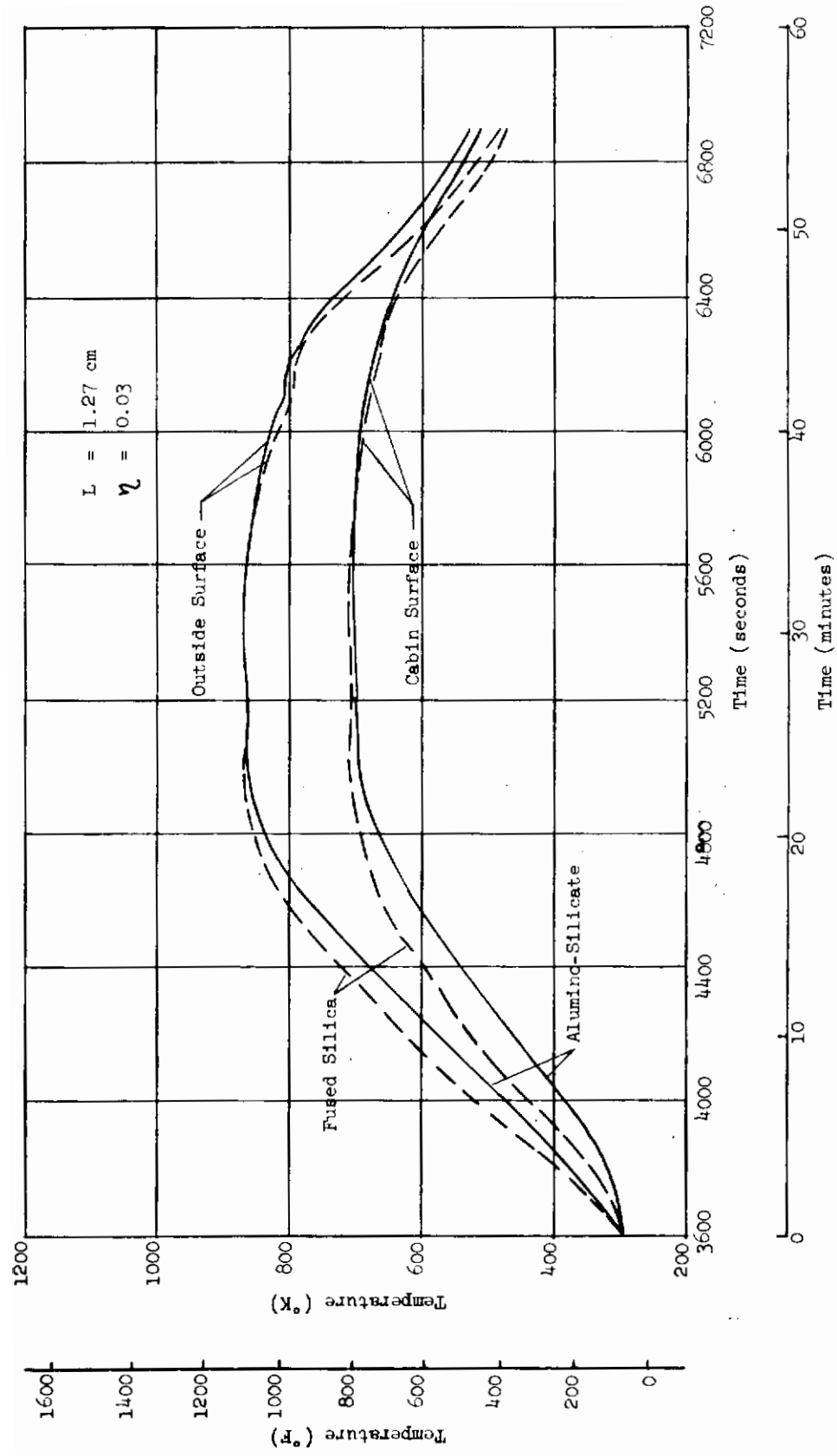

Figure 28 OPAQUE SURFACE TEMPERATURES FOR RTD TRAJECOTRY, HYPERSONIC SKIP-GLIDE

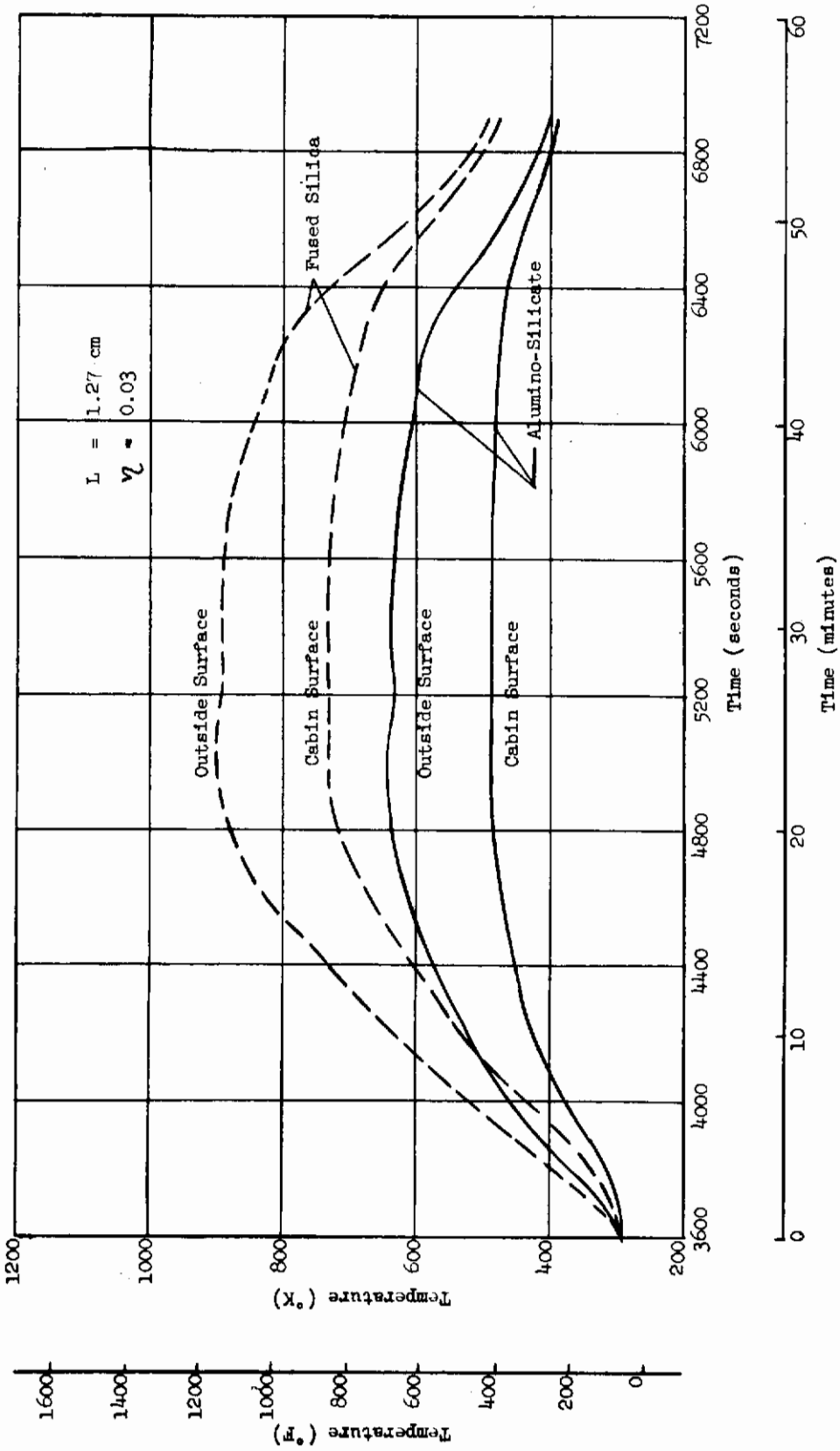

Figure 29 TRANSPARENT SURFACE TEMPERATURES FOR RTD TRAJECTORY, HYPERSONIC SKIP-GLIDE

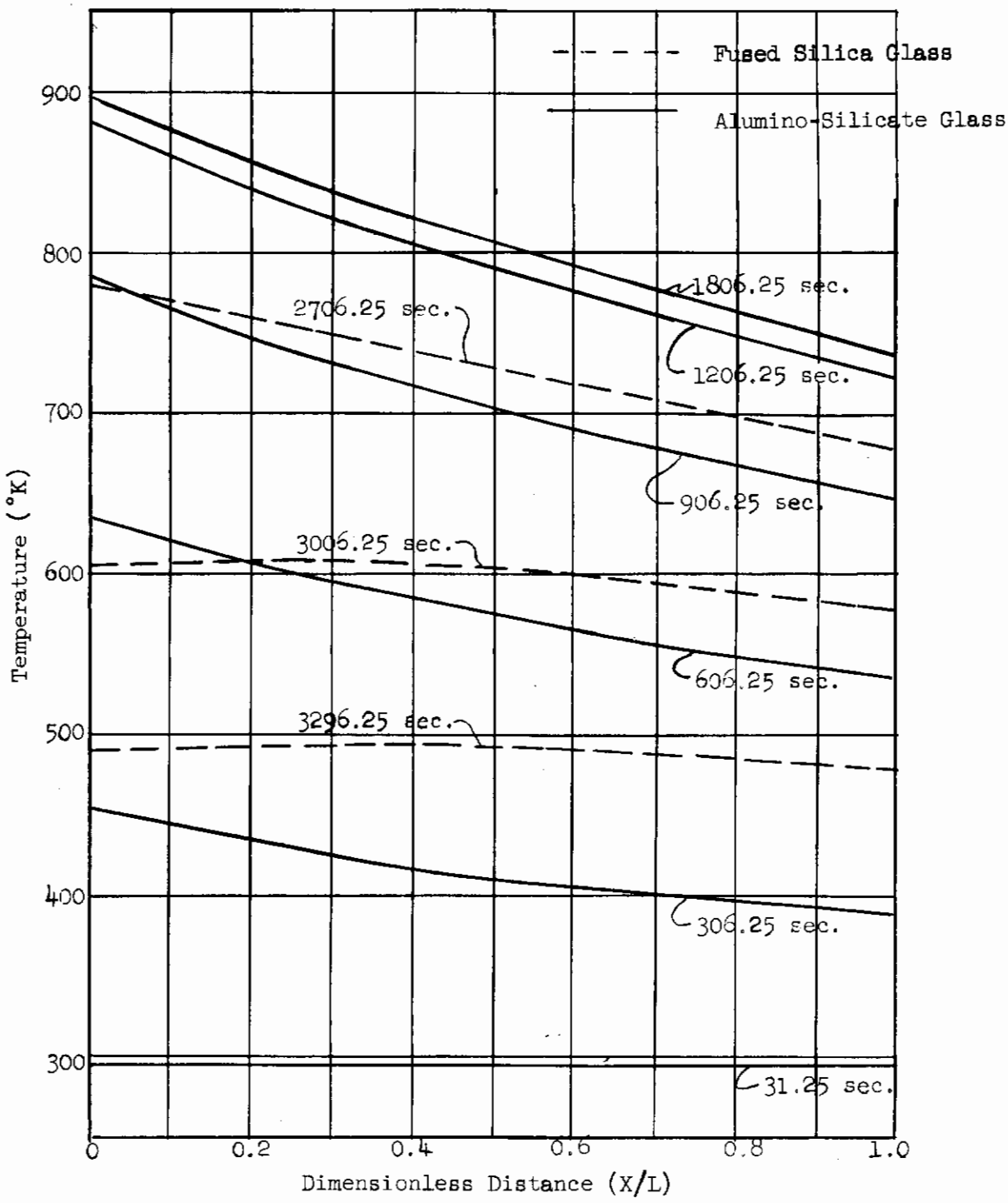

Figure 30 TRANSPARENT TEMPERATURE PROFILES DURING RTD TRAJECTORY, HYPERSONIC SKIP-GLIDE

31 to 44. As may be seen, the initial phase of the trajectory cools the window. In the heating phase, the temperatures rise sharply and remain relatively stable during the cruising phase of the trajectory. During descent the temperatures drop sharply and rise again during final leveling off.

The differences in the heating rates of the three materials considered is the same as previously discussed for hypersonic skip-glide, i.e., fused silica developed the highest temperature followed by soda-lime and alumino-silicate which developed the lowest temperatures. Fused silica temperatures predicted neglecting radiation show negligible variations from those including radiation. This is not true for the alumino-silicate and soda-lime glasses where significant differences occur in the temperatures predicted without considering radiation. The magnitude of the difference is much less than the differences noted for the hypersonic skip-glide calculations. The closer agreement between opaque and transparent calculations for supersonic calculations is due primarily to the lower temperatures developed. At lower temperatures the radiative mechanism is less capable of distributing the energy within the window. Thus, for example, from an initial temperature of 293°K the maximum front face temperature is 453°K based upon the opaque model and only 427°K based upon the transparent model.

3.3.4 Circular Earth Orbit

The temperature profiles that will develop in windows exposed to direct sunlight in an earth orbit are given in Figure 45. Two materials considered were soda-lime glass and Plexiglas. These calculations tend to show that solar radiative input, in direct sunlight does not impose stringent thermal conditions upon the window during orbit.

3.4 Results for Single-Glaze Window With Films

3.4.1 Interference Effect of Thin Transparent Films

In the development of the analysis for a coated glass certain extensions are necessary to account for the effects of the film. Since the film thickness is of the order of one wavelength or less in the visible spectrum, the film will produce interreflections which can affect the glass substrate temperature and its emission into the cabin.

Interference implies the existence of coherent radiant beams. For example, a point source external to the coated glass shown in Figure 46 will emit diffusely in all directions. A fan of beams enveloped between the two limits illustrated will interreflect within the film and arrive at the volume element δV non-collinearly. Since each of the beams emanated from one and the same source they are coherent having a constant relative phase difference due to their respective optical paths. The superposition of these beams at their point of culmination, δV, will produce varying degrees of constructive or destructive interference thereby affecting the intensity sensed at the elemental volume.

Consider a beam made up of a number of rays, parallel to each other and incident upon the filmed surface of the glass (Figure 47). A group of parallel rays incident upon the film surface interreflect within the film, superimpose, and refract into the glass. The reflection from the back face of the glass

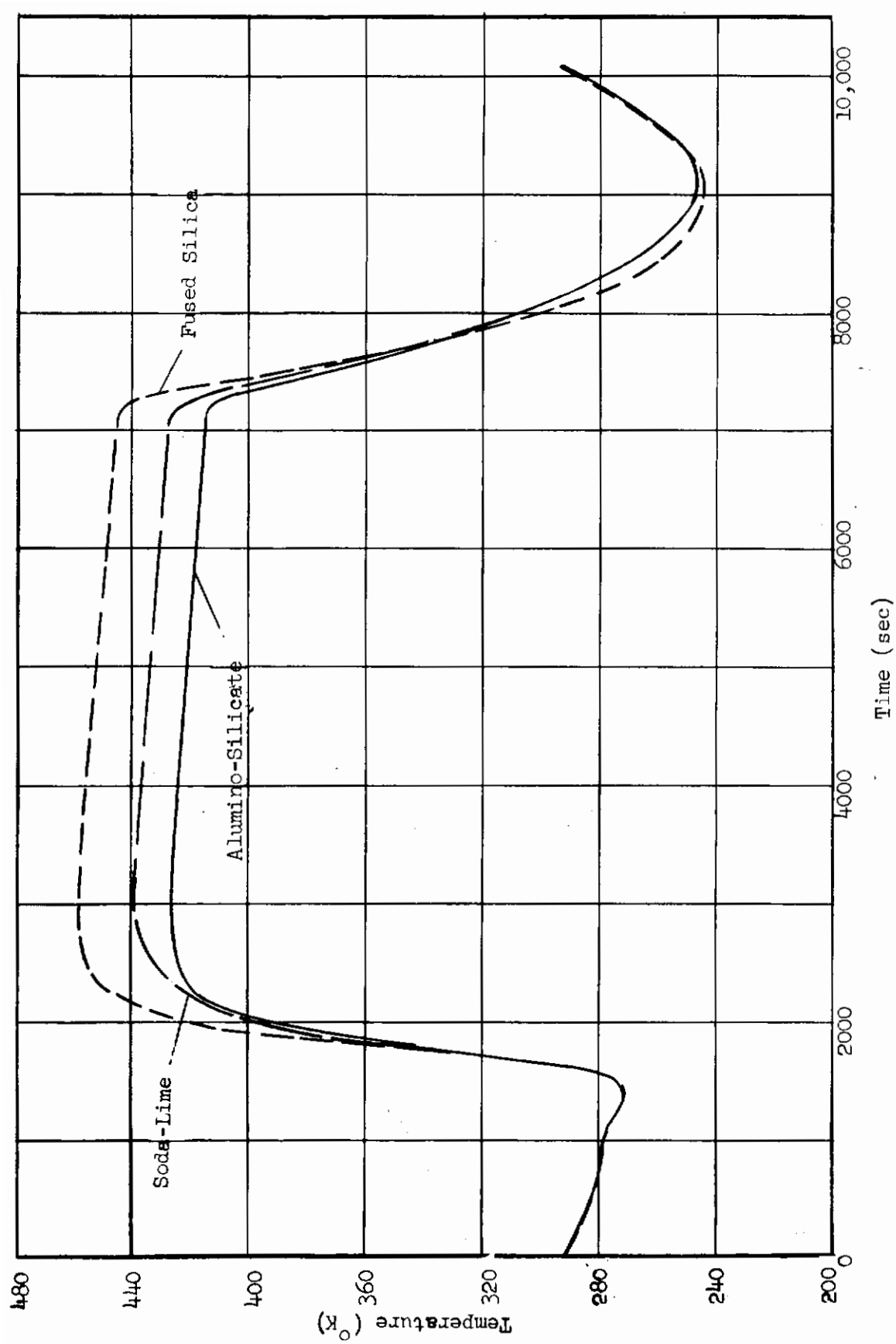

Figure 31 TRANSPARENT FRONT SURFACE TEMPERATURES FOR SUPERSONIC TRANSPORT TRAJECTORY

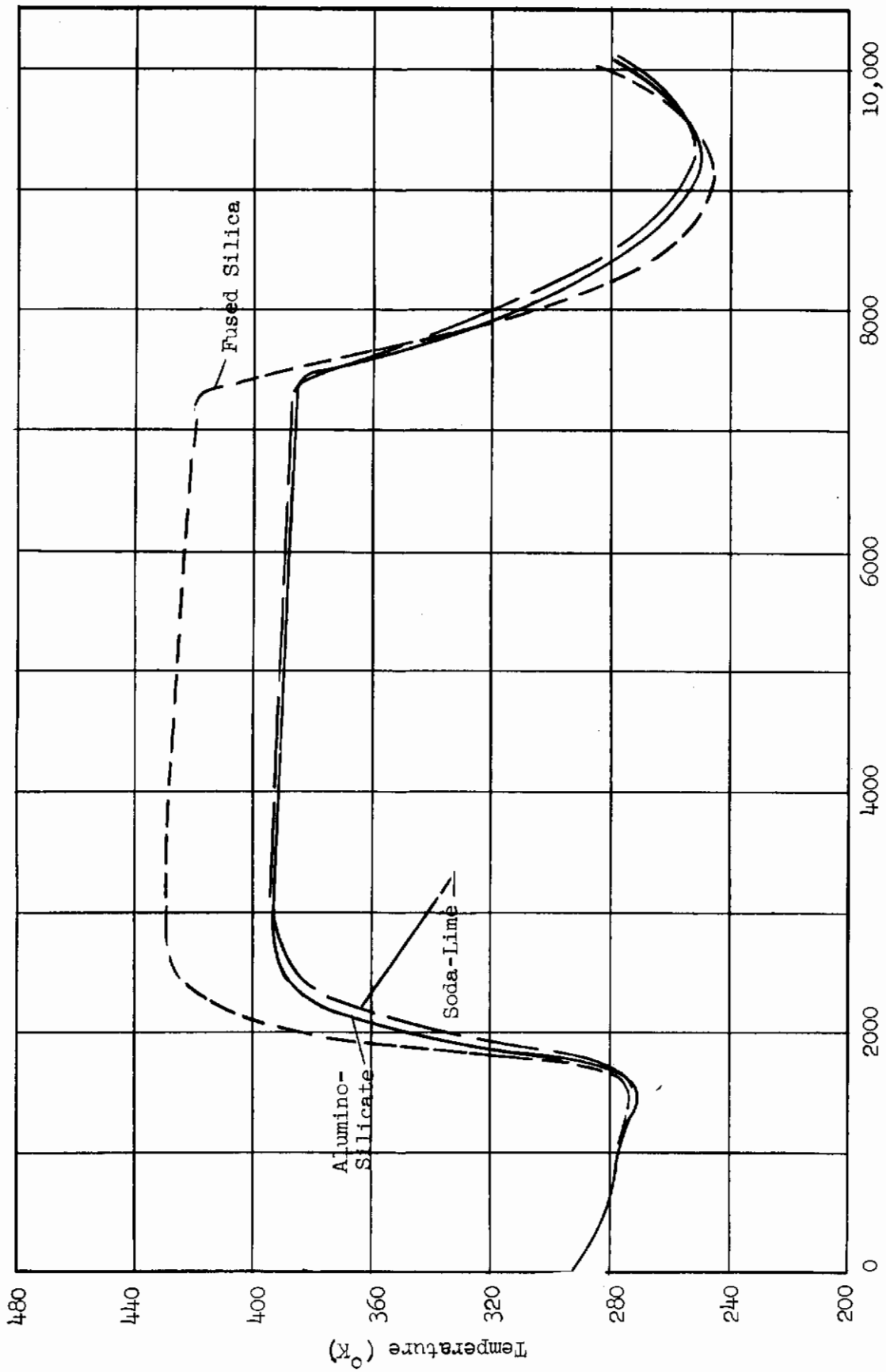

Figure 32 TRANSPARENT BACK SURFACE TEMPERATURES FOR SUPERSONIC TRANSPORT TRAJECTORY

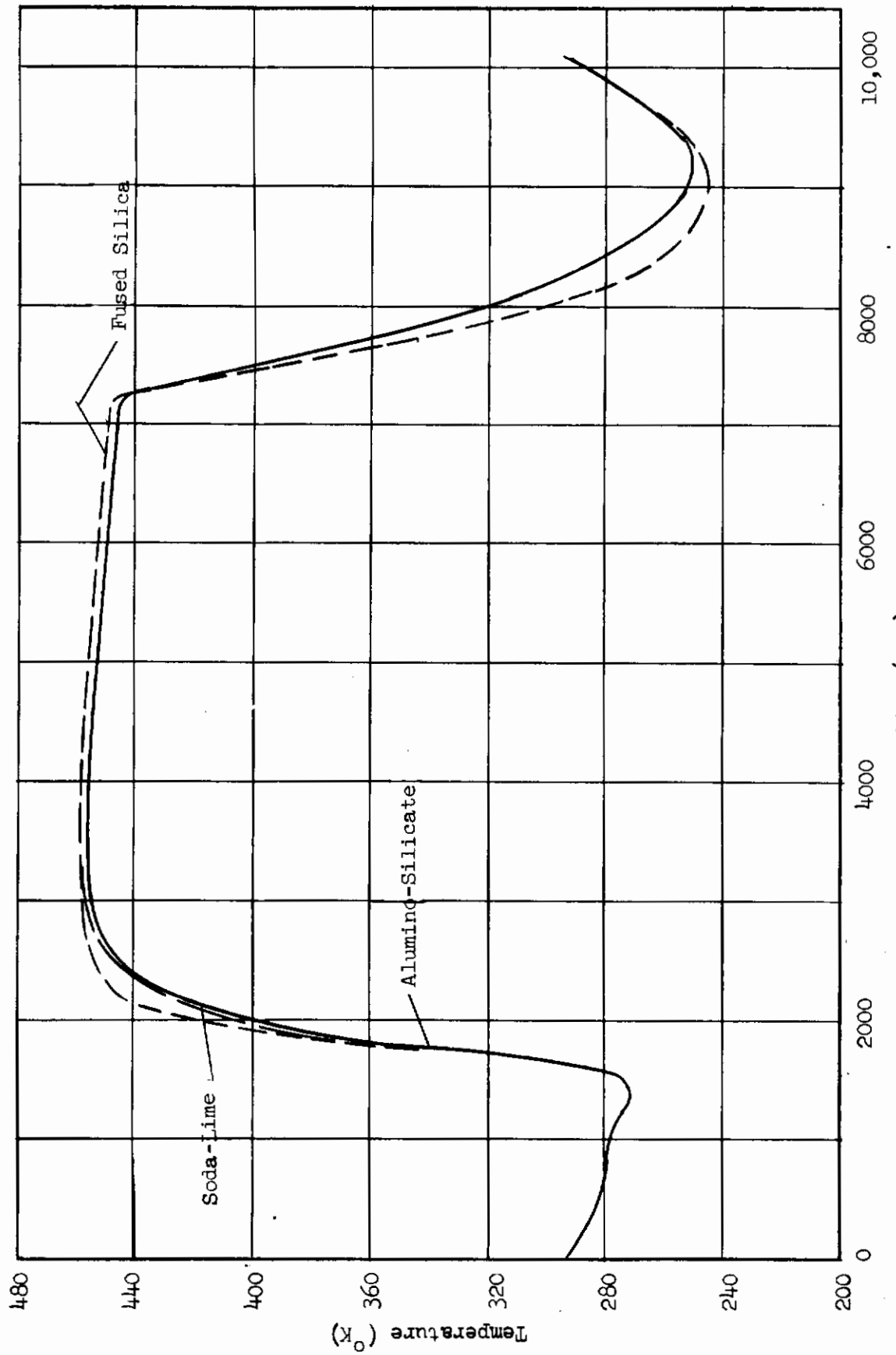

Figure 33 OPAQUE FRONT SURFACE TEMPERATURES FOR SUPERSONIC TRANSPORT TRAJECTORY

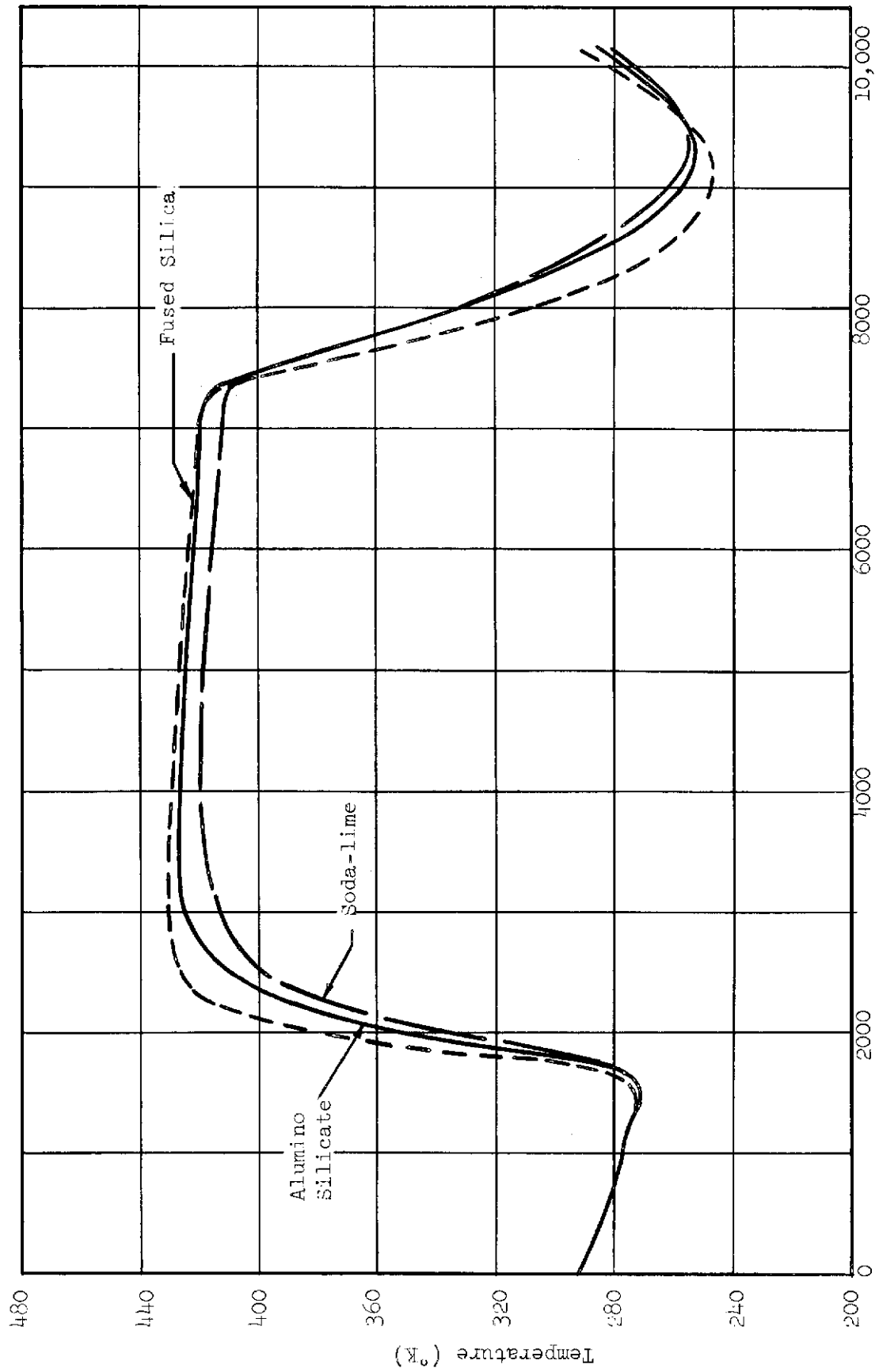

Figure 34 OPAQUE BACK SURFACE TEMPERATURES FOR SUPERSONIC TRANSPORT TRAJECTORY

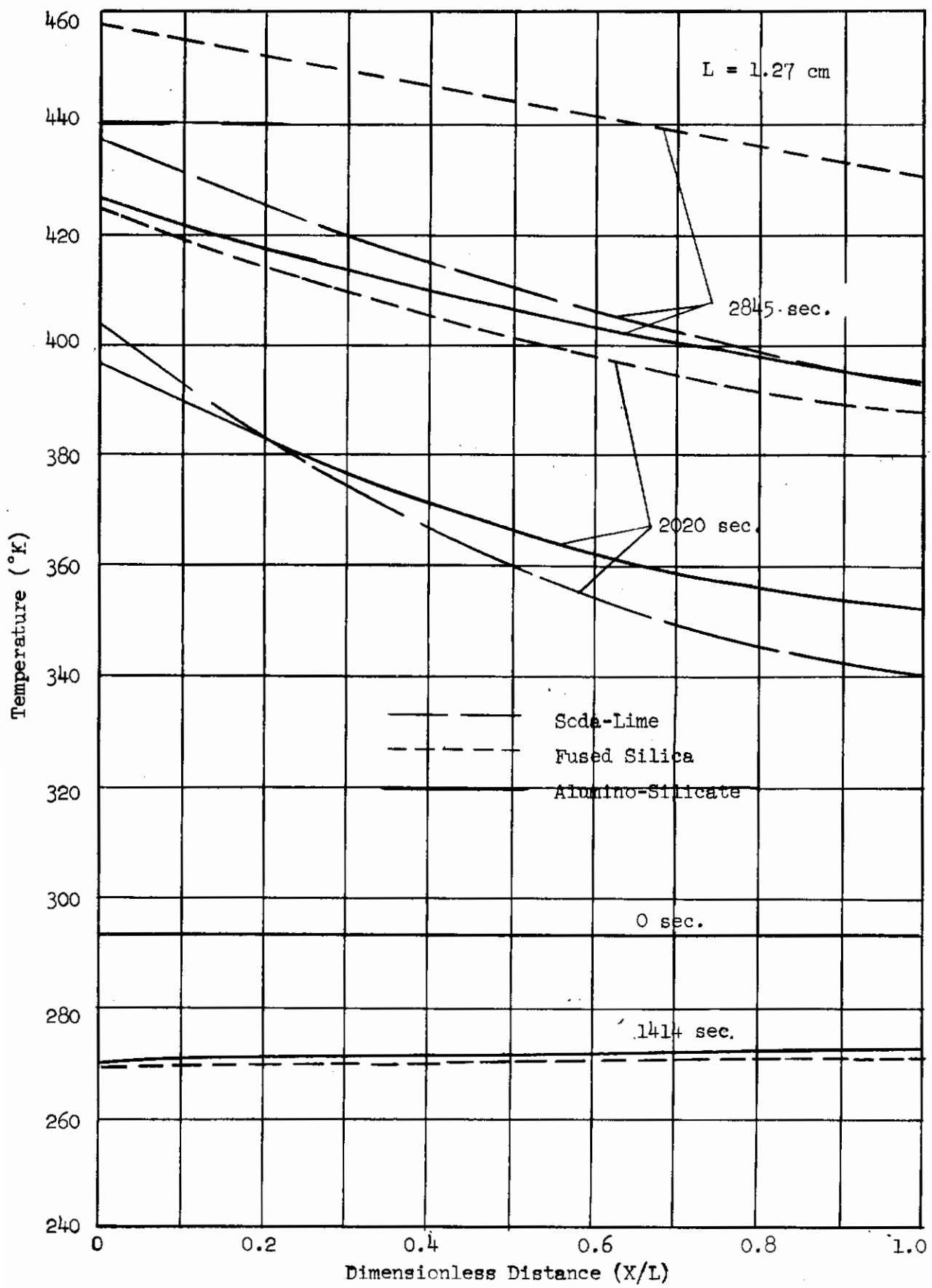

Figure 35 SUPERSONIC TRANSPORT TRANSPARENT PROFILES

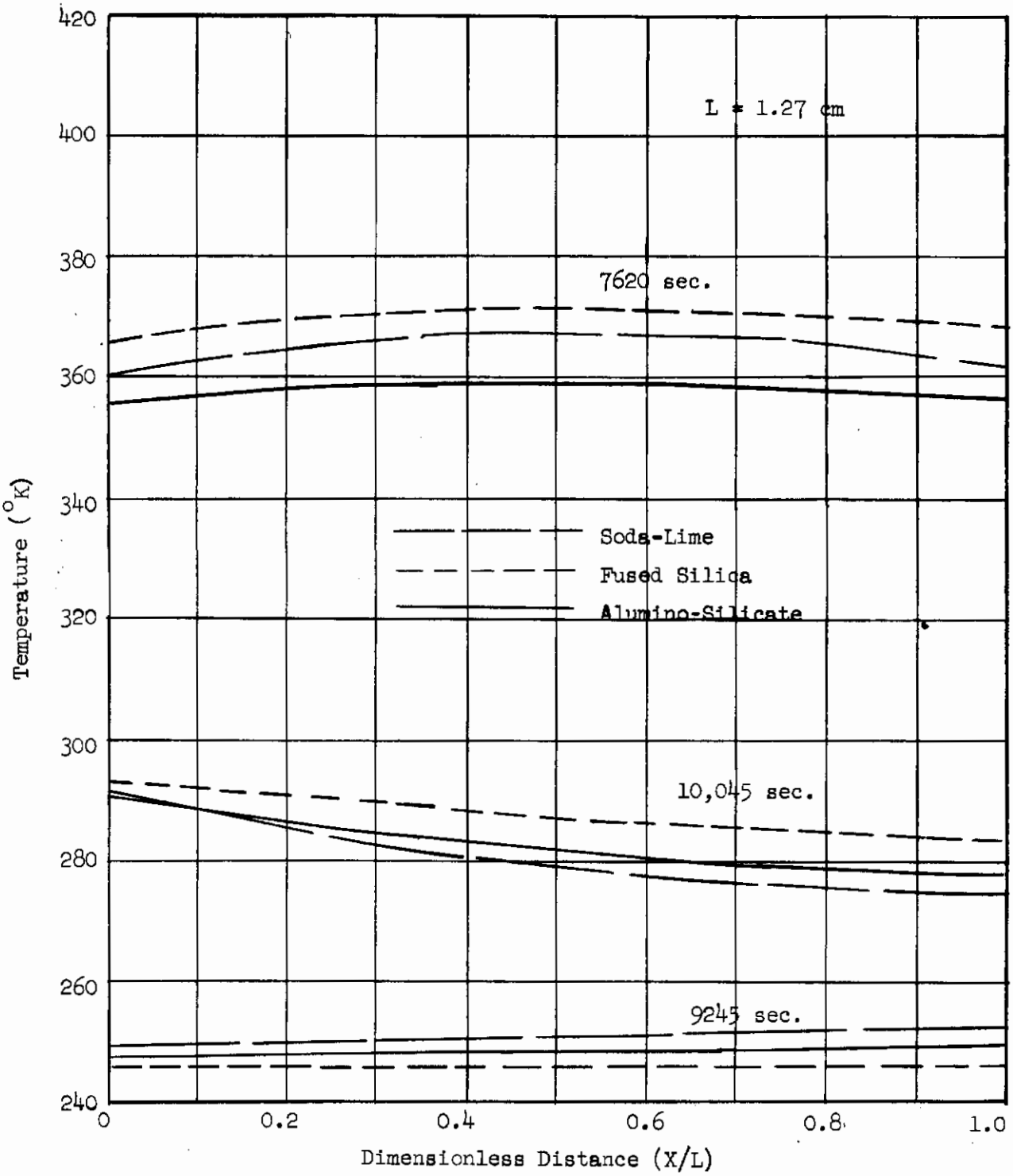

Figure 36 SUPERSONIC TRANSPORT TRANSPARENT PROFILES

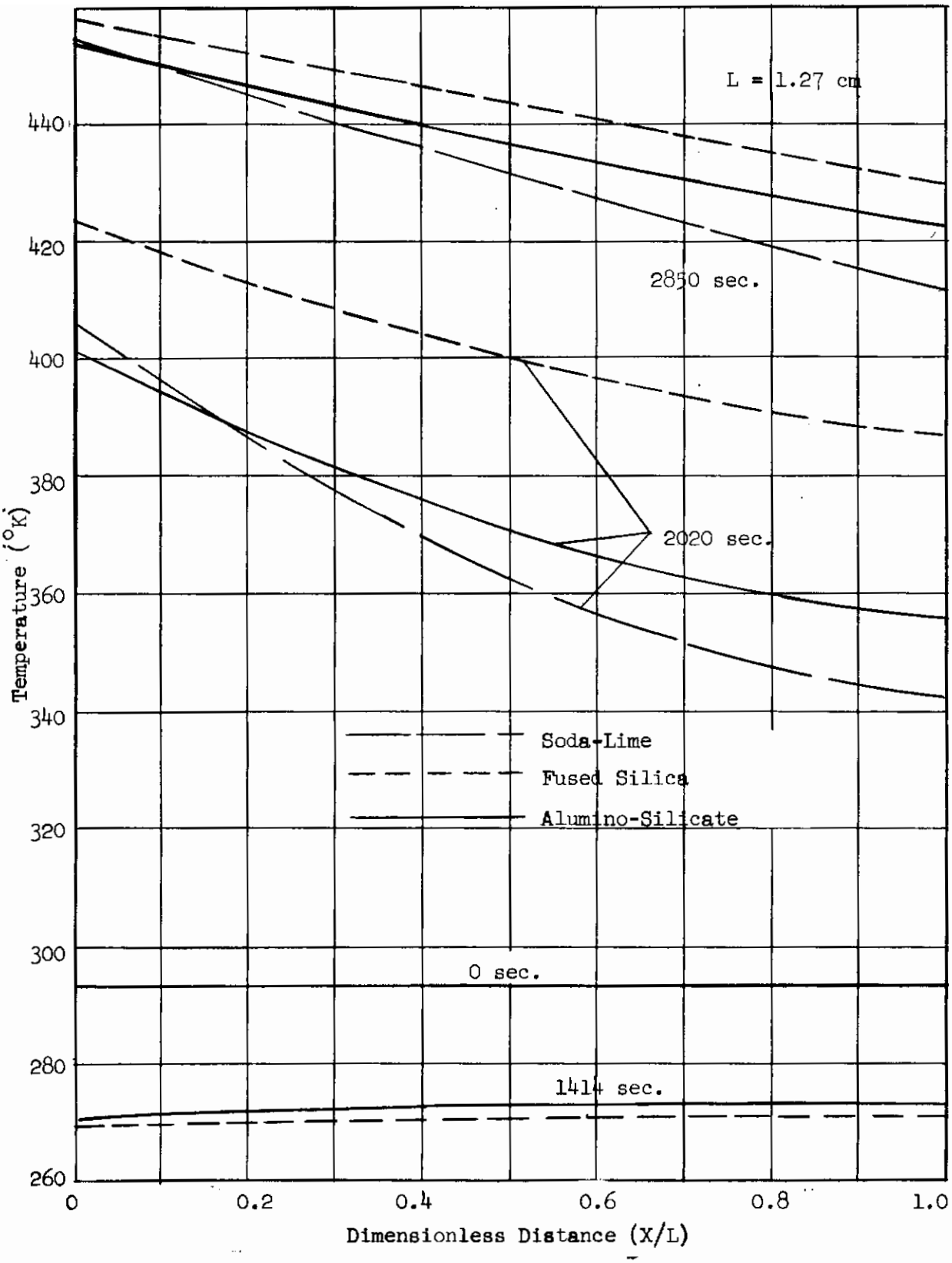

Figure 37 SUPERSONIC TRANSPORT OPAQUE PROFILES

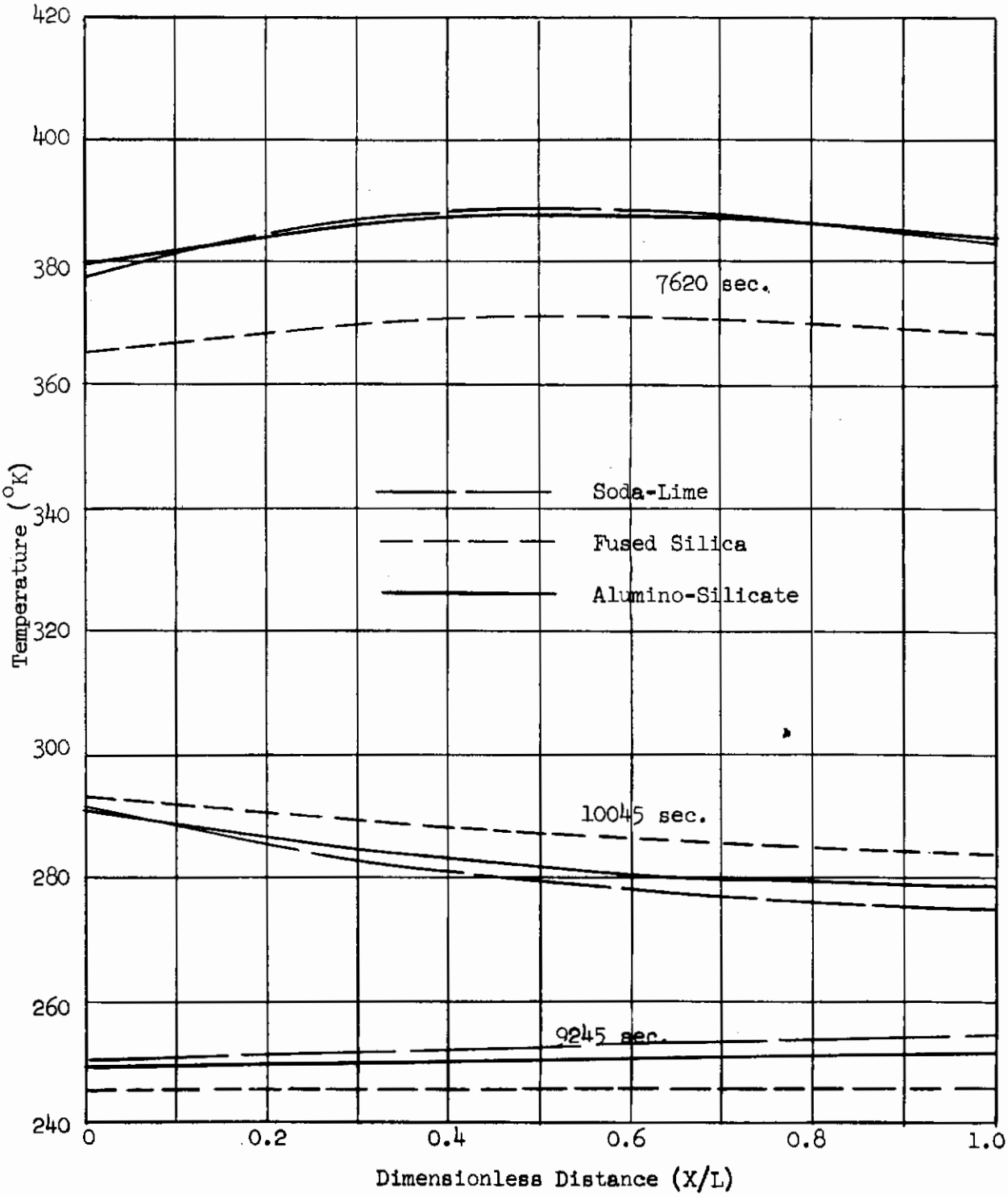

Figure 38 SUPERSONIC TRANSPORT OPAQUE PROFILES

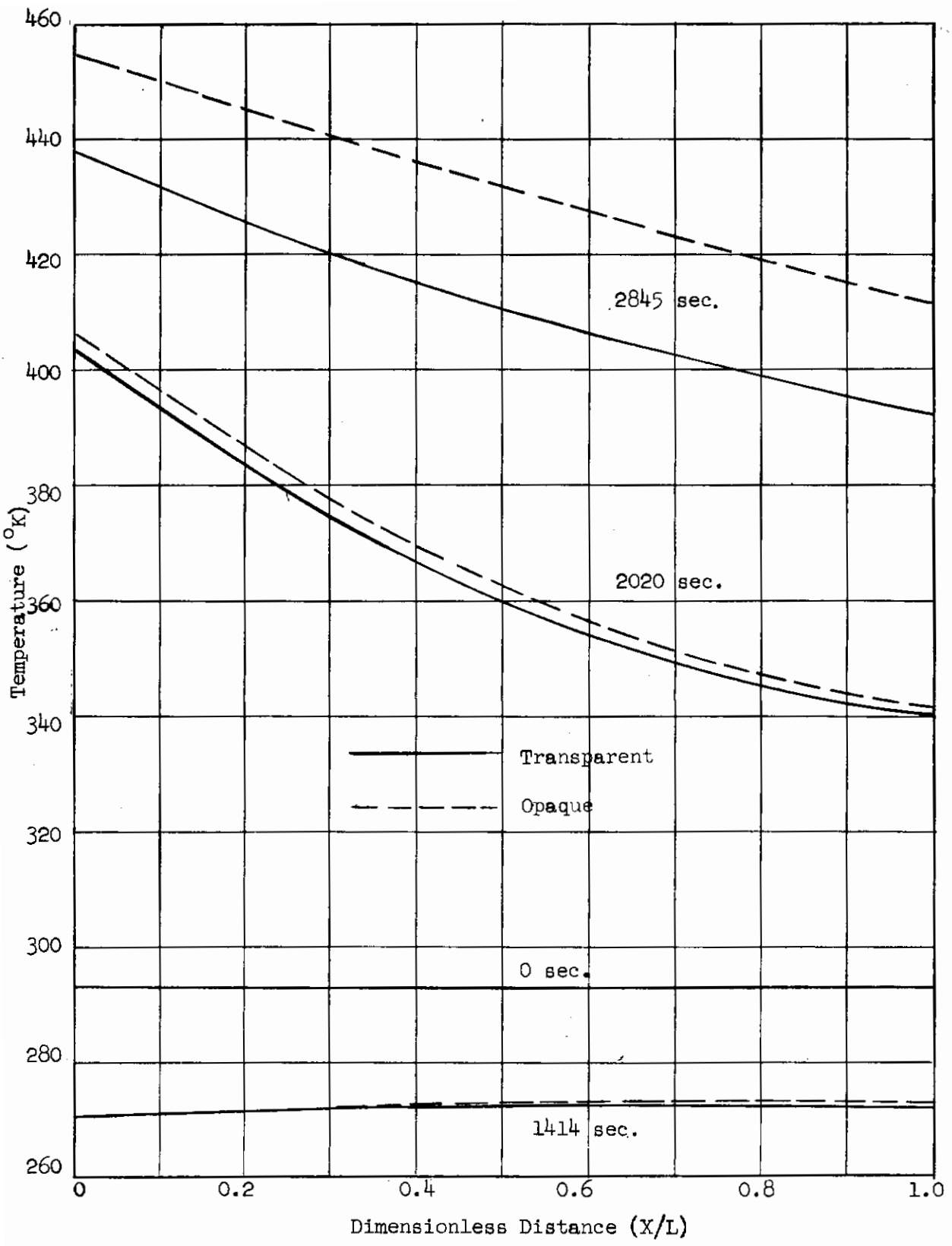

Figure 39 COMPARISON OF TEMPERATURE PROFILES AT BEGINNING OF SUPERSONIC TRANSPORT TRAJECTORY FOR SODA-LIME GLASS

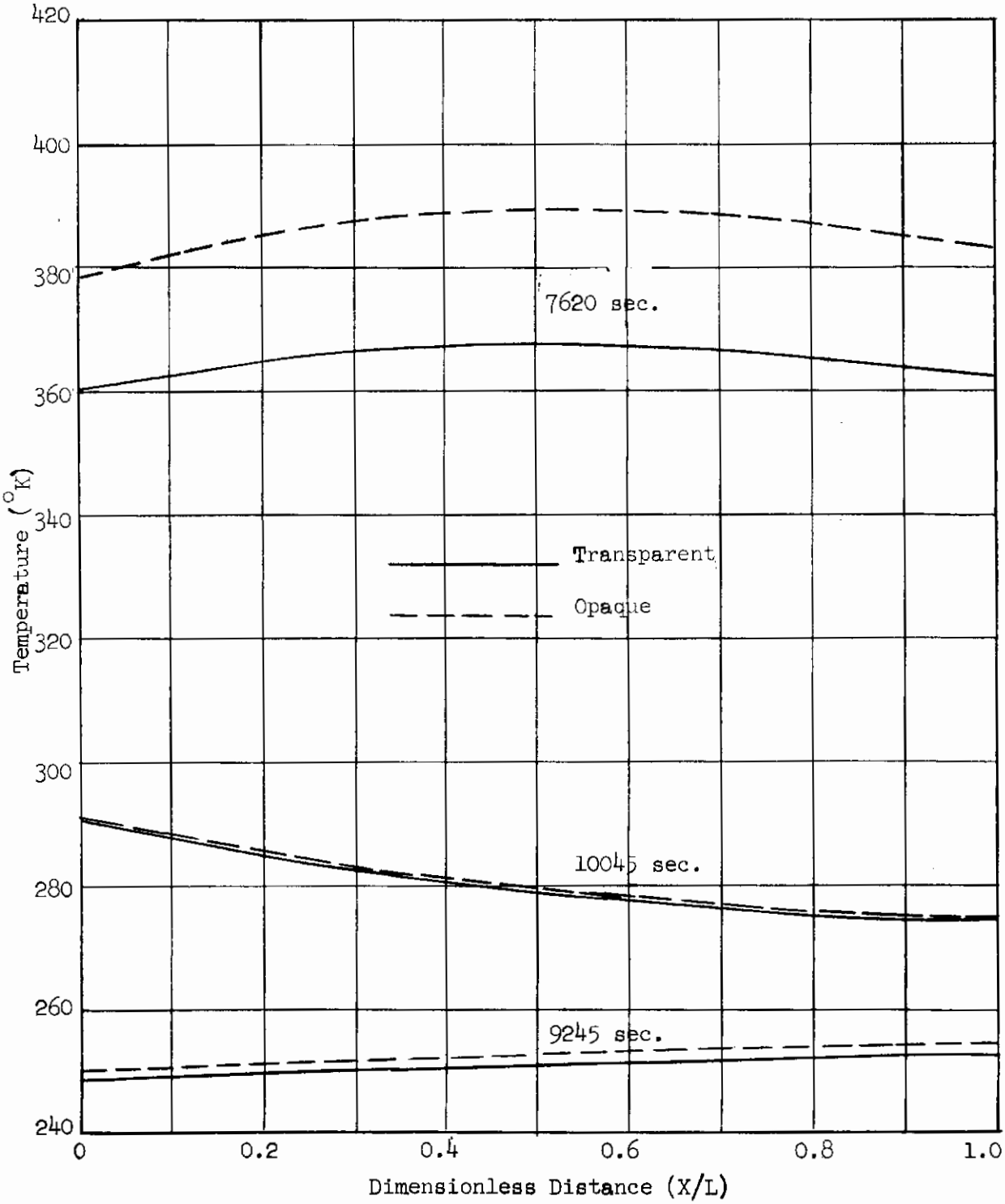

Figure 40 COMPARISON OF TEMPERATURE PROFILES AT END OF SUPERSONIC TRANSPORT TRAJECTORY FOR SODA-LIME GLASS

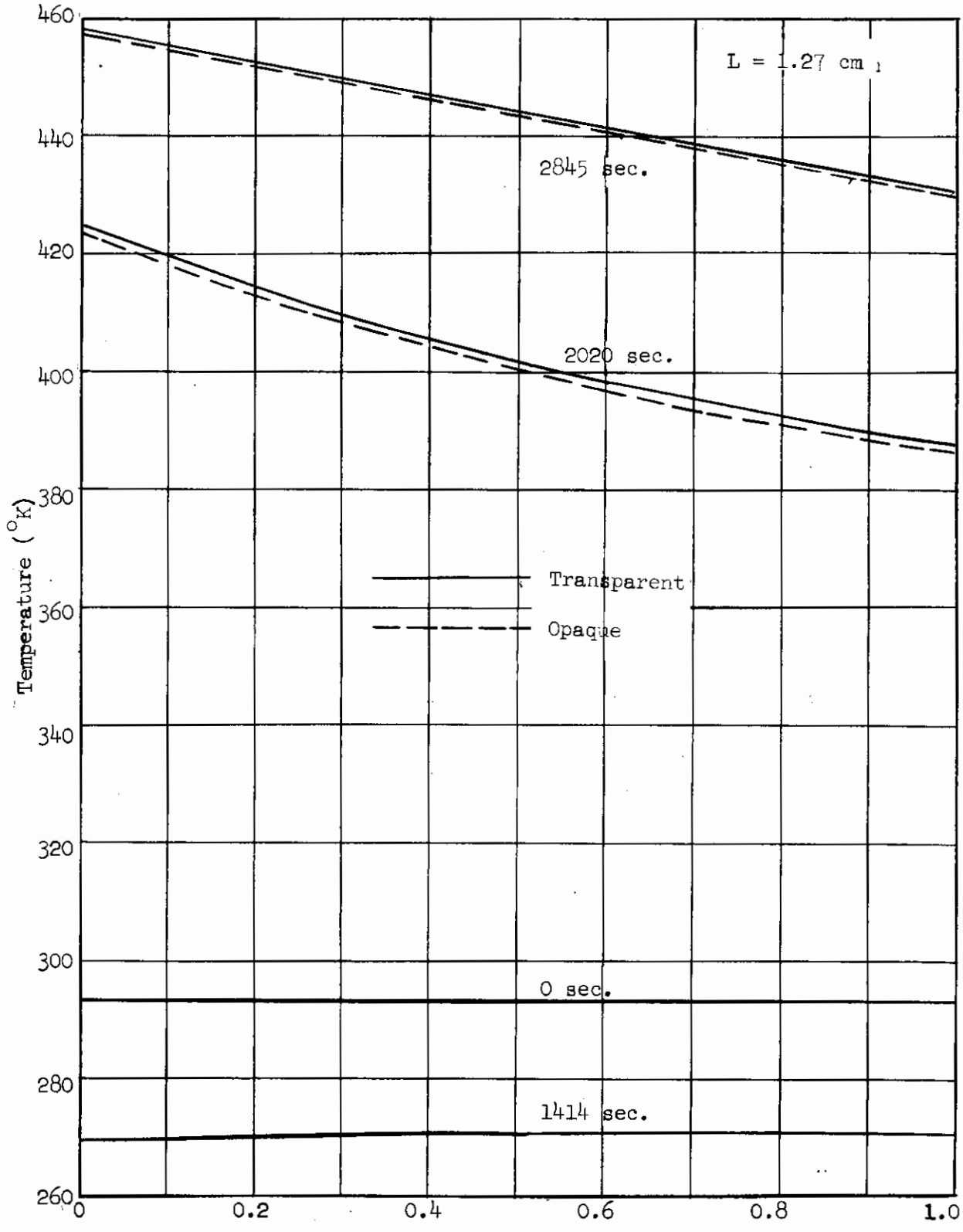

Figure 41 COMPARISON OF TEMPERATURE PROFILES AT BEGINNING OF SUPERSONIC TRANSPORT TRAJECTORY FOR FUSED SILICA GLASS

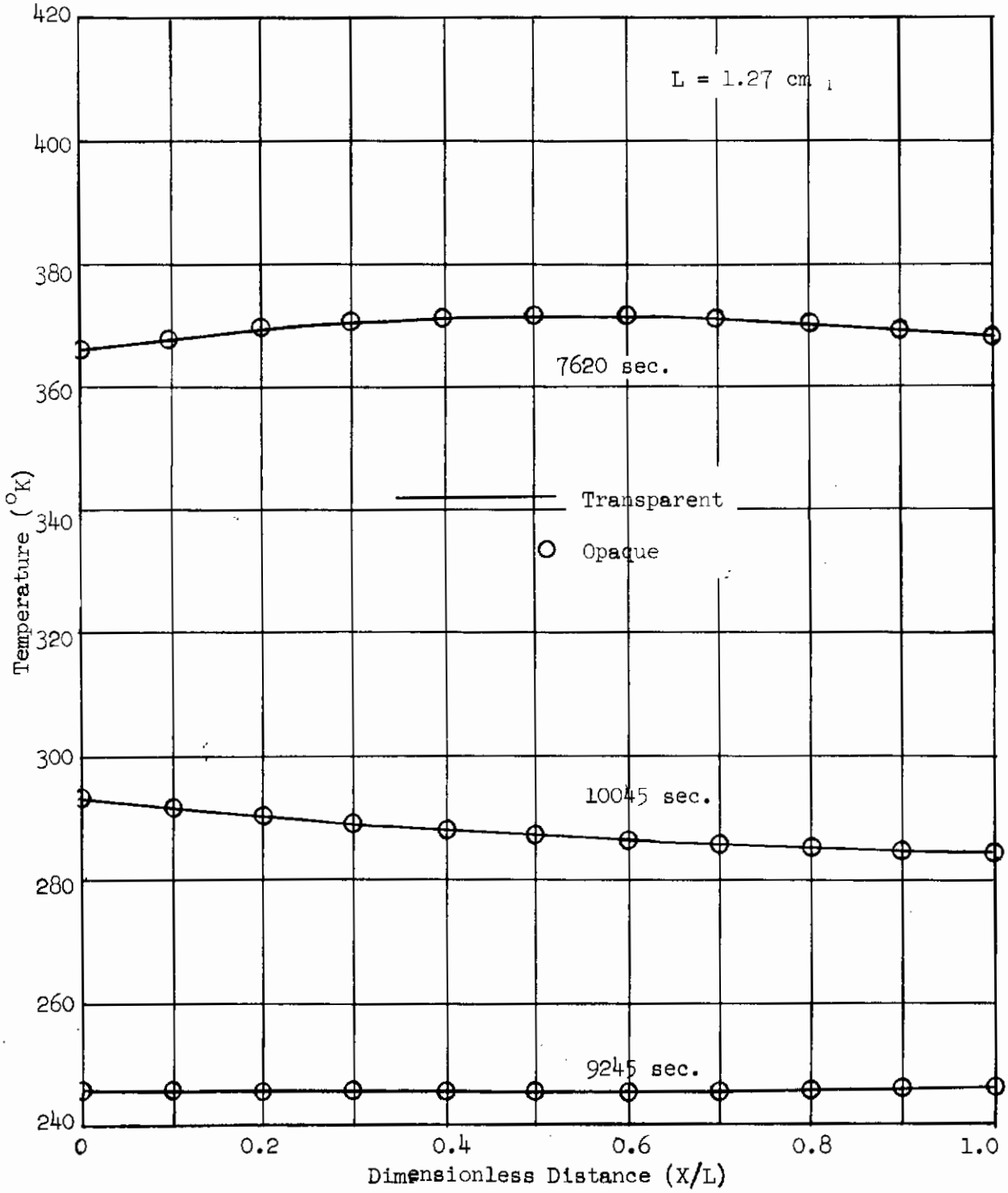

Figure 42 COMPARISON OF TEMPERATURE PROFILES AT END OF SUPERSONIC TRANSPORT TRAJECTORY FOR FUSED SILICA GLASS

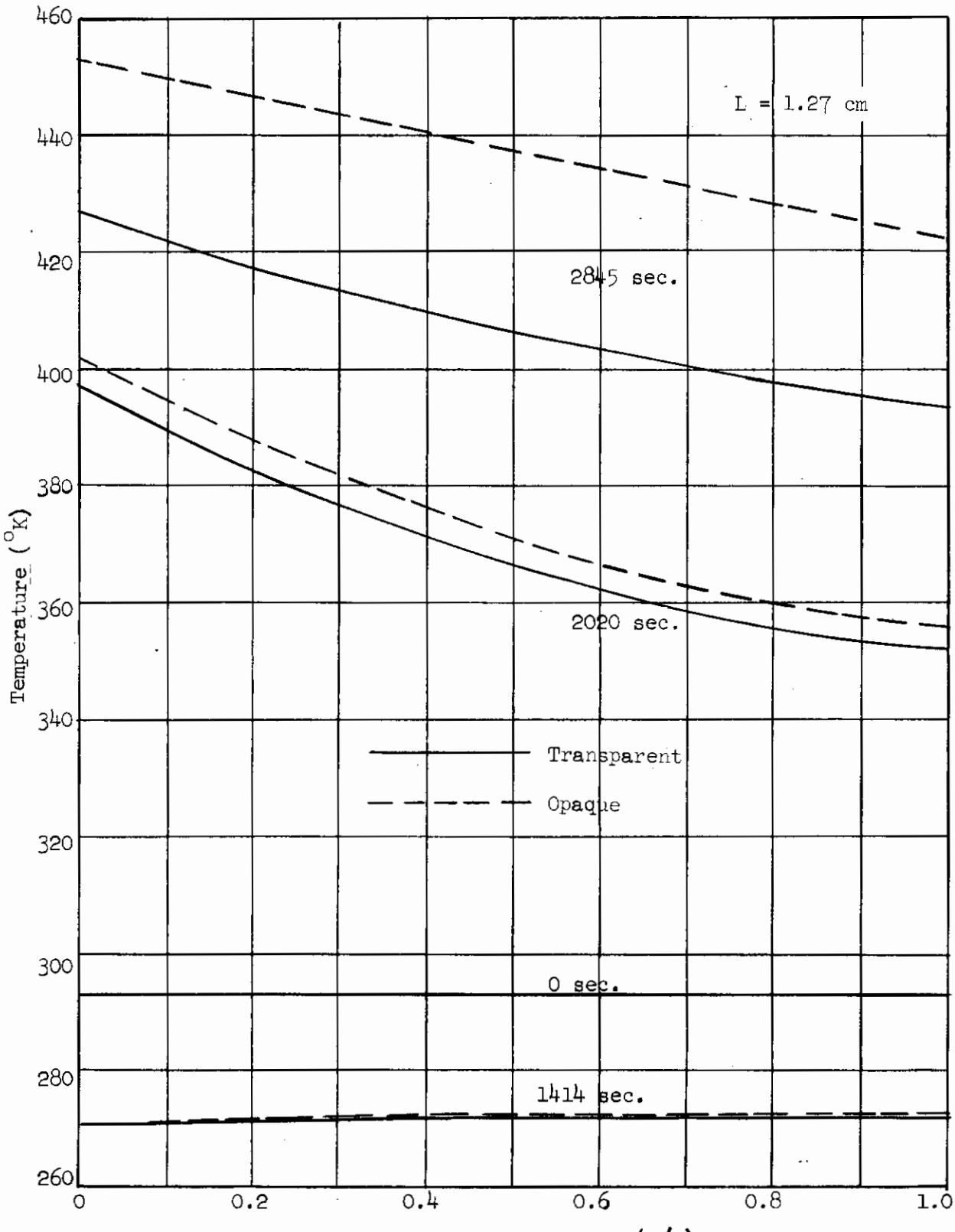

Figure 43 COMPARISON OF TEMPERATURE PROFILES AT BEGINNING OF SUPERSONIC TRANSPORT TRAJECTORY FOR ALUMINO-SILICATE GLASS

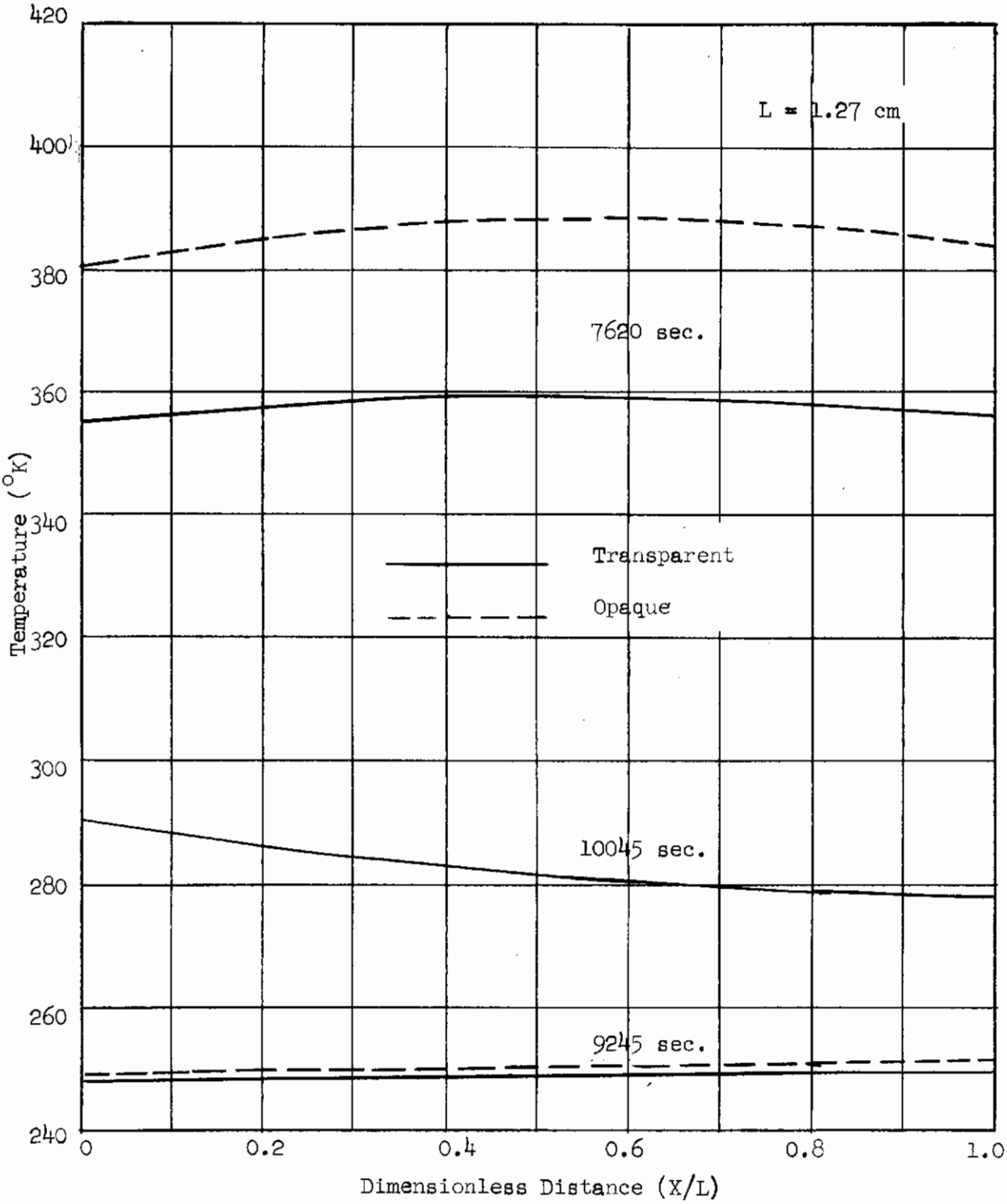

Figure 44 COMPARISON OF TEMPERATURE PROFILES AT END OF SUPERSONIC TRANSPORT TRAJECTORY FOR ALUMINO-SILICATE GLASS

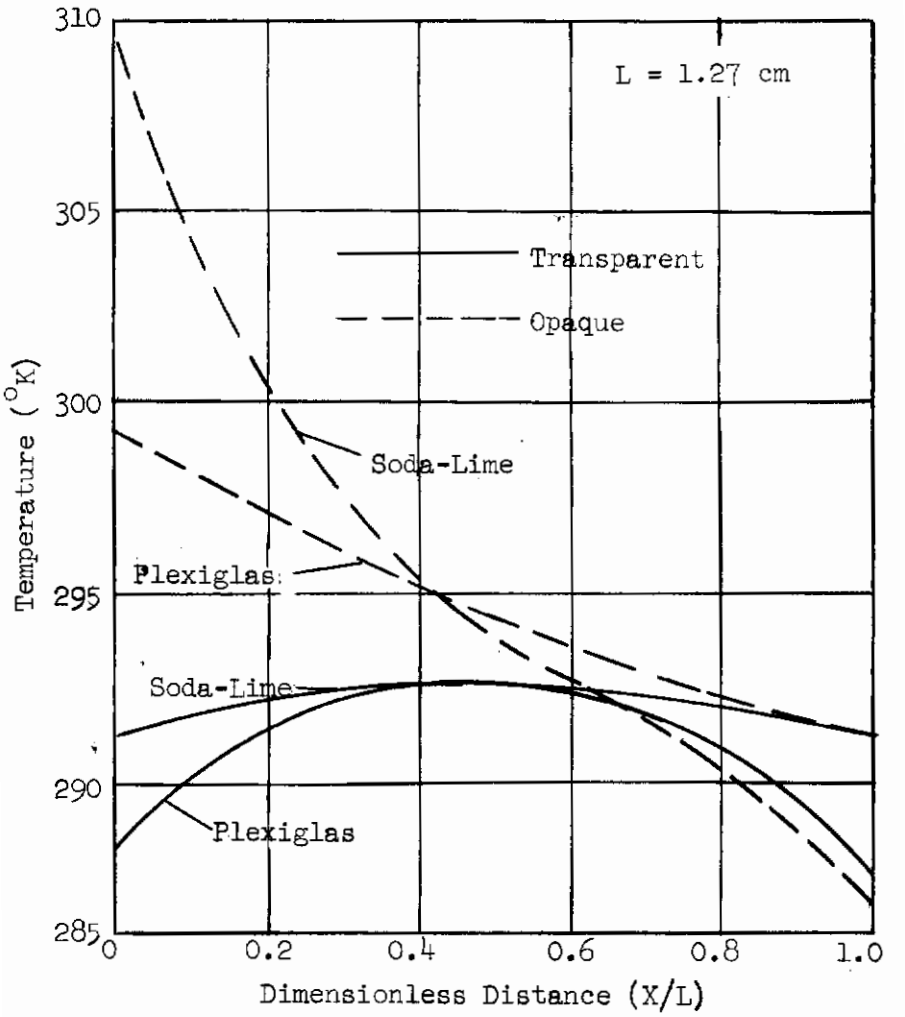

Figure 45 TEMPERATURE PROFILES AFTER 100 SECONDS OF CIRCULAR EARTH ORBIT

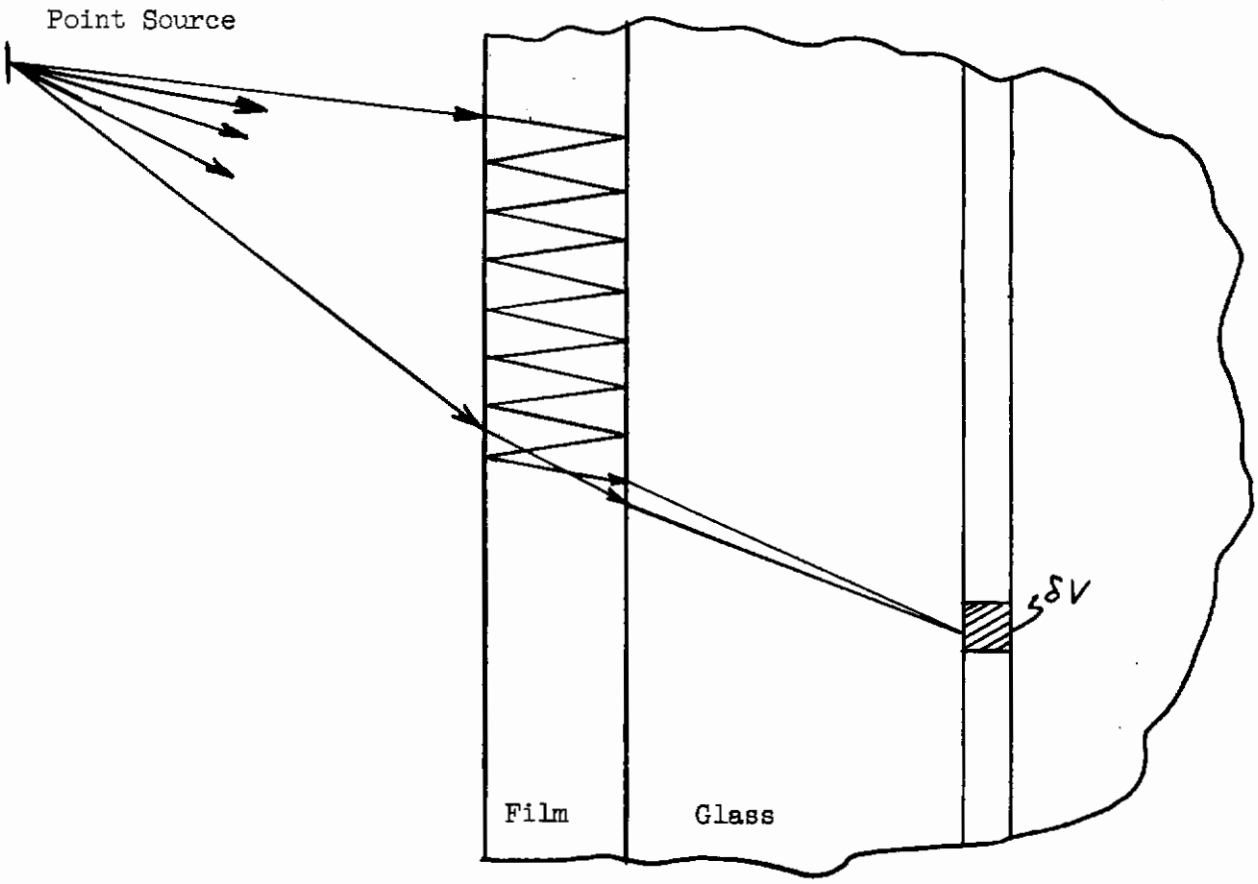

Figure 46 INTERFERENCE FROM A POINT SOURCE

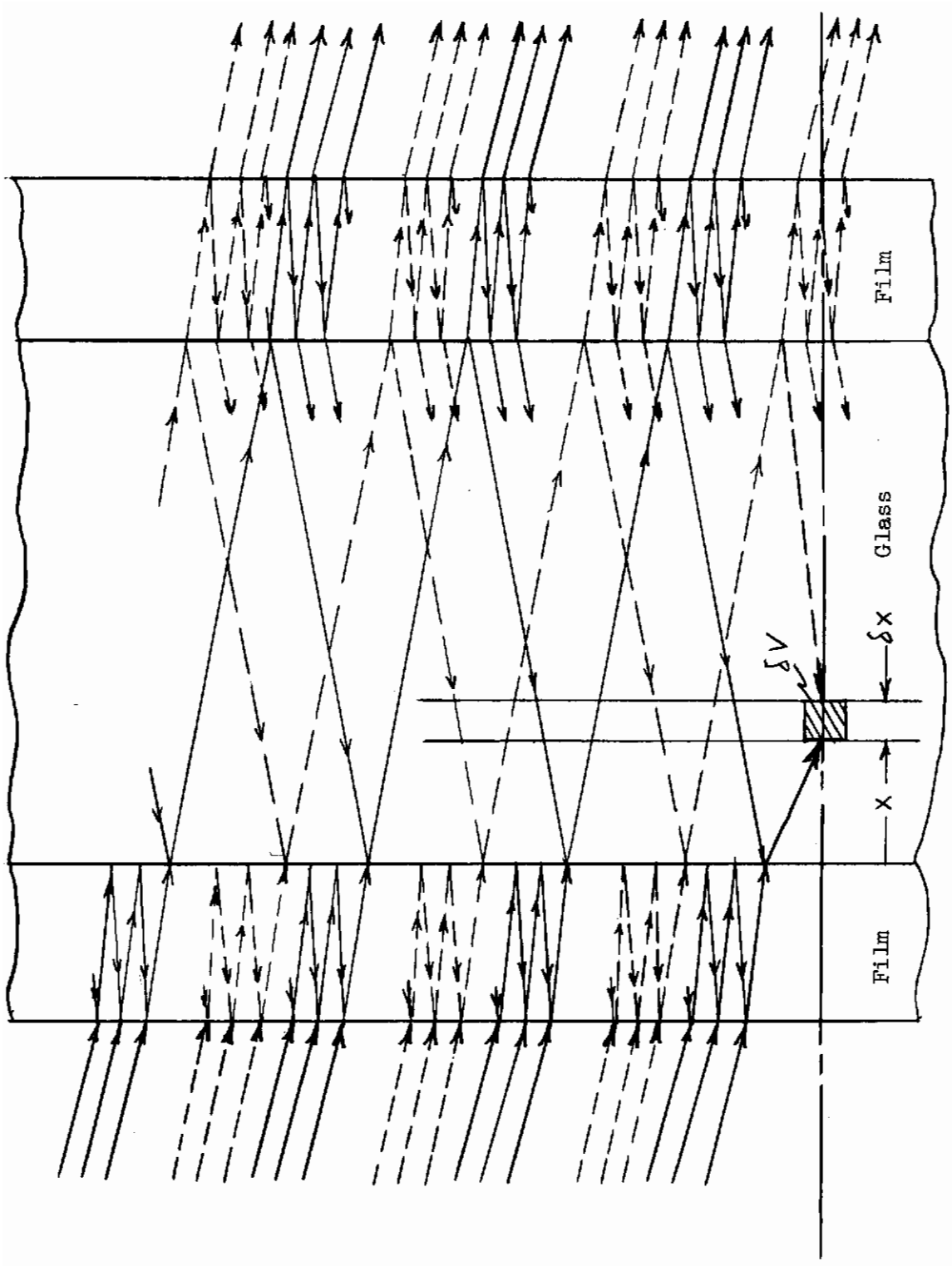

Figure 47 INTERFERENCE FROM MANY SOURCES

can be followed in a similar manner to produce back reflections which again produce superposition. Each bundle of rays may produce interference with the rays in their respective bundle but are generally incoherent with other bundles.

Parallel rays emanating from one and the same source, produce interference effects and are treated by the thin film theory. Treating these bundles as the individual beams were treated (c.f. Section 2.1.1), a geometric series evolves which yields the total intensity passing through the elemental volume. The absorption of the total intensity yields the net absorption from the external source.

A similar argument can be presented for the emission of a series of sources within the glass. These sources may behave in like manner to produce interference upon superposition of their interreflected beams due to the films. A hot gas cap does not radiate as a surface but radiates in depth within the hot gas layer. In this case the external beams are not from one and the same source and therefore must be added incoherently. However, internal emitting sources do produce coherence and therefore will interfere.

The second order effects of interference due to the existence of thin films on a glass substrate can produce striking effects in the directional emission of the filmed glass. For example, at certain angles of incidence complete destruction of an incident beam to the system may occur and at other angles of incidence bright spots will be displayed. The consequences of interference upon the temperature distribution has been investigated only for a limited number of cases during this study.

3.4.2 Film Optical Properties

The variations of the optical properties of gold and tin oxide presents additional complexities since the calculation of the temperature distribution through the window assumes that the radiations are piecewise graybodies, i.e., the absorption coefficients can be represented by step functions in broad wavelength bands (see Figures 7 to 10). These same approximations are applied to the index of refraction and extinction coefficient data for gold and tin oxide. Accordingly, the spectral data for these film materials are used to compute the apparent reflectivity and transmissivity for the filmed interfaces over the same wavelength bands considered for the glasses. Typical resulting apparent reflectivities are shown in Figures 48 and 49. It must be emphasized that, like the absorption coefficient approximations, the apparent properties for the film materials are a gross simplification to the actual data and are used as a necessary first approximation to the actual data. As can be seen, the tin oxide apparent reflectivity is fairly well approximated in the gross, two-wavelength band regions. However, gold film apparent reflectivity is poorly represented by only two wavelength bands. The refinement of the wavelength bands to conform to substrate materials as well as film materials is necessary. This refinement of the wavelength bands was not an authorized task of the present study and consequently could not be performed to increase the accuracy of the calculations.

3.4.3 Temperature Profiles

The temperature profiles for 1/2-inch thick alumino-silicate windows subjected to the hypersonic skip-glide trajectory with either no film, a 0.2 μ

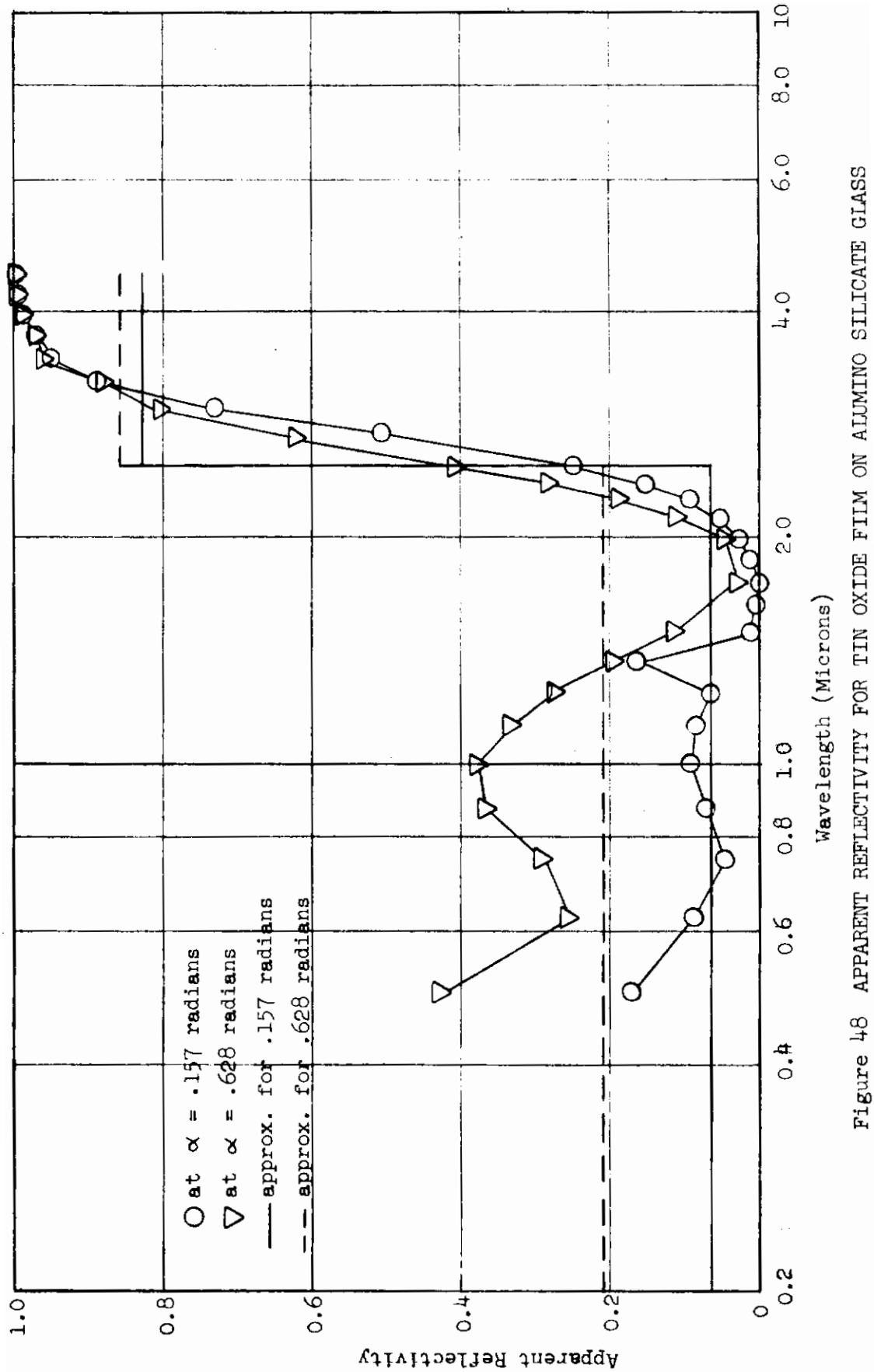

Figure 48 APPARENT REFLECTIVITY FOR TIN OXIDE FIIM ON AIJMINO SILICATE GIASS

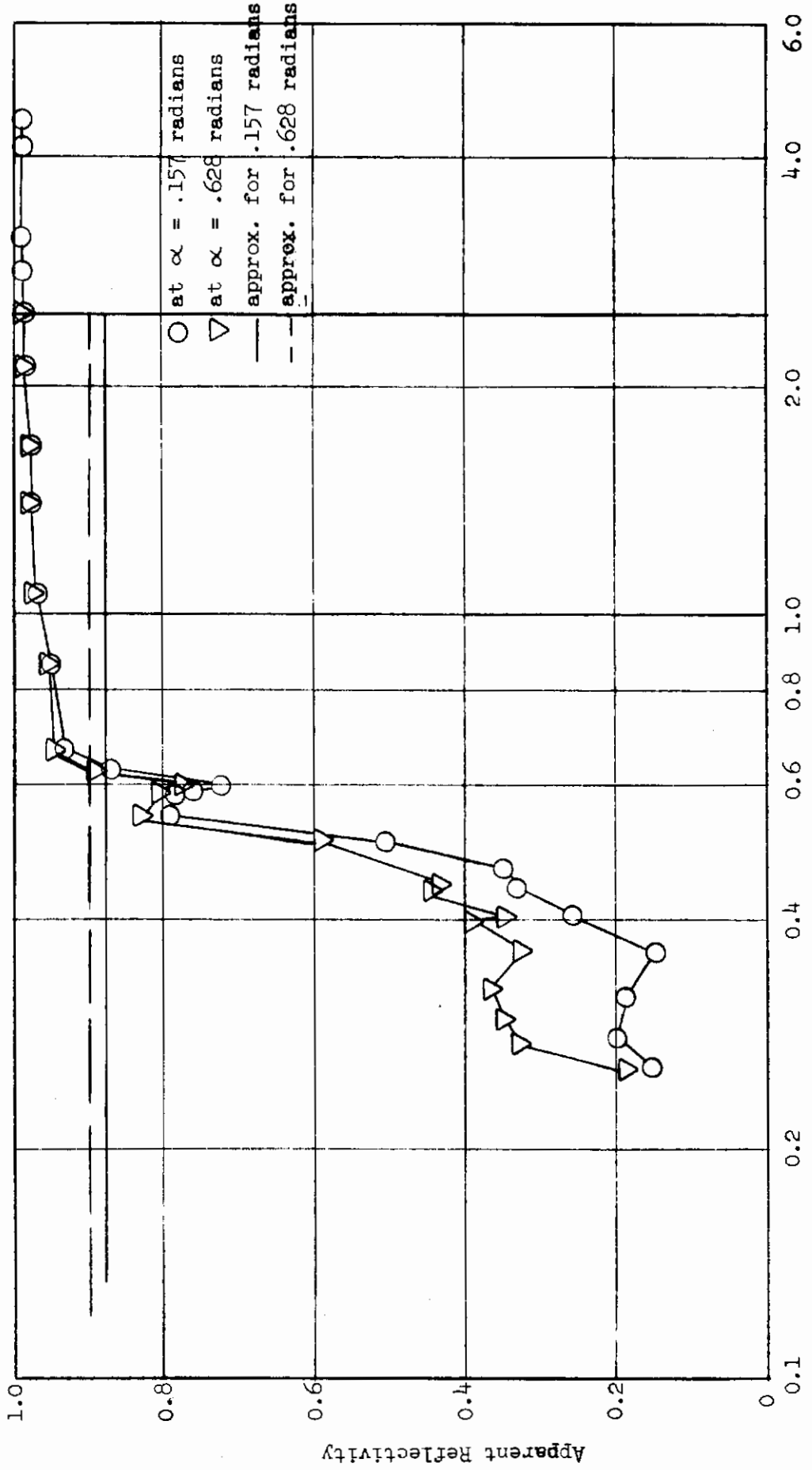

Figure 49 APPARENT REFLECTIVITY FOR GOLD FIIM ON ALUMINO SILICATE GLASS

gold film, or a 0.2μ tin oxide film on the incident or back surface are shown in Figures 50 to 53. The glazings with a gold film on their incident face consistently develop the highest temperatures while the glazings with a tin oxide film on their incident face are slightly cooler. Both coatings, however, produce temperature profiles above those predicted for uncoated glass.

These results agree with intuitive feelings of how the coating effects the glass temperature. Consider the apparent reflectivities for a glass with coatings and without any coatings. The uncoated glass surface would reflect the least amount of energy back into itself while gold coating would best reflect these internally-generated long wavelength radiations. Since more energy is reflected back into a gold-coated glass, it should develop a higher temperature profile than the uncoated glass.

3.4.4 Heat Flux into the Cabin

The net radiant heat flux into the cabin is given in Figures 54 to 56 for the hypersonic skip-glide trajectory. A gold coating on the emergent face reduces the cabin radiant heat flux to 1% of that for an uncoated glass. An uncoated glass develops less cabin radiant heat flux than a glass coated on the incident face only.

3.4.5 Discussion of Results

The results given for the temperature distributions and radiant heat flux emitted into the cabin are initial values obtained from the SIGTRAN computer program. In view of the film properties approximations (Section 3.4.2) the resulting temperature predictions may well be in error. Further verification of their accuracy is required using finer wavelength subdivisions. However, the trends and comparisons made between the coated and uncoated glasses are valid and serve to illustrate the prominent effects of the film materials to raise the temperature distribution and lower total heat flux into the cabin in some instances.

From the results it would appear that the minimum heat flux glazing is a window with a gold film on its emergent face. However, the increase of interface reflectivity which is produced by a gold film also increases the temperature within the window and decreases the overall apparent transmissivity of the window system. As can be seen from Table 6 the apparent total hemispherical transmissivity (in the visible spectrum) is four orders of magnitude lower for a 0.2μ gold-filmed glass than either uncoated or tin oxide-coated glass.

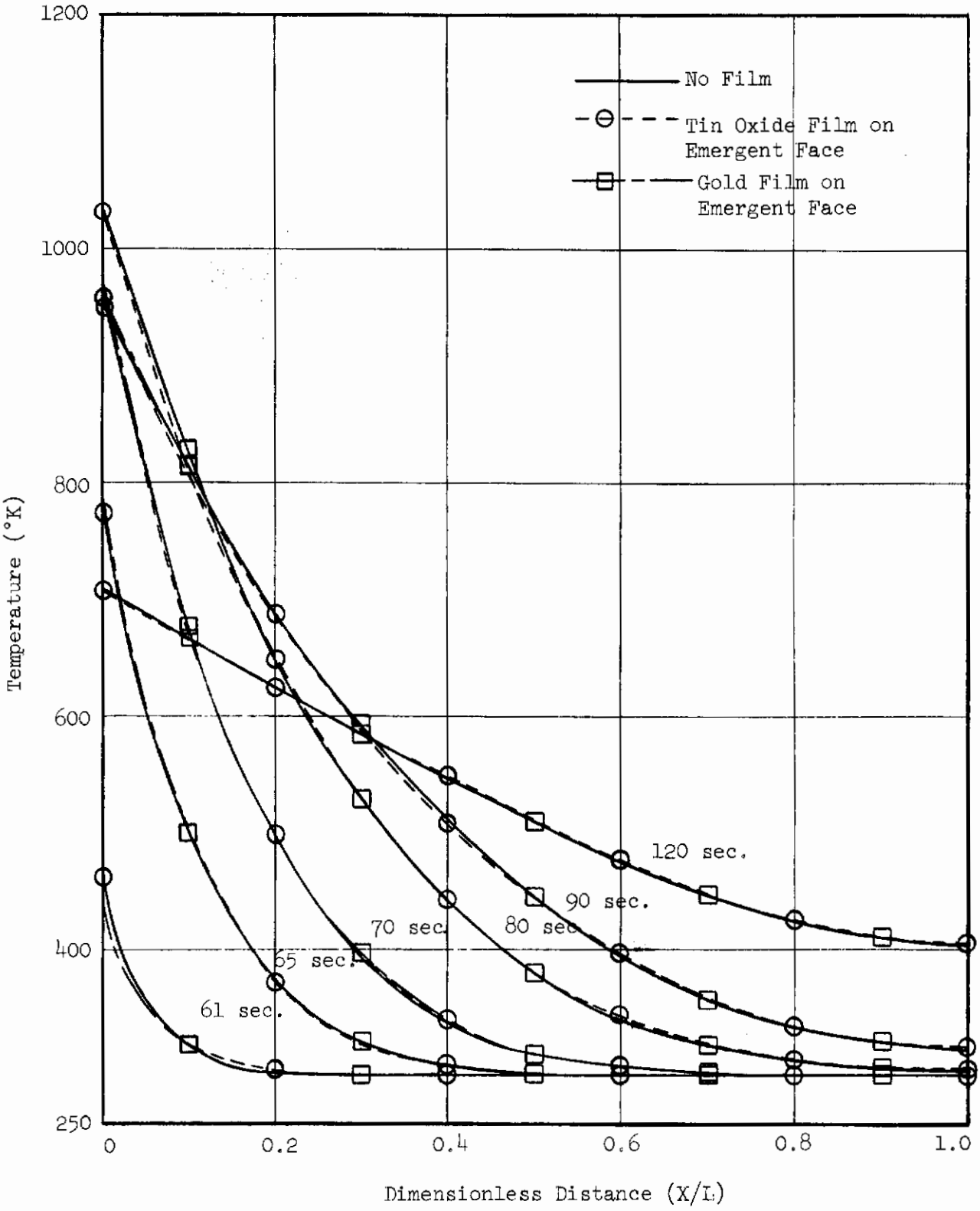

Figure 50 TEMPERATURE PROFILES - ALUMINO-SILICATE GLASS - NC FILMS ON INCIDENT FACE

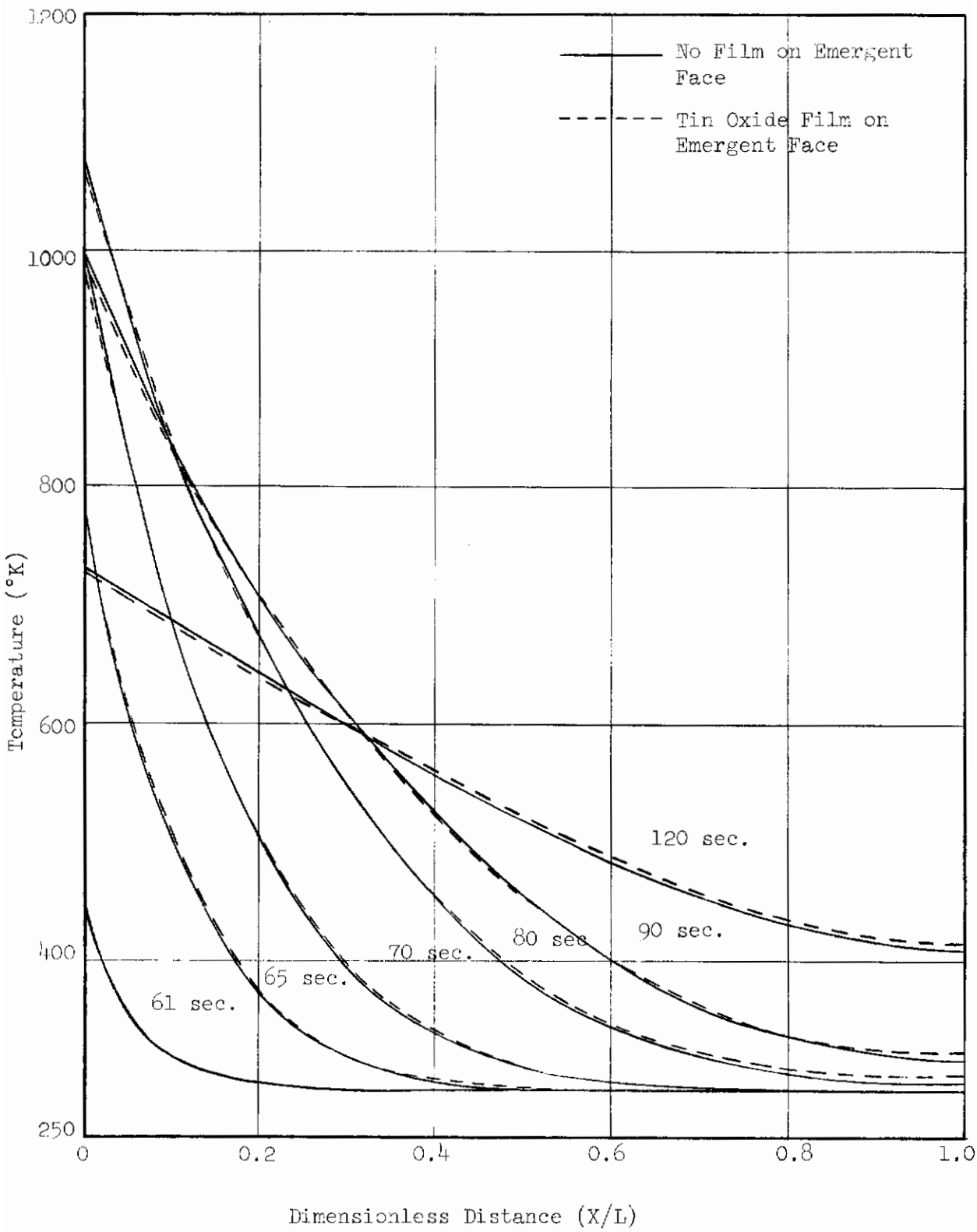

Figure 51 TEMPERATURE PROFILES - ALUMINO-SILICATE GLASS - TIN OXIDE FILM ON INCIDENT FACE

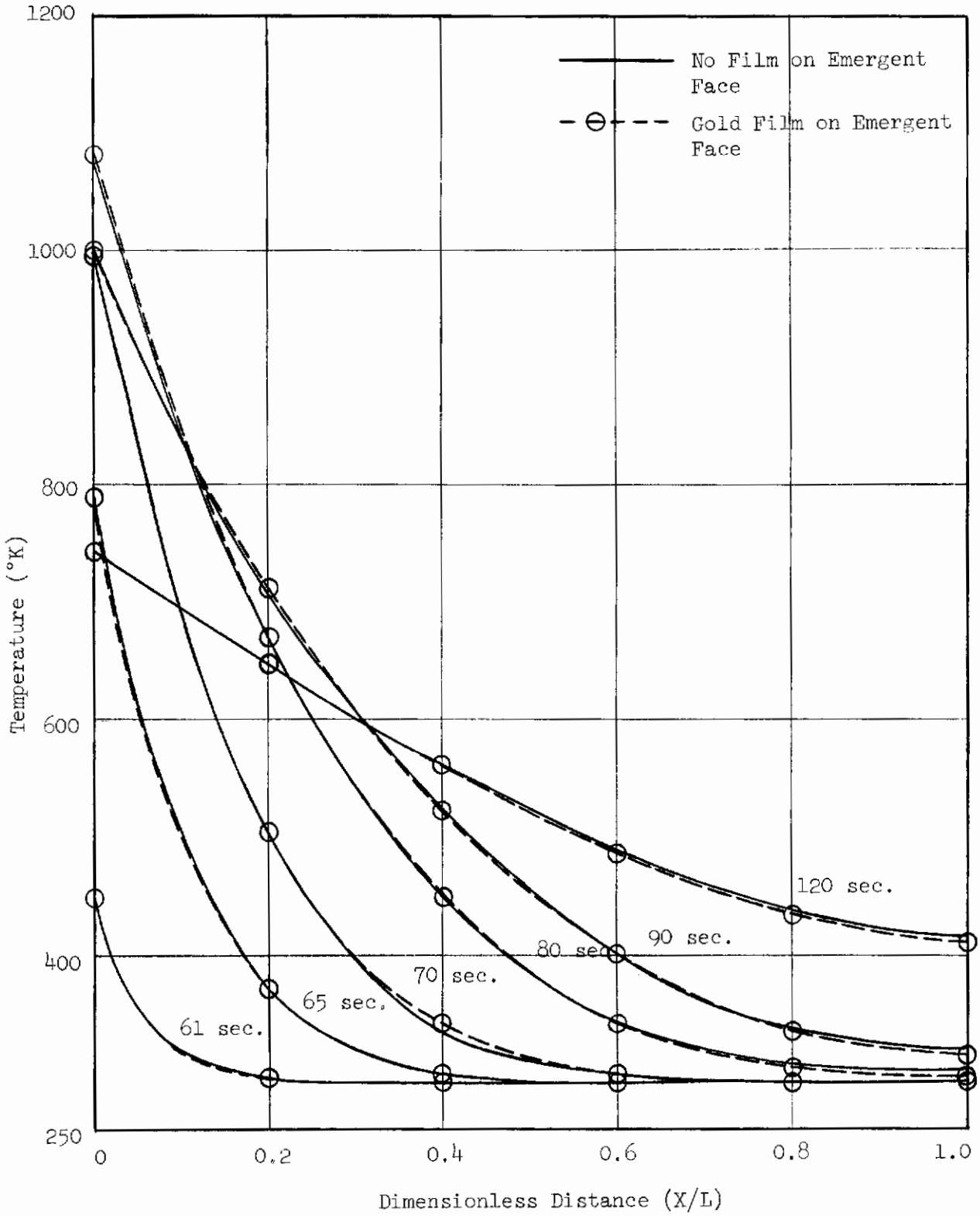

Figure 52 TEMPERATURE PROFILES - ALUMINO-SILICATE GLASS - GOLD FILM ON INCIDENT FACE

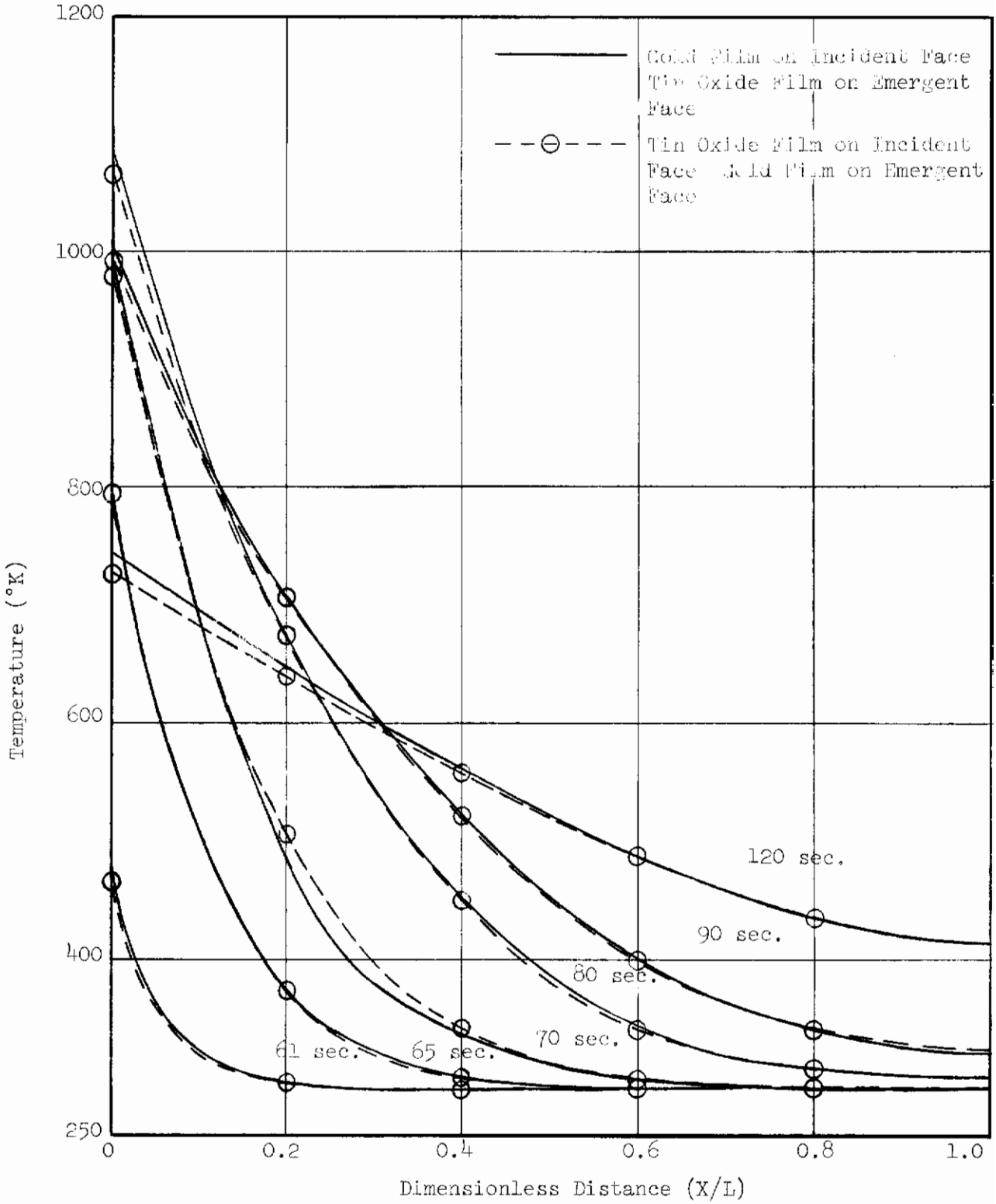

Figure 53 TEMPERATURE PROFILES - ALUMINO-SILICATE GLASS - GOLD AND TIN OXIDE FILMS

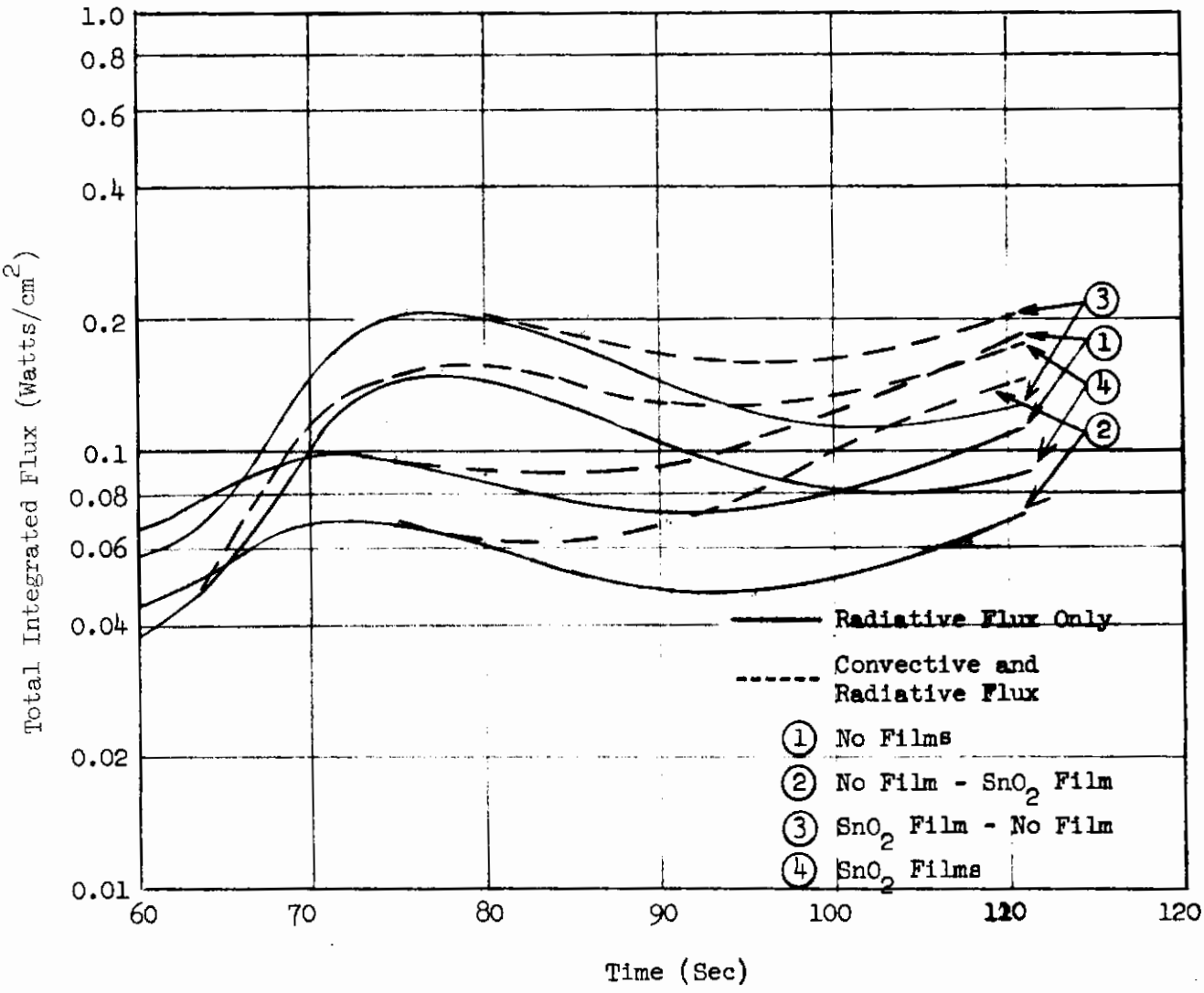

Figure 54 CABIN HEAT FLUX - TIN OXIDE COATED ALUMINO SILICATE GLASS

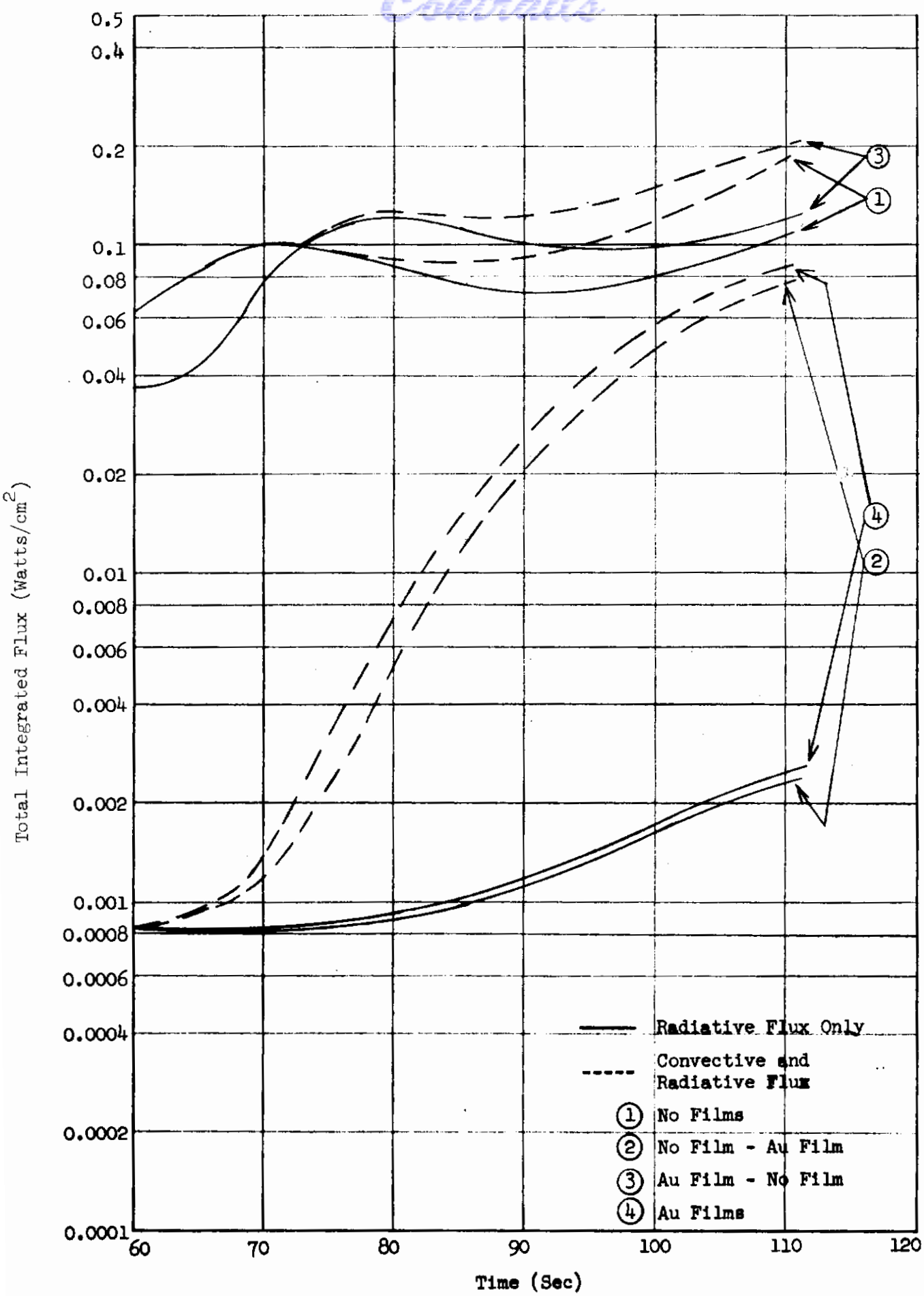

Figure 55 CABIN HEAT FLUX - GOLD COATED ALUMINO SILICATE GLASS

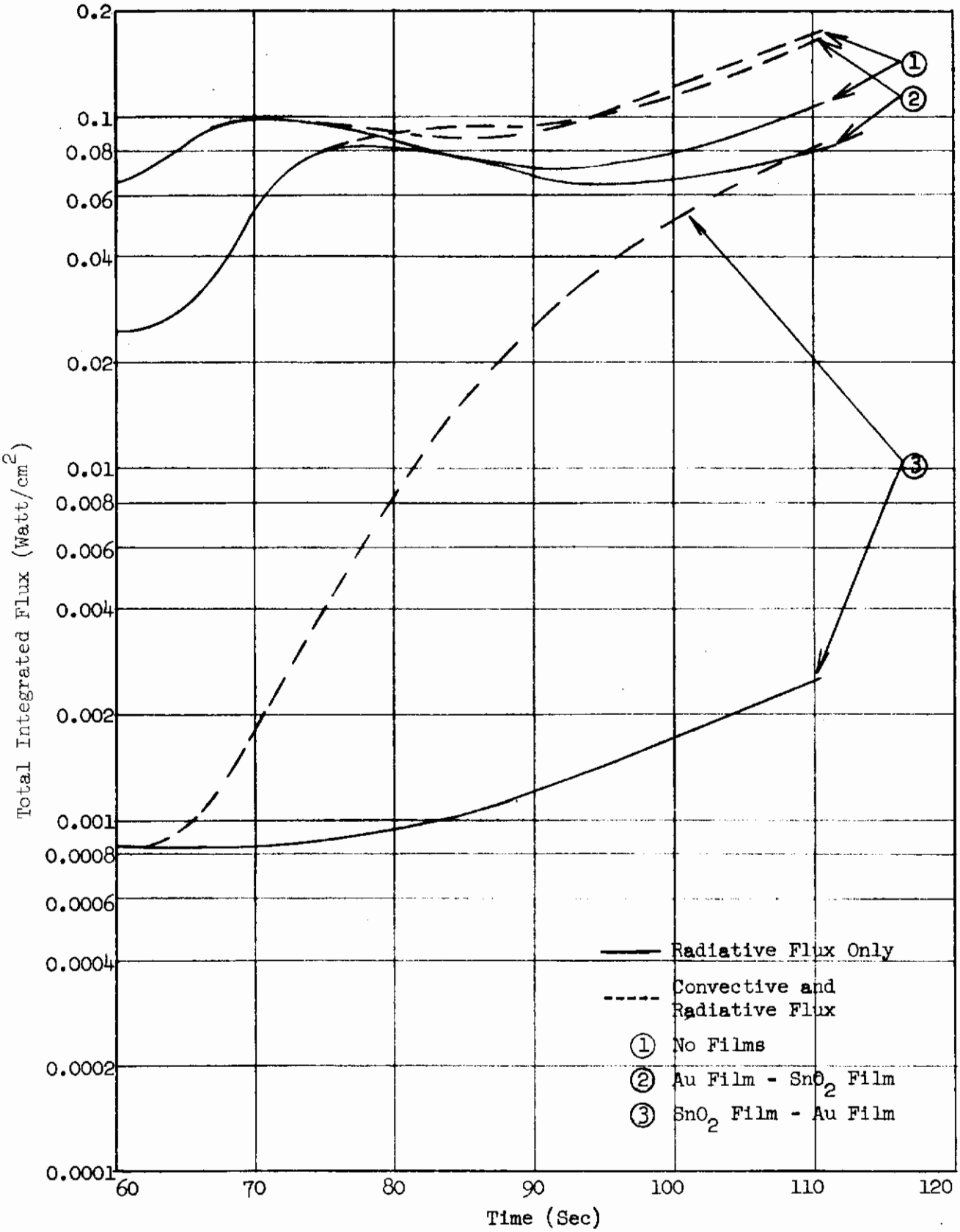

Figure 56 CABIN HEAT FLUX - GOLD AND TIN OXIDE COATED ALUMINO SILICATE GLASS

TABLE 6

APPARENT TOTAL HEMISPHERICAL TRANSMISSIVITY
OF A FILMED ALUMINO-SILICATE GLAZING*

Incident Face	Emergent Face	Transmissivity
No Film	No Film	.816
No Film	0.2 μ SnO_2 Film	.600
0.2 μ SnO_2 Film	No Film	.587
0.2 μ SnO_2 Film	0.2 μ SnO_2 Film	.432
No Film	0.2 μ Au Film	3.8×10^{-5}
0.2 μ Au Film	No Film	4.8×10^{-5}
0.2 μ Au Film	0.2 μ Au Film	2.9×10^{-9}
0.2 μ Au Film	0.2 μ SnO_2 Film	3.6×10^{-5}
0.2 μ SnO_2 Film	0.2 μ Au Film	3.0×10^{-5}

*These values were computed from the average properties values in the first wavelength band for tin oxide and from optical properties data at 0.406 μ for gold. Both film materials were computed as 0.2 μ thick on a 1/2-inch thick substrate of alumino-silicate glass.

SECTION 4

CONCLUSIONS AND RECOMMENDATIONS

Any accurate analysis of heat transfer within a partially transparent medium must include the radiative mode of heat transfer as well as the conductive mode whenever the medium is exposed to radiations within the diathermous spectrum or, whenever the medium itself is at a high temperature. The basis for radiative interchange has been extended from earlier theories so that window system configurations can be handled and temperature predictions can be made for a variety of thermal inputs. High aerodynamic heating rates, as associated with hypersonic flights, produce high temperature levels within the window. At these high temperatures radiative heat transfer becomes important and must be included in the analysis. At temperatures above approximately 1000°K it is necessary to consider radiant interchange if the surface temperatures are to be predicted to within ± 150°K.

The work summarized in this report provides a basic description of the heat transfer within a single layer of semitransparent window material. Computer programs have been written and developed for specific trajectories and missions as input conditions with several options available such as the option of using the opaque analysis and/or a constant convective input. The influence of computational accuracy, particularly as associated with the numerical integration of the radiative interchange for nearly transparent materials should be investigated further. There is a need for additional study to modify and refine the digital computer program into a more useful tool applicable to more general problems as well as the specific applications thus far incorporated.

Additional work that is recommended includes:

(1) Reduce and simplify the input information presently required in the trajectories by incorporating canned subroutines available in the RTD computer facilities library

(2) Refine spectral bands to include more accurate step-function fits to the material optical properties

(3) Remove the absorption approximation so that any material of any thickness may be handled, and

(4) Include temperature dependent thermal properties.

The work completed on the effects of a thin transparent film is extremely limited and is only a beginning to the analysis and understanding of this important technique of controlling heat transfer in an aerospace vehicle. Only one film thickness has been considered and therefore does not cover the phenomenon of interference of optically very thin films. It is recommended, therefore, that an extended study be undertaken to study further the interference effects of thinner transparent films.

The theory utilized in the development of the solution for temperature distributions within windows and thermal flux into the cabin of an aerospace vehicle introduces new concepts which are not encountered in more conventional heat transfer problems. As a result, the solution is quite complex and

predicts phenomena which are sometimes difficult to perceive. To establish confidence in the theory as well as to verify predictions derived from computed results an experimental program is recommended wherein temperature and radiation measurements are made under laboratory conditions and compared with computed predictions for these conditions. The experimental verification program must be designed such that:

(1) the boundary conditions are accurately known without interjecting extraneous experimental errors

(2) the radiative interchange mechanism of heat transfer is prominent

(3) the sensors used must not influence the test sample

These requirements emphasize that a very specialized approach is needed which departs from ordinary heat transfer experiments. Only by adhering to these requirements will a valid verification program be achieved.

Furthermore it is strongly recommended that techniques to simplify the analysis be investigated. These simplifications may take the form of idealizing the window system thermal input which analytically could yield approximate closed form solutions. A parameter study using the digital computer would profitably expose sensitive parameters which play a major role in radiative interchange within semitransparent materials. In this manner dimensionless correlations based upon characteristic properties would lead to advantageous simplification of the analytical maze inherent to this most complex heat transfer problem.

SECTION 5

REFERENCES

1. Gardon, R., "A Review of Radiant Heat Transfer in Glass", J. Amer. Cer. Soc. 44 (1961) No. 7, pp. 305-312.

2. Gardon, R., "The Emissivity of Transparent Materials", J. Amer. Cer Soc. 39 (1956) No. 8, pp. 278-287.

3. Kingery, W. D., "Heat Conductivity Processes in Glass", J. Amer. Cer. Soc. 44 (1961) No. 7, pp. 302-304.

4. Lee, D. W. and Kingery, W. D., "Radiation Energy Transfer and Thermal Conductivity of Ceramic Oxides", J. Amer. Cer. Soc. 43 (1960) No. 11, pp. 594-607.

5. Charnock, H., "Experimental and Theoretical Comparison of Radiation Conductivity Predicted by Steady State Theory With That Effective Under Periodic Temperature Conditions", J. Amer. Cer. Soc. 44 (1961) No. 7, pp. 313-317.

6. Gardon, R., "Calculation of Temperature Distributions in Glass Plates Undergoing Heat Treatment", J. Amer. Cer. Soc. 41 (1958) pp. 200-209.

7. Digges, K. H., Private Communication, 26 April 1963.

8. Hanshaw, C. E., Jacobsen, W. E., Strasser, G., Study of Structural Requirements of Re-entry from Outer Space WADD TR 60-886 (May 1961).

9. Staff: Langley Research Center, The Supersonic Transport - A Technical Summary NASA TND423 June 1960.

10. Kemp, N. H. and Riddell, F. R., "Heat Transfer to Satellite Vehicles Re-entering the Atmosphere", Jet Propulsion 27 (1957) pp. 132-137.

11. Fay, J. A. and Riddell, F. R., "Theory of Stagnation Point Heat Transfer in Dissociated Air", J. Aero. Sci. 25 (Feb. 1958).

12. Lighthill, M. J., "Dynamics of a Dissociating Gas Part I Equilibrium Flow", J. Fluid Mech. 2 (1957) pp. 1-32.

13. Kivel, B. and Bailey, K., Tables of Radiation from High Temperature Air AVCO Research Laboratory RR21 Dec. (1957).

14. Keck, J. C., Comm, J. C., Kivel, B. and Wentink, "Radiation from Hot Air Part II Shock Tube Study of Absolute Intensities", Ann. Phys. 7 (1959) p. 1-38.

15. Myerott, R E., Sokoloff, J. and Nicholls, R. W., "Absorption Coefficients of Air", Geo. Res. Papers No. 68, July 1960 (ASTIA AD 252003).

16. Koh, J. C. Y., "Radiation from Non-isothermal Gas to the Stagnation Point of a Hypersonic Blunt Body", ARS J. 32 (1962) pp. 1374-7.

REFERENCES (Cont.)

17. Kenneth, H. and Strack, S. L., "Stagnation Point Radiation Transfer", ARS J. 31 (1961) pp. 370-2.

18. Stevenson, G. T., Black-Body Radiation Functions NAVWEPS REPORT 7621 (ASTIA AD 273559), 1961.

19. Serbin, H., "Supersonic Flow about Blunt Bodies", J. Aero Sci. 25 (1958) No. 1, p. 58.

20. Lighthill, M. J., "Dynamics of a Dissociating Gas, Part 2 Quasi-Equilibrium Theory", J. Fluid Mech. 8 (1960), No. 2.

21. Corning Materials Handbook, Sixth Ed., April 1963, Corning Glass Works, Corning, New York.

22. Plexiglas Bulletin 53e, Rohm and Haas Co., (Nov. 1962).

23. McMahon, H. O., "Thermal Radiation from Partially Transparent Reflecting Bodies", J. Opt. Soc. of Amer. 40 (1950) No. 6, pp. 376-80.

24. Salvadori, M. G., Numerical Methods in Engineering, Prentice Hall (1952) pp. 72-75.

25. Crout, P. D., "A Short Method for Evaluating Determinants", Trans. AIEE 60, (1941).

26. Carslaw and Jaeger, Conduction of Heat in Solids, Clarendon Press, Oxford (1959) 2nd Ed. p. 112.

27. Vasicek, A., Optics of Thin Films, North-Holland Publ. Co., Amsterdam (1960) Chapter 5.

28. Przemieniecki, J. S., "Design of Transparencies", J. Roy. Aero, Soc. 63 (1959), p. 620.

29. Handbook of Physics and Chem. 34th Ed., Chem. Rubber Publ. Co., Cleveland, p. 2875.

APPENDIX I

ANALYSIS FOR A SINGLE-GLAZE FILMED TRANSPARENCY

TABLE OF CONTENTS

NOMENCLATURE

		Units
ρc	volumetric specific heat	(Watt sec/cm^3 °C)
F	form factor	
h	convection coefficient	(Watt/cm^2 °C)
g, G	intensity	(Watt/cm^2 -ster-μ)
i	index on the spatial coordinate being considered	
I	intensity	(Watt/cm^2 -ster-μ)
j	index on the spatial coordinate of influence	
j_λ	volume emissive power	(Watt/cm^3 -ster-μ)
k	thermal conductivity	(Watt/cm °C)
L	thickness of the slab	(cm)
m	number of wavelength bands	
n	refractive index	
P	auxiliary function defined in test	
p_m	fraction of blackbody energy	
Q	rate of absorption of energy per unit volume	(Watt/cm^3)
S	surface	
t	time	(sec)
T	absolute temperature	(°K)
W	radiant flux	(Watt/cm^2)
X	position coordinate	(cm)
y	auxiliary position coordinate	(cm)
α	angle between the direction of beam (within the slab) and the normal to the slab	(Radians)
β, β_1	angle external to the slab	(Radians)
γ_λ	absorption coefficient	(cm^{-1})
ϵ	emissivity	
λ	wavelength	(μ)
ρ'	directional reflectivity	
ρ'_H	mean reflectivity of surface for diffuse external radiation	
$\rho'_\perp$, $\rho'_\parallel$	directional reflectivity for perpendicularly and parallel polarized radiation, respectively.	
τ'	directional transmissivity of the surface	
ϕ	auxiliary function defined in test	

Subscripts

$\perp$	denotes perpendicularly polarized
$\parallel$	denotes parallel polarized
o	denotes initial or just prior to first reflection
H	denotes external radiation source
i	denotes incident
α, β, β_1	denotes angular dependence on α, β, β_1, respectively
λ	denotes wavelength dependence
A	denotes absorbed from external source
E	denotes emitted
L	denotes at the back surface: X = L
R	denotes reabsorbed
S	denotes surface
X	denotes at position X
$\rightarrow$, $\leftarrow$	denotes direction to the right and left, respectively

Introduction

The basic investigation of window system requirements for advanced aerospace vehicles undertaken under Contract AF 33(657)-9138 required a detailed analysis of heat transferred and temperature distributions in windows occurring during a variety of manned missions. These windows will be subjected to aerodynamic heating as well as thermal radiation as they traverse specified trajectories for these missions. This appendix discusses the derivations and solutions to a single-glaze of partially transparent window material subjected to the thermal environments of hypersonic, supersonic, and orbiting flights. The digital computer program written to solve these problems numerically on the IBM 7090 is discussed and computer program logic is illustrated schematically.

Thermal Analysis

A partially transparent or diathermanous medium such as glass when subjected to an environment of combined convection and radiation heat transfer will absorb thermal energy at its boundary and within its body and will propagate the energy within the glass by the combined mechanisms of conduction and radiation. Within a transparent medium, the temperature distribution is governed by the equation:

$$\rho c \frac{\partial T_i}{\partial t} = \sum_j q'''_i(T_j) + k \frac{\partial^2 T_i}{\partial X^2} \qquad (16)$$

where ρc = volumetric specific heat

T = temperature

t = time

k = "true" thermal conductivity

X = spatial coordinate

q''' = energy absorbed per unit volume per unit time

i = index on the spatial coordinate being considered

j = index on the spatial coordinate of influence

The nature of simultaneous transport of energy by conduction and radiation inherent in partially transparent materials requires the study and formulation of the mechanisms by which energy is exchanged and influenced at any level within the medium by surrounding levels in the medium and by external sources. The conduction represented by the last term of equation (16) is relatively straightforward and requires no further explanation. However, the radiant term requires considerable development and is dealt with in detail.

The flux absorbed from radiations in the transparent portion of the spectrum at any level, X, within or at the surface of the transparent medium may be expressed per unit volume as:

$$\sum_j q'''_i(T_j) = Q_A(X_i) - Q_E(X_i) + Q_R(X_i) \qquad (17)$$

Thus, an elemental slice of material at X_i will absorb flux from external radiations, $Q_A(X_i)$; will emit, $Q_E(X_i)$, its own radiation, and will re-absorb radiations, $Q_R(X_i)$, from other elemental slices within the medium. Each of these terms is derived individually in the following sections.

Multiple Reflections of a Single Beam

As a preliminary step to the derivation of the expression for radiation absorbed from external sources, consider a monochromatic, perpendicularly polarized beam of intensity g_o arriving at the internal boundary of a partially transparent medium at an angle of incidence, α, as shown in Figure 57. The two bounding surfaces have directional reflectivities, ρ and ρ_1, for the exposed and internal surfaces, respectively. At the internal surface the beam is partially refracted and partially reflected. The reflected component is attenuated as it passes through the sheet, partially re-reflected at the external boundary whence it is attenuated further by refraction and the balance is re-reflected over and over again. A layer of thickness δX within the glazing, at a distance X from the exposed surface, is traversed by multiple reflected beams in both directions. Let g^I, g^{II}, g^{III}, g^{IV},.... denote the intensities of these beams as they pass through the layer δX the first, second, third, etc. time. Then:

$$g_{\longrightarrow} = g^{II} + g^{IV} + g^{VI} + \ldots.$$

and

$$g_{\longleftarrow} = g^{I} + g^{III} + g^{V} + \ldots. \qquad (18)$$

represent the sums of intensities traveling, respectively, to the right and to the left. The intensity of each of these beams is:

$$\begin{aligned}
g^I &= g_o\rho_1 e^{-\gamma(L - X)\sec\alpha} \\
g^{II} &= g_o\rho\rho_1 e^{-\gamma L \sec\alpha}\left(e^{-\gamma X \sec\alpha}\right) \\
g^{III} &= g_o\rho\rho_1^2 e^{-2\gamma L \sec\alpha}\left(e^{-\gamma(L - X)\sec\alpha}\right) \\
g^{IV} &= g_o\rho^2\rho_1^2 e^{-3\gamma L \sec\alpha}\left(e^{-\gamma X \sec\alpha}\right) \\
g^{V} &= g_o\rho^2\rho_1^3 e^{-4\gamma L \sec\alpha}\left(e^{-\gamma(L - X)\sec\alpha}\right) \\
g^{VI} &= g_o\rho^3\rho_1^3 e^{-5\gamma L \sec\alpha}\left(e^{-\gamma X \sec\alpha}\right) \qquad (19)
\end{aligned}$$

so that equations (18) become:

$$\begin{aligned}
g_{\longrightarrow} &= g_o\rho\rho_1 e^{-\gamma(L + X)\sec\alpha}\left[1 + \rho\rho_1 e^{-2\gamma L \sec\alpha} + \rho^2\rho_1^2 e^{-4\gamma L \sec\alpha} + \ldots\right] \\
g_{\longleftarrow} &= g_o\rho_1 e^{-\gamma(L - X)\sec\alpha}\left[1 + \rho\rho_1 e^{-2\gamma L \sec\alpha} + \rho^2\rho_1^2 e^{-4\gamma L \sec\alpha} + \ldots\right] \qquad (20)
\end{aligned}$$

where, for the sake of brevity, the subscripts have been omitted and:

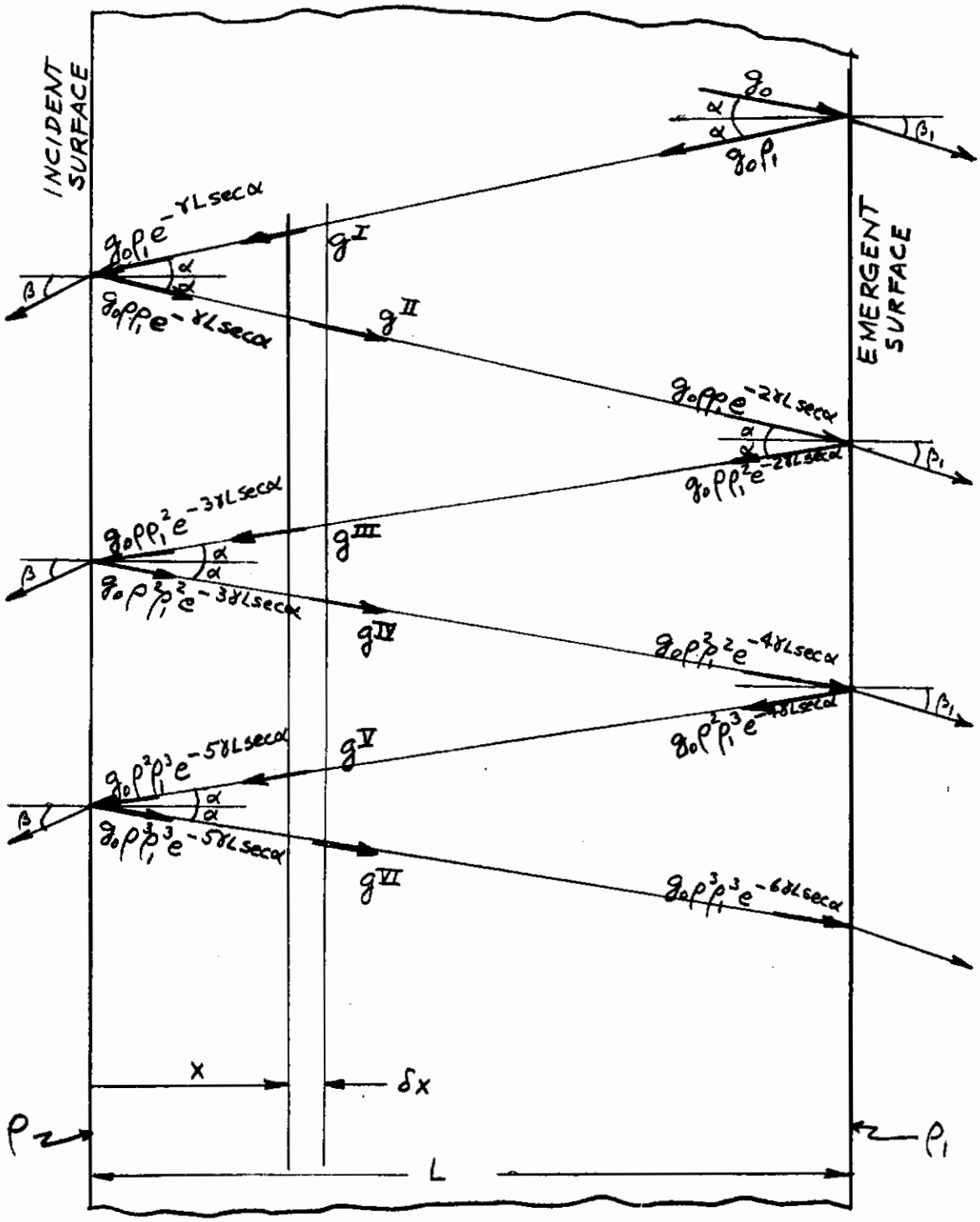

Figure 57 MULTIPLE REFLECTIONS OF A SINGLE BEAM

ρ, ρ_1 = fractional reflectivities of the exposed and internal surfaces, respectively

γ = spectral absorption coefficient

L = thickness of the glazing

α = angle of incidence, and

X = ccordinate of layer δX

The total intensity of beams crossing δX therefore is:

$$g^* = g_{\longrightarrow} + g_{\longleftarrow}$$

$$g^* = g_o\rho_1 \{ \rho e^{-\gamma(L + X) \sec \alpha} [1 + \rho\rho_1 e^{-2\gamma L \sec \alpha} + \rho^2\rho_1^2 e^{-4\gamma L \sec \alpha} + \ldots] + e^{-\gamma(L - X) \sec \alpha} [1 + \rho\rho_1 e^{-2\gamma L \sec \alpha} + \rho^2\rho_1^2 e^{-4\gamma L \sec \alpha}] \} \quad (21)$$

Each of the bracketed expressions above form a geometric series. Equation (21) may therefore be written in closed form as:

$$g^* = g_o\rho_1 \left\{ \frac{\rho e^{-\gamma(L + X) \sec \alpha}}{1 - \rho\rho_1 e^{-2\gamma L \sec \alpha}} + \frac{e^{-\gamma(L - X) \sec \alpha}}{1 - \rho\rho_1 e^{-2\gamma L \sec \alpha}} \right\}$$

or

$$g^* = \frac{g_o \rho_1}{1 - \rho\rho_1 e^{-2\gamma L \sec \alpha}} \{\rho e^{-\gamma(L + X) \sec \alpha} + e^{-\gamma(L - X) \sec \alpha}\} \quad (22)$$

Including the necessary subscripts, equation (22) becomes:

$$g^*_{\lambda\alpha X\perp} = \frac{g_{\lambda\alpha o\perp} \rho'_{1\perp}}{1 - \rho'_\perp\rho'_{1\perp} e^{-2\gamma L \sec \alpha}} \{ \rho'_\perp e^{-\gamma_\lambda(L + X) \sec \alpha} + e^{-\gamma_\lambda(L - X) \sec \alpha} \} \quad (23)$$

A similar expression may be written for parallel polarized, monochromatic beams:

$$g^*_{\lambda\alpha X\parallel} = \frac{g_{\lambda\alpha o\parallel} \rho'_{1\parallel}}{1 - \rho'_\parallel\rho'_{1\parallel} e^{-2\gamma_\lambda L \sec \alpha}} \{ \rho'_\parallel e^{-\gamma_\lambda(L + X) \sec \alpha} + e^{-\gamma_\lambda(L - X) \sec \alpha} \} \quad (24)$$

For initially unpolarized beams it follows that:

$$g^*_{\lambda\alpha X} = \frac{g_{\lambda\alpha o}}{1 + \frac{\tau'_{||}}{\tau'_{\perp}}} \left\{ \frac{\rho'_{1\perp}\, e^{-\gamma_\lambda L \sec\alpha}}{1 - \rho'_{\perp}\rho'_{1\perp}\, e^{-2\gamma_\lambda L \sec\alpha}} \left[\rho'_{\perp}\, e^{-\gamma_\lambda X \sec\alpha} + e^{+\gamma_\lambda X \sec\alpha} \right] \right. \tag{25}$$

$$\left. + \frac{\tau'_{||}}{\tau'_{\perp}} \frac{\rho'_{1||}\, e^{-\gamma_\lambda L \sec\alpha}}{1 - \rho_{||}\rho'_{1||}\, e^{-2\gamma_\lambda L \sec\alpha}} \left[\rho'_{||}\, e^{-\gamma_\lambda X \sec\alpha} + e^{+\gamma_\lambda X \sec\alpha} \right] \right\}$$

Equation (25) expresses the total intensity at a position X due to multiple reflections of a beam arriving at an internal boundary with an intensity of $g_{\lambda\alpha o}$.

Absorption of External Radiation

Consider a partially transparent glazing exposed to a radiant flux W_H during a time increment t to t + Δt. If the flux is perfectly diffuse the intensity of beams incident upon a plane surface at an angle β is:

$$I_{H\lambda\beta} = \frac{W_{H\lambda}}{\pi} \cos\beta \tag{26}$$

At the incident surface the beams are partially reflected and partially refracted. Their refracted portion enters the glazing at an angle α and has the intensity

$$I_{H\lambda\alpha o} = I_{H\lambda\beta} n^2 \frac{\cos\alpha}{\cos\beta} \tau' \tag{27}$$

where for initially unpolarized, incident beams

$$\tau' = \frac{1}{2}(\tau'_{\perp} + \tau'_{||}) \tag{28}$$

Thus, the intensity of a beam originating from a diffuse source, arriving at an angle of incidence β, and refracted into a material of index of refraction n_2 from a medium of refractive index n_1 is:

$$I_{H\lambda\alpha o} = \frac{W_{H\lambda}}{\pi} \left(\frac{n_2}{n_1}\right)^2 \cos\alpha\, \tau' \tag{29}$$

The refracted beams are partially absorbed as they traverse the glazing. They reach the level X within the glazing with an intensity:

$$I^*_{H\lambda\alpha X \longrightarrow} = \frac{W_{H\lambda}}{\pi} \left(\frac{n_2}{n_1}\right)^2 \tau' \cos\alpha\, e^{-\gamma_\lambda X \sec\alpha} \tag{30}$$

The level X is also traversed by multiple reflections of the beam originating from the outside the glazing. The intensity of the refracted beam just prior to the first refraction at the interior boundary is:

$$I_{H\lambda\alpha L} = \frac{W_{H\lambda}}{\pi}\left(\frac{n_2}{n_1}\right)^2 \tau' \cos\alpha\, e^{-\gamma_\lambda L \sec\alpha} \tag{31}$$

Thus the treatment for multiple reflections of $I_{H\lambda\alpha L}$ takes the same form as that for $g_{\lambda\alpha_o}$ of equation (25). The sum of the intensities, at level X, for all multiple reflections is, therefore:

$$I^*_{H\lambda\alpha X} = \frac{W_{H\lambda}}{\pi} \frac{\left(\frac{n_2}{n_1}\right)^2 \tau' \cos\alpha\, e^{-\gamma_\lambda L \sec\alpha}}{1 + \frac{\tau'_{\parallel}}{\tau'_{\perp}}} \left\{ \frac{\rho'_{1\perp}\, e^{-\gamma_\lambda L \sec\alpha}}{1 - \rho'_{\perp}\rho'_{1\perp}\, e^{-2\gamma_\lambda L \sec\alpha}} \right.$$

$$\left[\rho'_{\perp}\, e^{-\gamma_\lambda X \sec\alpha} + e^{+\gamma_\lambda X \sec\alpha}\right] + \frac{\tau'_{\parallel}}{\tau'_{\perp}} \frac{\rho'_{1\parallel} e^{-\gamma_\lambda L \sec\alpha}}{1 - \rho_{\parallel}\rho'_{1\parallel}\, e^{-2\gamma_\lambda L \sec\alpha}} \tag{32}$$

$$\left.\left[\rho'_{\parallel}\, e^{-\gamma_\lambda X \sec\alpha} + e^{+\gamma_\lambda X \sec\alpha}\right]\right\}$$

The total spectral intensity of all beams at level X is then:

$$I_{H\lambda\alpha X} = I^*_{H\lambda\alpha X \rightarrow} + I^*_{H\lambda\alpha X}$$

$$I_{H\lambda\alpha X} = \frac{W_{H\lambda}}{\pi}\left(\frac{n_2}{n_1}\right)^2 \tau' \cos\alpha \left\{ e^{-\gamma_\lambda X \sec\alpha} + \frac{e^{-2\gamma_\lambda L \sec\alpha}}{1 + \frac{\tau'_{\parallel}}{\tau'_{\perp}}} \left[\frac{\rho'_{1\perp}}{1 - \rho'_{\perp}\rho'_{1\perp} e^{-2\gamma_\lambda L \sec\alpha}}\right.\right.$$

$$\left.\left.\left(\rho'_{\perp}\, e^{-\gamma_\lambda X \sec\alpha} + e^{+\gamma_\lambda X \sec\alpha}\right) + \frac{\tau'_{\parallel}}{\tau'_{\perp}} \frac{\rho'_{1\parallel}}{1 - \rho'_{\parallel}\rho'_{1\parallel}\, e^{-2\gamma_\lambda L \sec\alpha}} \left(\rho'_{\parallel}\, e^{-\gamma_\lambda X \sec\alpha} + e^{+\gamma_\lambda X \sec\alpha}\right)\right]\right\} \tag{33}$$

To determine the rate of absorption of energy from these beams consider an elemental slice of material at X, having a thickness δX. The path of beams through the slice is

$$\delta S = \delta X \sec\alpha$$

By the Lambert-Bouguer Law

$$I_\lambda = I_{o\lambda}\, e^{-\gamma_\lambda \delta S}$$

is transmitted, or in other words, a fraction

$$1 - \frac{I_\lambda}{I_{o\lambda}} = 1 - e^{-\gamma_\lambda \delta S}$$

is absorbed within the increment. Therefore the absorbed intensity in a slice δX is:

$$\delta I_{H\lambda\alpha X} = (1 - e^{-\gamma_\lambda \delta S}) I_{H\lambda\alpha X} \tag{34}$$

Actually, beams from outside the glazing cross the glazing at all angles varying from zero to the critical angle, α_{cr}. The intensity of all these beams is reduced in their passage through the slice. The corresponding rate of accumulation of energy within the slice is equal to the rate of absorption of spectral flux:

$$\delta W_{H\lambda X} = 2\left(\frac{n_2}{n_1}\right)^2 \delta X \, W_{H\lambda} \phi(X)$$

where

$$\phi(X) = \int_0^{\alpha_{cr}} \tau' \left\{ e^{-\gamma_\lambda X \sec\alpha} + \frac{e^{-2\gamma_\lambda L \sec\alpha}}{1 + \frac{\tau'_{||}}{\tau'_{\perp}}} \left[\frac{\rho'_{1\perp}}{1 - \rho'_{\perp}\rho'_{1\perp} e^{-2\gamma_\lambda L \sec\alpha}} \right.\right.$$

$$\left. (\rho'_{\perp} e^{-\gamma_\lambda X \sec\alpha} + e^{+\gamma_\lambda X \sec\alpha}) + \frac{\tau'_{||}}{\tau'_{\perp}} \frac{\rho'_{1||}}{1 - \rho'_{||}\rho'_{1||} e^{-2\gamma_\lambda L \sec\alpha}} \right. \tag{35}$$

$$\left.\left. (\rho'_{||} e^{-\gamma_\lambda X \sec\alpha} + e^{+\gamma_\lambda X \sec\alpha}) \right] \right\} \left(\frac{1 - e^{-\gamma_\lambda \delta X \sec\alpha}}{\delta X}\right) \sin\alpha \cos\alpha \, d\alpha$$

The absorption of spectral flux per unit volume is:

$$Q_{A\lambda}(X) = \frac{\delta W_{H\lambda X}}{\delta X}$$

so that the integral over-all wavelengths yield the total rate of absorption of radiation energy per unit volume as

$$Q_A(X) = 2\left(\frac{n_2}{n_1}\right)^2 \int_0^\infty W_{H\lambda} \phi \, d\lambda \tag{36}$$

Internal Emission

If at any time the temperature of a layer at a position X in the glazing is known, the spectral volume emissive power is given by:

$$j_\lambda(X) = \frac{\left(\frac{n_2}{n_1}\right)^2 \gamma_\lambda W_{B\lambda}(X)}{\pi} \tag{37}$$

where $W_{B\lambda}$ is the hemispherical spectral emissive power of a blackbody radiator at the given temperature. The rate of internal emission of radiation

per unit volume at the level X is therefore:

$$Q_E(X) = 4\pi \int_0^\infty j_\lambda(X)\, d\lambda$$

or

$$Q_E(X) = 4\left(\frac{n_2}{n_1}\right)^2 \int_0^\infty \gamma_\lambda W_{B\lambda}(X)\, d\lambda \qquad (38)$$

Re-Absorption of Internally Emitted Radiation

Radiation emitted at any one level within a partially transparent material is partly radiated from the material and partly re-absorbed at other levels within the material. To determine the rate that energy is re-absorbed at level X it is necessary to consider the rate of emission from all other levels, such as y. Any time the temperature at y is known the volume emissive power $J_\lambda(y)$ is also known.

Primary Radiation-Re-Absorption

An elemental slice at y of thickness δy emits radiation having in its respective direction the intensity:

$$\delta I_{\lambda \rightarrow} = j_{\lambda \rightarrow}(y)\, \delta y \qquad \text{and} \qquad \delta I_{\lambda \leftarrow} = j_{\lambda \leftarrow}(y)\, \delta y$$

These beams are attenuated by absorption as they traverse the glazing. They reach the level X within the glazing with the intensities:

$$\delta I_{\lambda \alpha X \rightarrow} = j_{\lambda \rightarrow}(y)\, \delta y\, e^{-\gamma_\lambda (X - y) \sec \alpha} \qquad \text{for } X > y$$

and

$$\delta I_{\lambda \alpha X \leftarrow} = j_{\lambda \leftarrow}(y)\, \delta y\, e^{-\gamma_\lambda (y - X) \sec \alpha} \qquad \text{for } X < y \qquad (39)$$

Thus the total spectral intensity of all the primary beams (emitted within the glazing) at an angle α and crossing X in either direction is:

$$I_{\lambda \alpha X} = \int_0^X j_{\lambda \rightarrow}(y)\, e^{-\gamma_\lambda (X - y) \sec \alpha}\, dy + \int_X^L j_{\lambda \leftarrow}(y)\, e^{-\gamma_\lambda (y - X) \sec \alpha}\, dy$$

$$+ \epsilon' \frac{W_{B\lambda}(0)}{\pi} \cos \alpha\, e^{-\gamma_\lambda X \sec \alpha} + \epsilon_1' \frac{W_{B\lambda}(L)}{\pi} \cos \alpha\, e^{-\gamma_\lambda (L - X) \sec \alpha} \qquad (40)$$

At the level X the beams cross an elemental slice of the material of thickness δX so that their paths are

$$\delta X \sec \alpha$$

and their intensity is reduced as

$$\delta I^*_{\lambda\alpha X} = (1 - e^{-\gamma_\lambda \delta X \sec\alpha})\, I_{\lambda\alpha X} \tag{41}$$

The spectral flux absorbed in the slice is the sum of intensities absorbed from the beams traversing the slice in all directions so that:

$$\delta W^*_{\lambda X} = 2\int_0^{\pi/2} \sin\alpha\,(1 - e^{-\gamma_\lambda \delta X \sec\alpha})\left[\left(\frac{n_2}{n_1}\right)^2 \int_0^L \gamma_\lambda(y) W_{B\lambda}(y)\, e^{-\gamma_\lambda |X - y| \sec\alpha}\, dy\right.$$

$$\left. + \epsilon' W_{B\lambda}(0) \cos\alpha\, e^{-\gamma_\lambda X \sec\alpha} + \epsilon_1' W_{B\lambda}(L) \cos\alpha\, e^{-\gamma_\lambda (L - X)\sec\alpha}\right] d\alpha \tag{42}$$

Let:

$$P_1 = \int_0^{\pi/2} \sin\alpha (1 - e^{-\gamma_\lambda \delta X \sec\alpha})\, e^{-\gamma_\lambda |X - y| \sec\alpha}\, d\alpha$$

$$P_2 = \int_0^{\pi/2} \epsilon' \sin\alpha \cos\alpha\, (1 - e^{-\gamma_\lambda \delta X \sec\alpha})\, e^{-\gamma_\lambda X \sec\alpha}\, d\alpha \tag{43}$$

$$P_3 = \int_0^{\pi/2} \epsilon_1' \sin\alpha \cos\alpha\, (1 - e^{-\gamma_\lambda \delta X \sec\alpha})\, e^{-\gamma_\lambda (L - X)\sec\alpha}\, d\alpha$$

then

$$\delta W^*_{\lambda X} = 2\left\{\left(\frac{n_2}{n_1}\right)^2 \int_0^L \gamma_\lambda(y)\, W_{B\lambda}(y)\, P_1\, dy + P_2\, W_{B\lambda}(0) + P_3\, W_{B\lambda}(L)\right\} \tag{44}$$

which is the expression for the flux absorbed in an element δX at X due to primary radiation from y.

Multiple Reflections of Double Beams

Consider two internally generated beams (monochromatic, perpendicularly polarized) which arrive at their respective surfaces with the intensities: G_o and g_o as shown in Figure 58. At the surface they are partly refracted and partly reflected. Their reflected components are attenuated as they pass through the thickness of the glazing, partly re-reflected at the other surface and attenuated further again and again. At the level X the two beams cross the element δX with each reflection and they may be summed in the following manner:

$$G_{\rightarrow} = G^{I} + G^{III} + G^{V} + \ldots.$$
$$G_{\leftarrow} = G^{II} + G^{IV} + G^{VI} + \ldots.$$
$$g_{\rightarrow} = g^{II} + g^{IV} + g^{VI} + \ldots.$$
$$g_{\leftarrow} = g^{I} + g^{III} + g^{V} + \ldots.$$

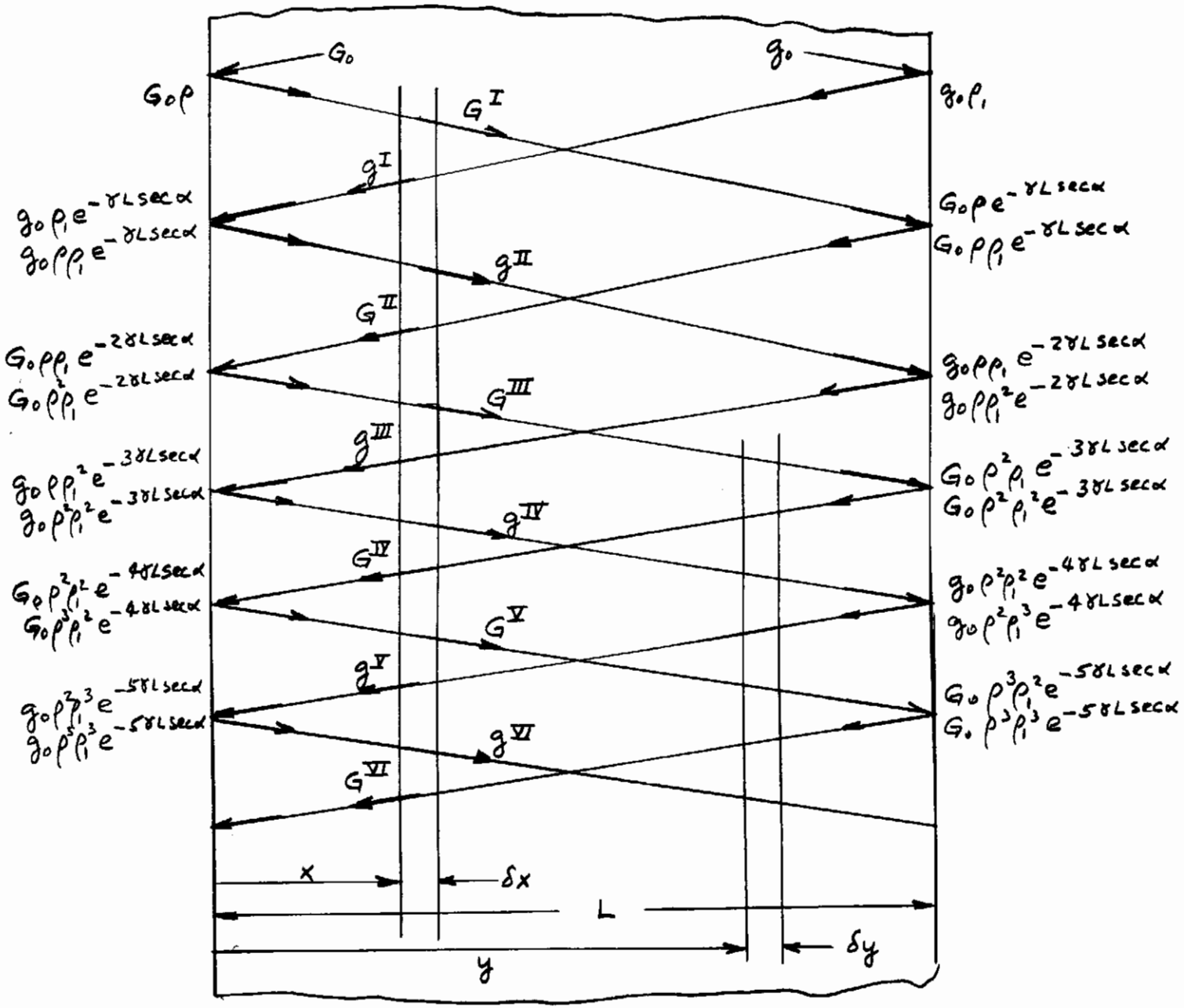

Figure 58 MULTIPLE REFLECTIONS OF A DOUBLE BEAM

where the individual intensities are:

$$
\begin{aligned}
G^{I} &= G_o \rho e^{-\gamma X \sec\alpha} \\
G^{II} &= G_o \rho \rho_1 e^{-\gamma L \sec\alpha} (e^{-\gamma(L - X)\sec\alpha}) \\
G^{III} &= G_o \rho^2 \rho_1 e^{-2\gamma L \sec\alpha} (e^{-\gamma X \sec\alpha}) \\
G^{IV} &= G_o \rho^2 \rho_1^2 e^{-3\gamma L \sec\alpha} (e^{-\gamma(L - X)\sec\alpha}) \\
G^{V} &= G_o \rho^3 \rho_1^2 e^{-4\gamma L \sec\alpha} (e^{-\gamma X \sec\alpha}) \\
G^{VI} &= G_o \rho^3 \rho_1^3 e^{-5\gamma L \sec\alpha} (e^{-\gamma(L - X)\sec\alpha})
\end{aligned} \tag{45}
$$

and

$$
\begin{aligned}
g^{I} &= g_o \rho_1 e^{-\gamma(L - X)\sec\alpha} \\
g^{II} &= g_o \rho \rho_1 e^{-\gamma L \sec\alpha} (e^{-\gamma X \sec\alpha}) \\
g^{III} &= g_o \rho \rho_1^2 e^{-2\gamma L \sec\alpha} (e^{-\gamma(L - X)\sec\alpha}) \\
g^{IV} &= g_o \rho^2 \rho_1^2 e^{-3\gamma L \sec\alpha} (e^{-\gamma X \sec\alpha}) \\
g^{V} &= g_o \rho^2 \rho_1^3 e^{-4\gamma L \sec\alpha} (e^{-\gamma(L - X)\sec\alpha}) \\
g^{VI} &= g_o \rho^3 \rho_1^3 e^{-5\gamma L \sec\alpha} (e^{-\gamma X \sec\alpha})
\end{aligned}
$$

Thus by substitution

$$
\begin{aligned}
G_{\rightarrow} &= G_o \rho e^{-\gamma X \sec\alpha} [1 + \rho\rho_1 e^{-2\gamma L \sec\alpha} + \rho^2\rho_1^2 e^{-4\gamma L \sec\alpha} + \ldots] \\
G_{\leftarrow} &= G_o \rho\rho_1 e^{-\gamma(2L - X)\sec\alpha} [1 + \rho\rho_1 e^{-2\gamma L \sec\alpha} + \rho^2\rho_1^2 e^{-4\gamma L \sec\alpha} + \ldots] \\
g_{\rightarrow} &= g_o \rho\rho_1 e^{-\gamma(L + X)\sec\alpha} [1 + \rho\rho_1 e^{-2\gamma L \sec\alpha} + \rho^2\rho_1^2 e^{-4\gamma L \sec\alpha} + \ldots] \\
g_{\leftarrow} &= g_o \rho_1 e^{-\gamma(L - X)\sec\alpha} [1 + \rho\rho_1 e^{-2\gamma L \sec\alpha} + \rho^2\rho_1^2 e^{-4\gamma L \sec\alpha} + \ldots]
\end{aligned} \tag{46}
$$

Summing all beams crossing δX and noting that the bracketed terms in equation (46) are a geometric series results in:

$$
\begin{aligned}
G^{**} = &\frac{G_o \rho}{1 - \rho\rho_1 e^{-2\gamma L \sec\alpha}} [e^{-\gamma X \sec\alpha} + \rho_1 e^{-\gamma(2L - X)\sec\alpha}] \\
&+ \frac{g_o \rho_1}{1 - \rho\rho_1 e^{-2\gamma L \sec\alpha}} [e^{-\gamma(L - X)\sec\alpha} + \rho e^{-\gamma(L + X)\sec\alpha}]
\end{aligned} \tag{47}
$$

With the appropriate subscripts equation (47) may be written for perpendicularly and parallel polarized beams as:

$$G^{**}_{\lambda\alpha X\perp} = \frac{G_{\lambda\alpha o\perp}\,\rho'_{\perp}}{1 - \rho'_{\perp}\rho'_{1\perp}\,e^{-2\gamma_\lambda L \sec\alpha}}\left[e^{-\gamma_\lambda X \sec\alpha} + \rho'_{1\perp}e^{-\gamma_\lambda(2L - X)\sec\alpha}\right]$$

$$+ \frac{g_{\lambda\alpha o\perp}\,\rho'_{1\perp}}{1 - \rho_{\perp}\rho'_{1\perp}e^{-2\gamma_\lambda L \sec\alpha}}\left[e^{-\gamma_\lambda(L - X)\sec\alpha} + \rho'_{\perp}\,e^{-\gamma_\lambda(L + X)\sec\alpha}\right] \tag{48}$$

and

$$G^{**}_{\lambda\alpha X\,\mathrm{II}} = \frac{G_{\lambda\alpha o\,\mathrm{II}}\,\rho'_{\mathrm{II}}}{1 - \rho'_{\mathrm{II}}\,\rho'_{1\,\mathrm{II}}\,e^{-2\gamma_\lambda L \sec\alpha}}\left[e^{-\gamma_\lambda X \sec\alpha} + \rho'_{1\,\mathrm{II}}e^{-\gamma_\lambda(2L - X)\sec\alpha}\right]$$

$$+ \frac{g_{\lambda\alpha o\,\mathrm{II}}\,\rho'_{1\,\mathrm{II}}}{1 - \rho'_{\mathrm{II}}\,\rho'_{1\,\mathrm{II}}e^{-2\gamma_\lambda L \sec\alpha}}\left[e^{-\gamma_\lambda(L - X)\sec\alpha} + \rho'_{\mathrm{II}}\,e^{-\gamma_\lambda(L + X)\sec\alpha}\right] \tag{49}$$

Summing the polarized components:

$$G^{**}_{\lambda\alpha X} = G^{**}_{\lambda\alpha X\perp} + G^{**}_{\lambda\alpha X\,\mathrm{II}}$$

and since all internally generated beams are non-polarized it follows that:

$$G_{\lambda\alpha o\perp} = G_{\lambda\alpha o\,\mathrm{II}} = \frac{1}{2}\,G_{\lambda\alpha o}$$

and

$$g_{\lambda\alpha o\perp} = g_{\lambda\alpha o\,\mathrm{II}} = \frac{1}{2}\,g_{\lambda\alpha o}$$

The sum becomes:

$$G^{**}_{\lambda\alpha X} = \frac{1}{2}\,G_{\lambda\alpha o}\left\{\left[\frac{\rho'_{\perp}}{1 - \rho'_{\perp}\rho'_{1\perp}\,e^{-2\gamma_\lambda L \sec\alpha}} + \frac{\rho'_{\mathrm{II}}}{1 - \rho'_{\mathrm{II}}\rho'_{1\,\mathrm{II}}e^{-2\gamma_\lambda L \sec\alpha}}\right]e^{-\gamma_\lambda X \sec\alpha}\right.$$

$$\left. + \left[\frac{\rho'_{\perp}\,\rho'_{1\perp}}{1 - \rho'_{\perp}\rho'_{1\perp}e^{-2\gamma_\lambda L \sec\alpha}} + \frac{\rho'_{\mathrm{II}}\,\rho'_{1\,\mathrm{II}}}{1 - \rho'_{\mathrm{II}}\,\rho'_{1\,\mathrm{II}}e^{-2\gamma_\lambda L \sec\alpha}}\right]e^{-\gamma_\lambda(2L - X)\sec\alpha}\right\}$$

$$+ \frac{1}{2}\,g_{\lambda\alpha o}\left\{\left[\frac{\rho'_{1\perp}}{1 - \rho'_{\perp}\rho'_{1\perp}e^{-2\gamma_\lambda L \sec\alpha}} + \frac{\rho'_{1\,\mathrm{II}}}{1 - \rho'_{\mathrm{II}}\rho'_{1\,\mathrm{II}}e^{-2\gamma_\lambda L \sec\alpha}}\right]e^{-\gamma_\lambda(L - X)\sec\alpha}\right.$$

$$\left. + \left[\frac{\rho'_{\perp}\rho'_{1\perp}}{1 - \rho'_{\perp}\rho'_{1\perp}e^{-2\gamma_\lambda L \sec\alpha}} + \frac{\rho'_{\mathrm{II}}\,\rho'_{1\,\mathrm{II}}}{1 - \rho'_{\mathrm{II}}\rho'_{1\,\mathrm{II}}e^{-2\gamma_\lambda L \sec\alpha}}\right]e^{-\gamma_\lambda(L + X)\sec\alpha}\right\} \tag{50}$$

Let:

$$P'_1 = \frac{1}{2}\left[\frac{\rho'_\perp}{1 - \rho'_\perp \rho'_{1\perp} e^{-2\gamma_\lambda L \sec\alpha}} + \frac{\rho'_{||}}{1 - \rho'_{||}\rho'_{1||} e^{-2\gamma_\lambda L \sec\alpha}}\right]$$

$$P'_2 = \frac{1}{2}\left[\frac{\rho'_{1\perp}}{1 - \rho'_\perp \rho'_{1\perp} e^{-2\gamma_\lambda L \sec\alpha}} + \frac{\rho'_{1||}}{1 - \rho'_{||}\rho'_{1||} e^{-2\gamma_\lambda L \sec\alpha}}\right] \qquad (51)$$

$$P'_{12} = \frac{1}{2}\left[\frac{\rho'_\perp \rho'_{1\perp}}{1 - \rho'_\perp \rho'_{1\perp} e^{-2\gamma_\lambda L \sec\alpha}} + \frac{\rho'_{||}\rho'_{1||}}{1 - \rho'_{||}\rho'_{1||} e^{-2\gamma_\lambda L \sec\alpha}}\right]$$

Then equation (50) becomes:

$$G^{**}_{\lambda\alpha X} = G_{\lambda\alpha o}\left\{P'_1 e^{-\gamma_\lambda X \sec\alpha} + P'_{12} e^{-\gamma_\lambda (2L - X)\sec\alpha}\right\}$$

$$+ g_{\lambda\alpha o}\left\{P'_2 e^{-\gamma_\lambda (L - X)\sec\alpha} + P'_{12} e^{-\gamma_\lambda (L + X)\sec\alpha}\right\} \qquad (52)$$

which is the expression for the total intensity crossing a position X due to multiple reflections of two beams arriving at respective internal boundaries with intensities $G_{\lambda\alpha o}$ and $g_{\lambda\alpha o}$.

Re-Absorption of Multiply Reflected Radiation

A part of the internally emitted radiation is multiply reflected between the surfaces of the glazing so that it will traverse the elemental slice again and again. Upon each traversal more of it is absorbed. The intensity of the beam just prior to the first reflection emanating from a layer δy at y is:

$$I^*_{\lambda\alpha o} = \int_o^L j_\lambda(y) \overleftarrow{\;} e^{-\gamma_\lambda y \sec\alpha}\, dy + \epsilon'_1 \frac{W_{B\lambda}(L)}{\pi} \cos\alpha\, e^{-\gamma_\lambda L \sec\alpha}$$

and

$$i^*_{\lambda\alpha o} = \int_o^L j_\lambda(y) \overrightarrow{\;} e^{-\gamma_\lambda (L - y)\sec\alpha}\, dy + \epsilon' \frac{W_{B\lambda}(0)}{\pi} \cos\alpha\, e^{-\gamma_\lambda L \sec\alpha} \qquad (53)$$

In the treatment of multiple reflections of double beams it is seen that the following identities are true:

$$I^*_{\lambda\alpha o} \equiv G_{\lambda\alpha o} \qquad \text{and} \qquad i^*_{\lambda\alpha o} \equiv g_{\lambda\alpha o}$$

So that substituting into equation (52)

$$I^{**}_{\lambda\alpha X} = I^*_{\lambda\alpha o}\left[P'_1 e^{-\gamma_\lambda X \sec\alpha} + P'_{12} e^{-\gamma_\lambda (2L - X)\sec\alpha}\right]$$

$$+ i^*_{\lambda\alpha o}\left[P'_2 e^{-\gamma_\lambda (L - X)\sec\alpha} + P'_{12} e^{-\gamma_\lambda (L + X)\sec\alpha}\right]$$

Or, by equations (53):

$$I^{**}_{\lambda\alpha X} = \Big[\int_0^L j_\lambda(y) \, e^{-\gamma_\lambda y \sec\alpha} dy + \epsilon_1' \frac{W_{B\lambda}(L)}{\pi} \cos\alpha \, e^{-\gamma_\lambda L \sec\alpha} \Big] \quad (\leftarrow)$$

$$\Big[P_1' \, e^{-\gamma_\lambda X \sec\alpha} + P_{12}' \, e^{-\gamma_\lambda (2L - X) \sec\alpha} \Big]$$

$$+ \Big[\int_0^L j_\lambda(y) \, e^{-\gamma_\lambda (L - y) \sec\alpha} \, dy + \epsilon' \frac{W_{B\lambda}(0)}{\pi} \cos\alpha \, e^{-\gamma_\lambda L \sec\alpha} \Big] \quad (\rightarrow)$$

$$\Big[P_2' \, e^{-\gamma_\lambda (L - X) \sec\alpha} + P_{12}' \, e^{-\gamma_\lambda (L + X) \sec\alpha} \Big] \qquad (54)$$

A fraction $(1 - e^{-\gamma_\lambda \delta X \sec\alpha})$ of the intensity $I^{**}_{\lambda\alpha X}$ is absorbed as it traverses δX. Thus, the rate of absorption of spectral flux becomes:

$$\delta W^{**}_{\lambda X} = 2\Big\{ \Big(\frac{n_2}{n_1}\Big)^2 \int_0^L \gamma_\lambda(y) W_{B\lambda}(y) P_i \, dy + W_{B\lambda}(L) \, P_{i1}$$

$$+ \Big(\frac{n_2}{n_1}\Big)^2 \int_0^L \gamma_\lambda(y) W_{B\lambda}(y) P_j \, dy + W_{B\lambda}(0) P_{j1} \Big\} \qquad (55)$$

where

$$P_i = \int_0^{\pi/2} \Big[P_1' \, e^{-\gamma_\lambda X \sec\alpha} + P_{12}' \, e^{-\gamma_\lambda (2L - X) \sec\alpha} \Big] \, e^{-\gamma_\lambda y \sec\alpha} \sin\alpha$$

$$(1 - e^{-\gamma_\lambda \delta X \sec\alpha}) \, d\alpha$$

$$P_{i1} = \int_0^{\pi/2} \epsilon_1' \sin\alpha \cos\alpha \, (1 - e^{-\gamma_\lambda \delta X \sec\alpha}) \Big[P_1' \, e^{-\gamma_\lambda X \sec\alpha} + P_{12}' \, e^{-\gamma_\lambda (2L - X) \sec\alpha} \Big]$$

$$e^{-\gamma_\lambda I \sec\alpha} \, d\alpha$$

$$P_j = \int_0^{\pi/2} \Big[P_2' \, e^{-\gamma_\lambda (L - X) \sec\alpha} + P_{12}' \, e^{-\gamma_\lambda (L + X) \sec\alpha} \Big] e^{-\gamma_\lambda (L - y) \sec\alpha} \sin\alpha$$

$$(1 - e^{-\gamma_\lambda \delta X \sec\alpha}) \, d\alpha$$

$$P_{j1} = \int_0^{\pi/2} \epsilon' \sin\alpha \cos\alpha \, (1 - e^{-\gamma_\lambda \delta X \sec\alpha}) \Big[P_2' \, e^{-\gamma_\lambda (L - X) \sec\alpha}$$

$$+ P_{12}' \, e^{-\gamma_\lambda (L + X) \sec\alpha} \Big] e^{-\gamma_\lambda L \sec\alpha} \, d\alpha \qquad (56)$$

Equation (55) is the expression for the flux absorbed in an element δX at X per unit volume due to multiple reflections from all layers y.

Total Rate of Re-Absorption

The total spectral rate of re-absorption per unit volume is the sum of the re-absorption from primary radiation (equation 44) and the re-absorption due to multiple reflections (equation 55). Thus:

$$Q_{R\lambda}(X) = \frac{\delta W^*_{\lambda X}}{\delta X} + \frac{\delta W^{**}_{\lambda X}}{\delta X} \tag{57}$$

This sum may be expressed as:

$$Q_{R\lambda}(X) = 2\left[\left(\frac{n_2}{n_1}\right)^2 \int_o^L \gamma_\lambda(y) W_{B\lambda}(y)\, \hat{P}(X)\, dy + W_{B\lambda}(o)\, \hat{P}_1(X) + W_{B\lambda}(L)\, \hat{P}_2(X)\right] \tag{58}$$

where

$$\hat{P}(X) = \int_o^{\pi/2} \sin\alpha \left(\frac{1 - e^{-\gamma_\lambda \delta X \sec\alpha}}{\delta X}\right) \left[e^{-\gamma_\lambda |X-y| \sec\alpha} + \left(P'_1\, e^{-\gamma_\lambda X \sec\alpha} + P'_{12}\, e^{-\gamma_\lambda (2L-X)\sec\alpha}\right) e^{-\gamma_\lambda y \sec\alpha} + \left(P'_2\, e^{-\gamma_\lambda (L-X)\sec\alpha} + P'_{12} e^{-\gamma_\lambda (L+X)\sec\alpha}\right) e^{-\gamma_\lambda (L-y)\sec\alpha}\right] d\alpha$$

$$\hat{P}_1(X) = \int_o^{\pi/2} \epsilon' \sin\alpha\cos\alpha \left(\frac{1 - e^{-\gamma_\lambda \delta X \sec\alpha}}{\delta X}\right) \left[e^{-\gamma_\lambda X \sec\alpha} + \left(P'_2\, e^{-\gamma_\lambda (L-X)\sec\alpha} + P'_{12}\, e^{-\gamma_\lambda (L-X)\sec\alpha}\right) e^{-\gamma_\lambda L \sec\alpha}\right] d\alpha$$

$$\hat{P}_2(X) = \int_o^{\pi/2} \epsilon'_1 \sin\alpha\cos\alpha \left(\frac{1 - e^{-\gamma_\lambda \delta X \sec\alpha}}{\delta X}\right) \left[e^{-\gamma_\lambda (L-X)\sec\alpha} + \left(P'_1\, e^{-\gamma_\lambda X \sec\alpha} + P'_{12}\, e^{-\gamma_\lambda (2L-X)\sec\alpha}\right) e^{-\gamma_\lambda L \sec\alpha}\right] d\alpha \tag{59}$$

and for all wavelengths, the total rate of reabsorption becomes:

$$Q_R(X) = \int_o^\infty Q_{R\lambda}(X)\, d\lambda \tag{60}$$

Inter-Face Reflectivities and Transmissivities

Fresnel's equations relate the amplitudes of the electric waves of the incident, reflected, and refracted beams at an interface. Comparing the energy of the incident and reflected beams which are two beams within the same medium, the Fresnel equations lead to the following expressions for the

directional reflectivities of a dielectric material for perpendicularly and parallel polarized beams, respectively:

$$\rho'_{\perp} = \frac{\sin^2(\beta - \alpha)}{\sin^2(\beta + \alpha)} \qquad \text{and} \qquad \rho'_{1\perp} = \frac{\sin^2(\beta_1 - \alpha)}{\sin^2(\beta_1 + \alpha)}$$

$$\rho'_{\parallel} = \frac{\tan^2(\beta - \alpha)}{\tan^2(\beta + \alpha)} \qquad \text{and} \qquad \rho'_{1\parallel} = \frac{\tan^2(\beta_1 - \alpha)}{\tan^2(\beta_1 + \alpha)} \tag{61}$$

where β and β_1, are the angles of refraction of the incident and emergent medium, respectively. The angles of refraction and incidence are related by Snell's Law as:

$$n_1 \sin\beta = n_2 \sin\alpha = n_3 \sin\beta_1 \tag{62}$$

where the n's are the indices of refraction. It can be shown that a critical angle of incidence exists beyond which no energy is refracted or in other words all beams at angles of incidence greater than the critical angle are given by:

$$\alpha_{cr1} = \sin^{-1}\left(\frac{n_1}{n_2}\right) \qquad \text{and} \qquad \alpha_{cr2} = \sin^{-1}\left(\frac{n_3}{n_2}\right) \tag{63}$$

Furthermore, the directional transmissivities of a dielectric material interface for perpendicularly and parallel polarized beams respectively become:

$$\tau'_{\perp} = 1 - \rho'_{\perp} \qquad \text{and} \qquad \tau'_{\parallel} = 1 - \rho'_{\parallel} \tag{64}$$

For a filmed interface, the reflectivities and transmissivities occurring in the radiant interchange terms are apparent properties. The film causes inter-reflections to occur and the rays comprising a beam incident on the film will superimpose and may cause interference depending upon the origin of the beam. Therefore, with a filmed interface the source of radiant beam determines how the interface property is to be computed.

For coherent sources "thin" film theory is used which accounts for the phase lag upon superimposed rays. Thin film theory has been recently advanced by Vasicek (Reference 27) in which it is shown that the classical Murmann-Fosterling formulas derived for thin absorbing films violate the laws of conservation of energy. Consequently Vasicek derives the following equations for the component apparent reflectivities and transmissivities.

$$\rho^*_{\perp} = \frac{r'^2_{\perp} + r''^2_{\perp} e^{-2\xi'} + 2r'_{\perp} r''_{\perp} \cos(\xi + \delta'_{\perp} - \delta''_{\perp})}{1 + r'^2_{\perp} r''^2_{\perp} e^{-2\xi'} + 2r'_{\perp} r''_{\perp} e^{-\xi'} \cos(\xi + \delta'_{\perp} - \delta''_{\perp})}$$

$$\rho^*_{\parallel} = \frac{r'^2_{\parallel} + r''^2_{\parallel} e^{-2\xi'} + 2r'_{\parallel} r''_{\parallel} \cos(\xi + \delta'_{\parallel} - \delta''_{\parallel})}{1 + r'^2_{\parallel} r''^2_{\parallel} e^{-2\xi'} + 2r'_{\parallel} r''_{\parallel} \cos(\xi + \delta'_{\parallel} - \delta''_{\parallel})} \tag{65}$$

and

$$\tau_{\perp}^{*} = \frac{t_{\perp}'^{2} t_{\perp}''^{2} e^{-\xi'} \tan\beta \operatorname{ctn}\alpha}{1 + r_{\perp}'^{2} r_{\perp}''^{2} e^{-2\xi'} + 2 r_{\perp}' r_{\perp}'' e^{-\xi'} \cos(\xi + \delta_{\perp}' - \delta_{\perp}'')}$$

$$\tau_{\parallel}^{*} = \frac{t_{\parallel}'^{2} t_{\parallel}''^{2} e^{-\xi'} \tan\beta \operatorname{ctn}\alpha}{1 + r_{\parallel}'^{2} r_{\parallel}''^{2} e^{-2\xi'} + 2 r_{\parallel}' r_{\parallel}'' e^{-\xi'} \cos(\xi + \delta_{\parallel}' - \delta_{\parallel}'')} \qquad (66)$$

where the computational method and definitions for the component terms are given in reference 27. The above equations comprise the apparent properties for the polarized components of the filmed interface with coherent sources. For initially unpolarized beams the apparent properties become:

$$\rho^{*} = \tfrac{1}{2}(\rho_{\perp}^{*} + \rho_{\parallel}^{*})$$
$$\tau^{*} = \tfrac{1}{2}(\tau_{\perp}^{*} + \rho_{\parallel}^{*}) \qquad (67)$$

For incoherent sources the superposition of inter-reflected rays are random ("thick" film theory) and the phase differences between superimposed rays are averaged. The equations for the reflectivity and transmissivity of glass with an absorbent film are taken and the mean value of the integral for the reflectivity and transmissivity are computed which results in:

$$\langle \rho_{\perp}^{*} \rangle = \frac{r_{\perp}'^{2} - 2 r_{\perp}'^{2} r_{\perp}''^{2} e^{-2\xi'} + r_{\perp}''^{2} e^{-2\xi'}}{1 - r_{\perp}'^{2} r_{\perp}''^{2} e^{-2\xi'}}$$

$$\langle \rho_{\parallel}^{*} \rangle = \frac{r_{\parallel}'^{2} - 2 r_{\parallel}'^{2} r_{\parallel}''^{2} e^{-2\xi'} + r_{\parallel}''^{2} e^{-2\xi'}}{1 - r_{\parallel}'^{2} r_{\parallel}''^{2} e^{-2\xi'}} \qquad (68)$$

and

$$\langle \tau_{\perp}^{*} \rangle = \frac{t_{\perp}'^{2} t_{\perp}''^{2} e^{-\xi'} \tan\beta \operatorname{ctn}\alpha}{1 - r_{\perp}'^{2} r_{\perp}''^{2} e^{-2\xi'}}$$

$$\langle \tau_{\parallel}^{*} \rangle = \frac{t_{\parallel}'^{2} t_{\parallel}''^{2} e^{-\xi'} \tan\beta \operatorname{ctn}\alpha}{1 - r_{\parallel}'^{2} r_{\parallel}''^{2} e^{-2\xi'}} \qquad (69)$$

The above equations comprise the apparent properties for the polarized components of the filmed interface with incoherent sources. For initially unpolarized beams these apparent properties become:

$$\langle \rho^{*} \rangle = \tfrac{1}{2}(\rho_{\perp}^{*} + \rho_{\parallel}^{*})$$
$$\langle \tau^{*} \rangle = \tfrac{1}{2}(\tau_{\perp}^{*} + \tau_{\parallel}^{*}) \qquad (70)$$

It is evident from the above that the apparent properties of the filmed interface is directionally dependent, e.g., the apparent reflectivity for a

beam traveling from the glass to air will not in general be the same as the apparent reflectivity for a beam traveling from air to glass. Furthermore, the film itself absorbs energy so that, unlike the unfilmed interface, the sum of the apparent reflectivity and transmissivity is less than or equal to unity. Therefore, in applying the interface properties for a filmed interface a finite emissivity of the interface is included in the appropriate radiant interchange terms.

Boundary Absorption

The boundaries of the window are represented in finite difference form as an incremental element of half the thickness of internal elements. Therefore, at these elements (at X = 0 and X = L) the absorption of energy from traversing beams is less due to the shorter path length within the elements. Furthermore, at the surfaces, the absorption of the film is attributed to the element, thus, for surface elements of thickness $\delta X/2$ the absorbed intensity from external sources is:

$$\delta I_{H\lambda\alpha S} = [(1 - e^{-\gamma_\lambda \frac{\delta X}{2} \sec\alpha}) + \epsilon'] I_{H\lambda\alpha S} \tag{71}$$

and the rate of absorption of spectral flux becomes:

$$\delta W_{H\lambda S} = 2W_{H\lambda}(\frac{n_2}{n_1})^2 \phi(S) \tag{72}$$

where

$$\phi(S) = \int_0^{\alpha_{cr}} [(1 - e^{-\gamma_\lambda \frac{\delta X}{2} \sec\alpha}) + \epsilon'] \sin\alpha \cos\alpha \, \tau'$$

$$\{e^{-\gamma_\lambda X \sec\alpha} + \frac{e^{-2\gamma_\lambda L \sec\alpha}}{1 + \frac{\tau'_{||}}{\tau'_\perp}} [\frac{\rho'_{1\perp}}{1 - \rho'_\perp \rho'_{1\perp} e^{-2\gamma_\lambda L \sec\alpha}} (\rho'_\perp e^{-\gamma_\lambda X \sec\alpha} + e^{+\gamma_\lambda X \sec\alpha})$$

$$+ \frac{\tau'_{||}}{\tau'_\perp} \frac{\rho'_{1||}}{1 - \rho'_{||} \rho'_{1||} e^{-2\gamma_\lambda L \sec\alpha}} (\rho'_{||} e^{-\gamma_\lambda X \sec\alpha} + e^{\gamma_\lambda X \sec\alpha})]\} \, d\alpha \tag{73}$$

Similarly for re-absorbed radiation of internal sources, the spectral rate of re-absorption per unit volume becomes:

$$Q_{R\lambda}(S) = 2\{(\frac{n_2}{n_1})^2 \int_0^L \gamma_\lambda(y) W_{B\lambda}(y) \hat{P}(S) \, dy$$

$$+ W_{B\lambda}(0) \hat{P}_1(S) + W_{B\lambda}(L) \hat{P}_2(S)\} \tag{74}$$

where

$$\hat{P}(S) = \int_0^{\pi/2} \sin\alpha \left[\frac{(1 - e^{-\gamma_\lambda \frac{\delta X}{2} \sec\alpha}) + \epsilon' S}{\delta X/2}\right] \left[e^{-\gamma_\lambda |X-y| \sec\alpha}\right.$$

$$\left. + (P_1' e^{-\gamma_\lambda X \sec\alpha} + P_{12}' e^{-\gamma_\lambda (2L-X) \sec\alpha}) e^{-\gamma_\lambda y \sec\alpha}\right.$$

$$\left. + (P_2' e^{-\gamma_\lambda (L-X) \sec\alpha} + P_{12}' e^{-\gamma_\lambda (L+X) \sec\alpha}) e^{-\gamma_\lambda (L-y) \sec\alpha}\right] d\alpha$$

$$\hat{P}_1(S) = \int_0^{\pi/2} \epsilon' \sin\alpha \cos\alpha \left[\frac{(1 - e^{-\gamma_\lambda \frac{\delta X}{2} \sec\alpha}) + \epsilon' S}{\delta X/2}\right] \left[e^{-\gamma_\lambda X \sec\alpha}\right.$$

$$\left. + (P_2' e^{-\gamma_\lambda (L-X) \sec\alpha} + P_{12}' e^{-\gamma_\lambda (L-X) \sec\alpha}) e^{-\gamma_\lambda L \sec\alpha}\right] d\alpha$$

$$\hat{P}_2(S) = \int_0^{\pi/2} \epsilon_1' \sin\alpha \cos\alpha \left[\frac{(1 - e^{-\gamma_\lambda \frac{\delta X}{2} \sec\alpha}) + \epsilon' S}{\delta X/2}\right] \left[e^{-\gamma_\lambda (L-X) \sec\alpha}\right.$$

$$\left. + (P_1' e^{-\gamma_\lambda X \sec\alpha} + P_{12}' e^{-\gamma_\lambda (2L-X) \sec\alpha}) e^{-\gamma_\lambda L \sec\alpha}\right] d\alpha \qquad (75)$$

Summary of Energy Absorbed

The energy absorbed from internal radiations, lost by self-emission, and re-absorbed from other layers are summarized in Figure 59 for a layer at position X. The integrals shown can only be evaluated numerically due to the complex arguments involved. However, a simplification is made in the wavelength integration. The wavelength dependent quantities, i.e., the spectral absorption coefficient, γ_λ, and the blackbody distributions, $W_{B\lambda}$ are approximated by step functions over wavelength bands and beyond a cut-off wavelength, λm, the material may be considered opaque. Tables of integrals for blackbody distributions are available (i.e., Ref. 18) that can be applied to the wavelength bands corresponding to the spectral absorption coefficients. Thus, the energy absorbed terms may be computed by the finite summations:

$$Q_A(X) = 2\left(\frac{n_2}{n_1}\right)^2 \sum_1^m W_{B\lambda m} \phi(X)$$

$$Q_E(X) = 4\left(\frac{n_2}{n_1}\right)^2 \sum_1^m \gamma_{\lambda m} W_{B\lambda m}(X) \qquad (76)$$

$$Q_R(X) = 2 \sum_1^m \left[\left(\frac{n_2}{n_1}\right)^2 \int_0^L \gamma_{\lambda m}(y) W_{B\lambda m}(y) \hat{P}(X)\, dy + W_{B\lambda m}(0) \hat{P}_1 + W_{B\lambda m}(L) \hat{P}_2\right]$$

$$Q_A(X) = 2\left(\frac{n_2}{n_1}\right)^2 \int_o W_{H\lambda}\phi(X)d\lambda$$

$$\phi(X) = \int_o^{\alpha_{cr}} \tau' \{e^{-\gamma_\lambda X\sec\alpha} + \frac{e^{-2\gamma_\lambda L\sec\alpha}}{1+\frac{\tau_{||}'}{\tau_\perp'}}\left[\frac{\rho_{1\perp}'}{1-\rho_\perp'\rho_{1\perp}'e^{-2\gamma_\lambda L\sec\alpha}}(\rho_\perp' e^{-\gamma_\lambda X\sec\alpha} + e^{-\gamma_\lambda X\sec\alpha})\right.$$

$$\left. + \frac{\tau_{||}'}{\tau_\perp'}\frac{\rho_{1||}'}{1-\rho_{||}'\rho_{1||}'e^{-2\gamma_\lambda L\sec\alpha}}(\rho_{||}' e^{-\gamma_\lambda X\sec\alpha} + e^{+\gamma_\lambda X\sec\alpha})\right]\}\left(\frac{1-e^{-\gamma_\lambda \delta X\sec\alpha}}{\delta X}\right)\sin\alpha\cos\alpha\, d\alpha$$

$$Q_E(X) = 4\left(\frac{n_2}{n_1}\right)^2 \int_o^\infty \gamma_\lambda W_{B\lambda}(X)d\lambda$$

$$Q_R(X) = 2\int_o^\infty \left[\left(\frac{n_2}{n_1}\right)^2 \int_o^L \gamma_\lambda(y)W_{B\lambda}(y)\hat{F}(X)dy + W_{B\lambda}(0)\hat{P}_1(X) + W_{B\lambda}(L)\hat{P}_2(X)\right] d\lambda$$

$$\hat{F}(X) = \int_o^{\pi/2} \sin\alpha\left(\frac{1-e^{-\gamma_\lambda \delta X\sec\alpha}}{\delta X}\right)\left[e^{-\gamma_\lambda|X-y|\sec\alpha} + (P_1'e^{-\gamma_\lambda X\sec\alpha} + P_{12}'e^{-\gamma_\lambda(2L-X)\sec\alpha})e^{-\gamma_\lambda y\sec\alpha}\right.$$

$$\left. + (P_2'e^{-\gamma_\lambda(L-X)\sec\alpha} + P_{12}'e^{-\gamma_\lambda(L+X)\sec\alpha})e^{-\gamma_\lambda(L-y)\sec\alpha}\right]d\alpha$$

$$\hat{P}_1(X) = \int_o^{\pi/2} \epsilon' \sin\alpha\cos\alpha\left(\frac{1-e^{-\gamma_\lambda \delta X\sec\alpha}}{\delta X}\right)\left[e^{-\gamma_\lambda X\sec\alpha} + (P_2'e^{-\gamma_\lambda(L-X)\sec\alpha} + P_{12}'e^{-\gamma_\lambda(L-X)\sec\alpha})e^{-\gamma_\lambda L\sec\alpha}\right]d\alpha$$

$$\hat{P}_2(X) = \int_o^{\pi/2} \epsilon_1' \sin\alpha\cos\alpha\left(\frac{1-e^{-\gamma_\lambda \delta X\sec\alpha}}{\delta X}\right)\left[e^{-\gamma_\lambda(L-X)\sec\alpha} + (P_1'e^{-\gamma_\lambda X\sec\alpha} + P_{12}'e^{-\gamma_\lambda(2L-X)\sec\alpha})\right]d\alpha$$

$$P_1' = \frac{1}{2}\left[\frac{\rho_\perp'}{1-\rho_\perp'\rho_{1\perp}'e^{-2\gamma_\lambda L\sec\alpha}} + \frac{\rho_{||}'}{1-\rho_{||}'\rho_{1||}'e^{-2\gamma_\lambda L\sec\alpha}}\right]$$

$$P_2' = \frac{1}{2}\left[\frac{\rho_\perp'}{1-\rho_\perp'\rho_{1\perp}'e^{-2\gamma_\lambda L\sec\alpha}} + \frac{\rho_{||}'}{1-\rho_{||}'\rho_{1||}'e^{-2\gamma_\lambda L\sec\alpha}}\right]$$

$$P_{12}' = \frac{1}{2}\left[\frac{\rho_\perp'\rho_{1\perp}'}{1-\rho_\perp'\rho_{1\perp}'e^{-2\gamma_\lambda L\sec\alpha}} + \frac{\rho_{||}'\rho_{1||}'}{1-\rho_{||}'\rho_{1||}'e^{-2\gamma_\lambda L\sec\alpha}}\right]$$

Figure 59 SUMMARY OF ENERGY ABSORBED TERMS

Emission from a Non-Isothermal Glass

In order to formulate the emission of the radiation from a glazing, it is necessary to develop the emission of a partially transparent slab whose temperature is non-uniform. Consider a transparent medium as shown in Figure 60. In Figure 60a, a perpendicularly polarized beam arrives at the internal surface with an intensity $I_{\lambda\alpha\perp}$ just prior to its first reflection. Part of this beam is reflected and the part is refracted across the interface between medium (2) and medium (3). The refracted portion of this beam which emerges into the medium (3) has the intensity:

$$I_{\lambda\alpha\perp} \frac{\tau'_{1\perp} \cos\beta_1}{\left(\frac{n_2}{n_3}\right)^2 \cos\alpha}$$

The refracted portions of each inter-reflection of the beam $I_{\lambda\alpha\perp}$ may be described as shown in Figure 60a. Thus, from Figure 60a the sum of refracted intensities due to the intensity $I_{\lambda\alpha\perp}$ is:

$$I_{\lambda\alpha\perp} \frac{\tau'_{1\perp} \cos\beta_1}{\left(\frac{n_2}{n_1}\right)^2 \cos\alpha} \left\{1 + \rho'_{1\perp}\rho'_{1\perp} e^{-2\gamma_\lambda L \sec\alpha} + (\rho'_{1\perp}\rho'_{1\perp})^2 e^{-4\gamma_\lambda L \sec\alpha} + \ldots\right\}$$

$$= I_{\lambda\alpha\perp} \frac{\tau'_{1\perp} \cos\beta_1}{\left(\frac{n_2}{n_3}\right)^2 \cos\alpha} \left\{\frac{1}{1 - \rho'_{1\perp}\rho'_{1\perp} e^{-2\gamma_\lambda L \sec\alpha}}\right\} \qquad (77)$$

Figure 60b illustrates a similar treatment for the beam $I_{\lambda\alpha\perp}$. The sum of refracted beams due to the intensity $I_{\lambda\alpha\perp}$ is:

$$I_{\lambda\alpha\perp} \frac{\tau'_{1\perp} \cos\beta_1}{\left(\frac{n_2}{n_3}\right)^2 \cos\alpha} \left\{\rho'_{1\perp} e^{-\gamma_\lambda L \sec\alpha} + \rho'_{1\perp}\rho'_{1\perp} e^{-3\gamma_\lambda L \sec\alpha} + \rho'^3_{1\perp}\rho'^2_{1\perp} e^{-5\gamma_\lambda L \sec\alpha} + \ldots\right\}$$

$$= I_{\lambda\alpha\perp} \frac{\tau'_{1\perp} \cos\beta_1}{\left(\frac{n_2}{n_3}\right)^2 \cos\alpha} \left\{\frac{\rho'_{1\perp} e^{-\gamma_\lambda L \sec\alpha}}{1 - \rho'_{1\perp}\rho'_{1\perp} e^{-2\gamma_\lambda L \sec\alpha}}\right\} \qquad (78)$$

Thus, the combination of refracted beams from intensities $I_{\lambda\alpha\perp}$ and $I_{\lambda\alpha\perp}$ becomes

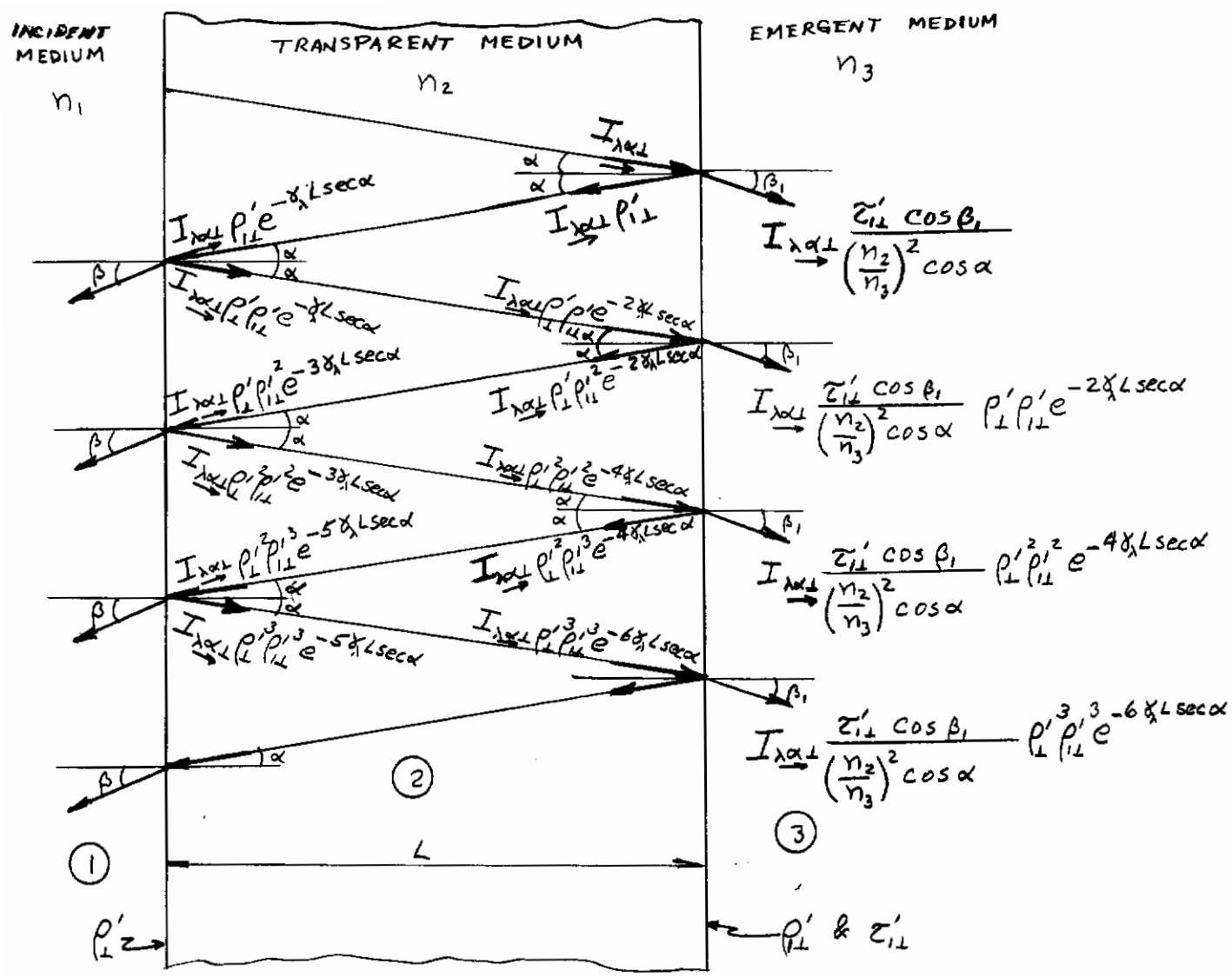

Figure 60a EMISSION FROM A NON-ISOTHERMAL GLASS
(Right Emanating Component)

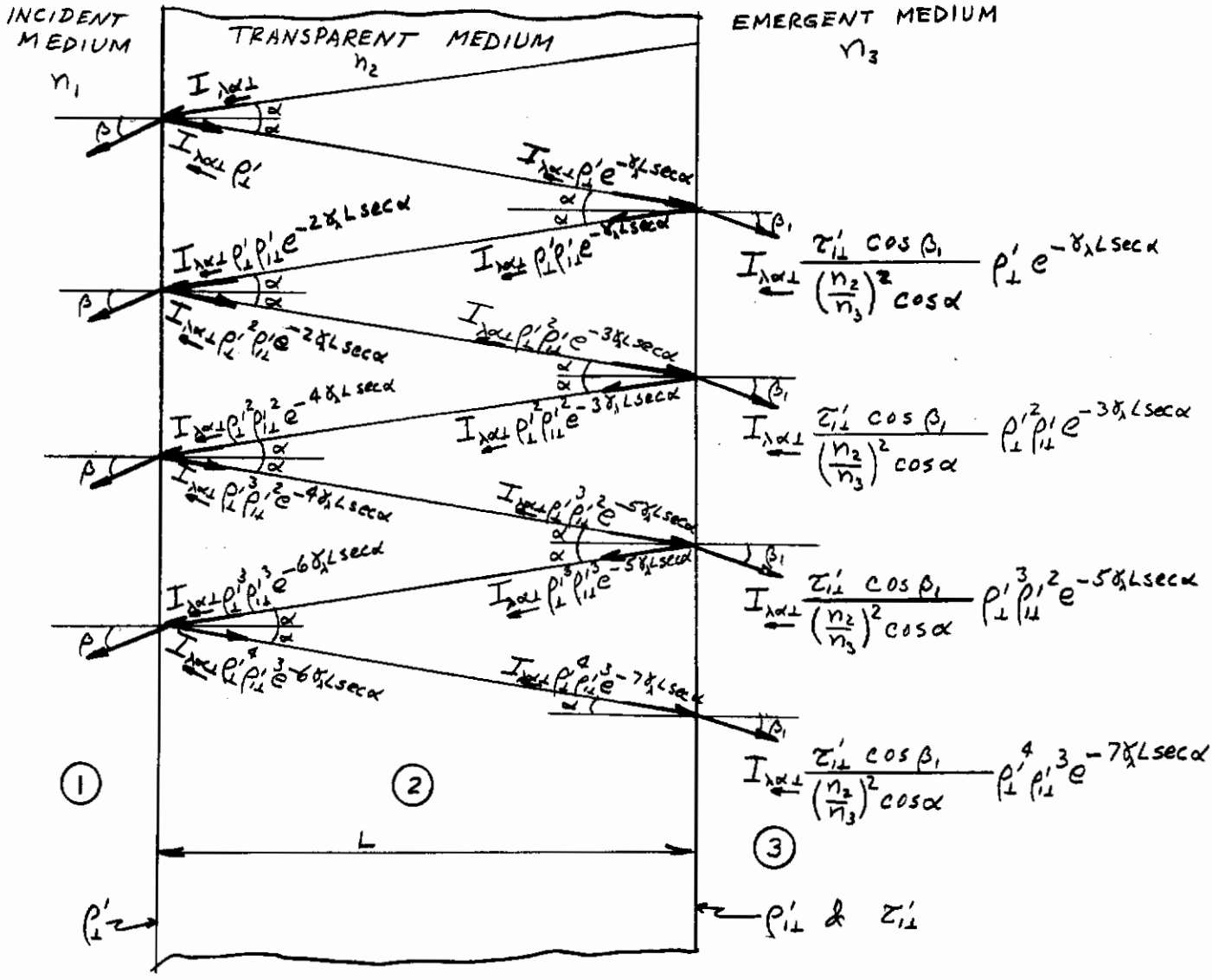

Figure 60b EMISSION FROM A NON-ISOTHERMAL GLASS
(Left Emanating Component)

$$I_{\lambda\beta_1\perp} = I_{\lambda\alpha\perp}\frac{\tau'_{1\perp}\cos\beta_1}{\left(\frac{n_2}{n_3}\right)^2\cos\alpha}\left\{\frac{1}{1-\rho'_\perp\rho'_{1\perp}e^{-2\gamma_\lambda L\sec\alpha}}\right\}$$

$$+ I_{\lambda\alpha\perp}\frac{\tau'_{1\perp}\cos\beta_1}{\left(\frac{n_2}{n_3}\right)^2\cos\alpha}\left\{\frac{\rho'_\perp e^{-\gamma_\lambda L\sec\alpha}}{1-\rho'_\perp\rho'_{1\perp}e^{-2\gamma_\lambda L\sec\alpha}}\right\}$$

or

$$I_{\lambda\beta_1\perp} = \frac{\tau'_{1\perp}\cos\beta_1}{\left(\frac{n_2}{n_3}\right)^2\cos\alpha}\left\{\frac{I_{\lambda\alpha\rightarrow\perp}+\rho'_\perp e^{-\gamma_\lambda L\sec\alpha}\,I_{\lambda\alpha\perp}}{1-\rho'_\perp\rho'_{1\perp}e^{-2\gamma_\lambda L\sec\alpha}}\right\} \tag{79}$$

Likewise, an expression for parallel polarized beams may be written as:

$$I_{\lambda\beta_1\parallel} = \frac{\tau'_{1\parallel}\cos\beta_1}{\left(\frac{n_2}{n_3}\right)^2\cos\alpha}\left\{\frac{I_{\lambda\alpha\rightarrow\parallel}+\rho'_\parallel e^{-\gamma_\lambda L\sec\alpha}\,I_{\lambda\alpha\parallel}}{1-\rho'_\parallel\rho'_{1\parallel}e^{-2\gamma_\lambda L\sec\alpha}}\right\} \tag{80}$$

The total intensity of refracted beams is:

$$I_{\lambda\beta_1 L} = I_{\lambda\beta_1\perp} + I_{\lambda\beta_1\parallel}$$

or

$$I_{\lambda\beta_1 L} = \left(\frac{n_3}{n_2}\right)^2\frac{\cos\beta_1}{\cos\alpha}\left\{\frac{\tau'_{1\perp}\left[I_{\lambda\alpha\rightarrow\perp}+\rho'_\perp e^{-\gamma_\lambda L\sec\alpha}\,I_{\lambda\alpha\perp}\right]}{1-\rho'_\perp\rho'_{1\perp}e^{-2\gamma_\lambda L\sec\alpha}}\right.$$

$$\left. + \frac{\tau'_{1\parallel}\left[I_{\lambda\alpha\rightarrow\parallel}+\rho'_\parallel e^{-\gamma_\lambda L\sec\alpha}\,I_{\lambda\alpha\parallel}\right]}{1-\rho'_\parallel\rho'_{1\parallel}e^{-2\gamma_\lambda L\sec\alpha}}\right\} \tag{81}$$

It is now necessary to determine the values of $I_{\lambda\alpha}$ and $I_{\lambda\alpha}$ in the two polarized components. Consider an element at X of the thickness δX. The intensity emitted by this element to the right is:

$$\delta I_{\lambda\alpha} = j_\lambda(X)\,\delta X$$

The volume emissive power is now directional since the emergent media are not necessarily the same on each side of the slab. The intensity emitted by element δX at X to the right becomes

$$\delta I_{\lambda\alpha\rightarrow} = \left(\frac{n_2}{n_3}\right)^2 \frac{\gamma_\lambda(X) W_{B\lambda}(X)\, \delta X}{\pi}$$

and will arrive at the interior boundary as:

$$\delta I_{\lambda\alpha L\rightarrow} = \left(\frac{n_2}{n_3}\right)^2 \frac{\gamma_\lambda(X) W_{B\lambda}(X)}{\pi} \delta X\, e^{-\gamma_\lambda (L-X) \sec\alpha}$$

So that the total integrated value for all positions X is:

$$I_{\lambda\alpha L\rightarrow} = \left(\frac{n_2}{n_3}\right)^2 \int_0^L \frac{\gamma_\lambda(X) W_{B\lambda}(X)}{\pi} e^{-\gamma_\lambda (L-X) \sec\alpha}\, dX + \epsilon' \frac{W_{B\lambda}(0)}{\pi} \cos\alpha\, e^{-\gamma_\lambda L \sec\alpha} \tag{82}$$

Since all these beams originated within the partially transparent medium they are unpolarized and it follows that

$$I_{\lambda\alpha\perp\rightarrow} = I_{\lambda\alpha\parallel\rightarrow} = \frac{1}{2} I_{\lambda\alpha L\rightarrow} \tag{83}$$

Using a similar argument for the intensity emitted by the element δX at X to the left:

$$\delta I_{\lambda\alpha\leftarrow} = j_{\lambda\leftarrow}(X)\, \delta X$$

and it follows that

$$\delta I_{\lambda\alpha\leftarrow} = \left(\frac{n_2}{n_1}\right)^2 \frac{\gamma_\lambda(X) W_{B\lambda}(X)}{\pi} \delta X$$

or at the exposed boundary

$$\delta I_{\lambda\alpha L\leftarrow} = \left(\frac{n_2}{n_1}\right)^2 \frac{\gamma_\lambda(X) W_{B\lambda}(X)}{\pi} e^{-\gamma_\lambda X \sec\alpha}\, \delta X$$

The total integrated value for all positions X is:

$$I_{\lambda\alpha L\leftarrow} = \left(\frac{n_2}{n_1}\right)^2 \int_0^L \frac{\gamma_\lambda(X) W_{B\lambda}(X)}{\pi} e^{-\gamma_\lambda X \sec\alpha}\, dX + \epsilon_1' \frac{W_{B\lambda}(L)}{\pi} \cos\alpha\, e^{-\gamma_\lambda L \sec\alpha} \tag{84}$$

And again since these beams originated within the partially transparent medium, they are unpolarized and it follows that:

$$I_{\lambda\alpha\perp\leftarrow} = I_{\lambda\alpha\parallel\leftarrow} = \frac{1}{2} I_{\lambda\alpha L\leftarrow} \tag{85}$$

Thus by equations (82) to (85), equation (81) may be written as:

$$I_{\lambda\beta_1 L} = \left(\frac{n_3}{n_2}\right)^2 \frac{\cos\beta_1}{\cos\alpha} \left\{\frac{1}{2} I_{\lambda\alpha L}\right\rightarrow \left[\frac{\tau'_{1\perp}}{1 - \rho'_\perp \rho'_{1\perp} e^{-2\gamma_\lambda L \sec\alpha}} + \frac{\tau'_{1\parallel}}{1 - \rho'_\parallel \rho'_{1\parallel} e^{-2\gamma_\lambda L \sec\alpha}}\right]$$

$$+ \frac{1}{2} I_{\lambda\alpha L}\left\leftarrow \left[\frac{\tau'_{1\perp}\rho'_\perp e^{-\gamma_\lambda L \sec\alpha}}{1 - \rho'_\perp \rho'_{1\perp} e^{-2\gamma_\lambda L \sec\alpha}} + \frac{\tau'_{1\parallel}\rho'_\parallel e^{-\gamma_\lambda L \sec\alpha}}{1 - \rho'_\parallel \rho'_{1\parallel} e^{-2\gamma_\lambda L \sec\alpha}}\right]\right\}$$

Let

$$\Gamma\rightarrow = \frac{1}{2}\left[\frac{\tau'_{1\perp}}{1 - \rho'_\perp \rho'_{1\perp} e^{-2\gamma_\lambda L \sec\alpha}} + \frac{\tau'_{1\parallel}}{1 - \rho'_\parallel \rho'_{1\parallel} e^{-2\gamma_\lambda L \sec\alpha}}\right]$$

$$\Gamma\leftarrow = \frac{1}{2}\left[\frac{\tau'_{1\perp}\rho'_\perp e^{-\gamma_\lambda L \sec\alpha}}{1 - \rho'_\perp \rho'_{1\perp} e^{-2\gamma_\lambda L \sec\alpha}} + \frac{\tau'_{1\parallel}\rho'_\parallel e^{-\gamma_\lambda L \sec\alpha}}{1 - \rho'_\parallel \rho'_{1\parallel} e^{-2\gamma_\lambda L \sec\alpha}}\right] \qquad (86)$$

Thus:

$$I_{\lambda\beta_1 L} = \left(\frac{n_3}{n_2}\right)^2 \frac{\cos\beta_1}{\cos\alpha}\left[I_{\lambda\alpha L}\right\rightarrow \Gamma\rightarrow + I_{\lambda\alpha L}\left\leftarrow \Gamma\leftarrow\right] \qquad (87)$$

which is the expression for total intensity refracted into the medium (3) due to the temperature distribution of medium (2).

Apparent Transmissivity

Consider a perpendicular polarized beam, $I_{\lambda\perp}$, within a medium of refractive index n_{i-1} and incident upon the interface to a medium of refractive index n_i as shown in Figure 61. A portion ($I_{\lambda\perp}\rho'_\perp$) is reflected at the interface and a portion is refracted. The refracted portion is attenuated by passage through the medium i and subsequently arrives at the back surface of medium i with the intensity

$$I_{\lambda\perp}\tau'_\perp e^{-\gamma_\lambda L \sec\alpha}$$

Part of this beam is reflected and part is refracted into the medium of refractive index n_{i+1}. Following the inter-reflections of the primary reflected beam as shown in Figure 61, the sum of refracted beams into the medium i+1 is seen to be:

$$I_{\lambda\tau\perp} = \frac{I_{\lambda\perp}\tau'_\perp\tau''_\perp e^{-\gamma_\lambda L \sec\alpha}}{1 - \rho'_\perp\rho''_\perp e^{-2\gamma_\lambda L \sec\alpha}} \qquad (88)$$

By definition the apparent directional transmissivity of perpendicularly polarized radiation is therefore:

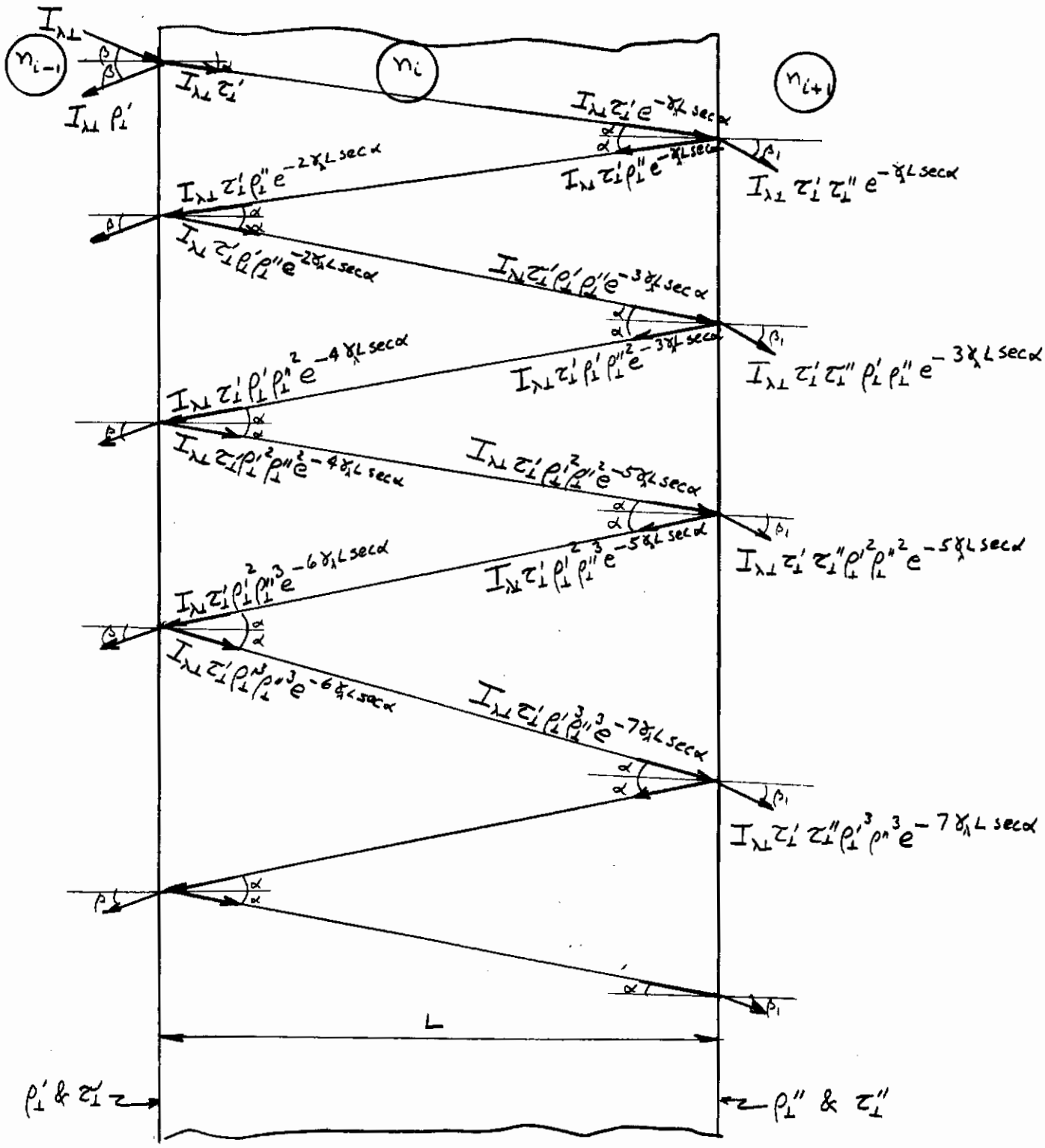

Figure 61 APPARENT TRANSMISSIVITY

$$\tau^*_{\lambda\perp} = \frac{I_{\lambda\tau\perp}}{I_{\lambda\perp}} = \frac{\tau'_\perp \tau''_\perp \; e^{-\gamma_\lambda L \sec\alpha}}{1 - \rho'_\perp \rho''_\perp \; e^{-2\gamma_\lambda L \sec\alpha}} \tag{89}$$

A similar expression may be written for the apparent directional transmissivity of parallel polarized radiation as:

$$\tau^*_{\lambda\parallel} = \frac{I_{\lambda\tau\parallel}}{I_{\lambda\parallel}} = \frac{\tau'_\parallel \tau''_\parallel \; e^{-\gamma_\lambda L \sec\alpha}}{1 - \rho'_\parallel \rho''_\parallel \; e^{-2\gamma_\lambda L \sec\alpha}} \tag{90}$$

Now, since the total incident intensity is the sum of its components,

$$I_{\lambda i} = I_{\lambda\perp} + I_{\lambda\parallel}$$

and furthermore for initially unpolarized radiation

$$I_{\lambda\perp} = I_{\lambda\parallel} = \frac{1}{2} I_{\lambda i} ,$$

and since the total transmitted intensity is the sum of its components,

$$I_{\lambda\tau} = I_{\lambda\tau\perp} + I_{\lambda\tau\parallel}$$

it follows by equations (89) and (90) that

$$I_{\lambda\tau} = I_{\lambda\perp} \tau^*_{\lambda\perp} + I_{\lambda\parallel} \tau^*_{\lambda\parallel}$$

By definition, the apparent directional transmissivity of the total intensity becomes:

$$\tau^*_{\lambda G} = \frac{I_{\lambda\tau}}{I_{\lambda i}} = \frac{I_{\lambda\perp}}{I_{\lambda i}} \tau^*_{\lambda\perp} + \frac{I_{\lambda\parallel}}{I_{\lambda i}} \tau^*_{\lambda\parallel}$$

or

$$\tau^*_{\lambda G} = \frac{1}{2} \left[\tau^*_{\lambda\perp} + \tau^*_{\lambda\parallel} \right] \tag{91}$$

Equation (91) is the desired expression for the apparent directional transmissivity.

Total Radiant Heat Flux

The total radiant heat flux into the cabin is made up of the following components:

(1) emission from the non-isothermal glazing
(2) transmission of external radiation
(3) emission from the emergent face film
(4) opaque emission of the emergent face.

From the foregoing developments the spectral heat flux into the cabin becomes:

$$W_\lambda = 2\pi \int_0^{\pi/2} \left[I_{\lambda,\beta_1} L + \left(\tau^*_{\lambda G} \frac{W_{H\lambda}}{\pi} + \epsilon'_1 \frac{W_{B\lambda}(L)}{\pi} \right) \cos \beta_1 \right] \sin \beta_1 \, d\beta_1 \qquad (92)$$

and the total heat flux becomes:

$$W = \sum_m W_{\lambda m} + \epsilon_m \left[1 - p(T_{11}) \right] \sigma T_{11}^4 \qquad (93)$$

Numerical Solution

From the foregoing discussion it is clear that the solution involves the evaluation of integro-differential equations. Numerical methods (REf. 24 and 25) are used to solve the equation:

$$\rho c \frac{\partial T_i}{\partial t} = \sum_j q_i'''(T_j) + k \frac{\partial^2 T_i}{\partial X^2} \qquad (94)$$

with appropriate boundary and initial conditions. It is seen that the temperature, T, is a function of position, X, and time, t. Expanding T(X, t) in a Taylor series for the spatial coordinates about a position X yields:

$$T(X + \Delta X, t) = T_{i+1} = T_i + \Delta X \frac{\partial T}{\partial X} + \frac{(\Delta X)^2}{2} \frac{\partial^2 T}{\partial X^2} + \ldots$$

$$T(X - \Delta X, t) = T_{i-1} = T_i - \Delta X \frac{\partial T}{\partial X} + \frac{(\Delta X)^2}{2} \frac{\partial^2 T}{\partial X^2} - \ldots \qquad (95)$$

Adding equations (95) yields

$$T_{i+1} + T_{i-1} \cong 2 T_i + (\Delta X)^2 \frac{\partial^2 T}{\partial X^2}$$

or

$$\frac{\partial^2 T}{\partial X^2} = \frac{T_{i+1} - 2T_i + T_{i-1}}{(\Delta X)^2} \qquad (96)$$

which neglects terms of 4th order and beyond. Similarly, a Taylor series expansion of T(X, t) with time yields:

$$T(X, t + \Delta t) = T^{n+1} = T_i^n + \Delta t \frac{\partial T}{\partial t} + \ldots$$

or

$$\frac{\partial T}{\partial t} \cong \frac{T_i^{n+1} - T_i^n}{\Delta t} \qquad (97)$$

Equation (94) may now be expressed as

$$\rho c \frac{T_i^{n+1} - T_i^n}{\Delta t} = \sum_j q_i'''(T_j) + k \frac{T_{i+1} - 2T_i + T_{i-1}}{(\Delta X)^2} \qquad (98)$$

where the superscript n is used as the time index. The question of the selection of a proper time index for the right hand side now arises. Since equation (95) could have been expanded at time $t + \Delta t$ at least two possible finite difference forms appear, namely:

$$\rho c \frac{T_i^{n+1} - T_i^n}{\Delta t} = \sum_j q_i'''(T_j^n) + k \frac{T_{i+1}^n - 2T_i^n + T_{i-1}^n}{(\Delta X)^2} \qquad (99)$$

and

$$\rho c \frac{T_i^{n+1} - T_i^n}{\Delta t} = \sum_j q_i'''(T_j^{n+1}) + k \frac{T_{i+1}^{n+1} - 2T_i^{n+1} + T_{i-1}^{n+1}}{(\Delta X)^2} \qquad (100)$$

Equation (99) will be referred to as the "explicit" form and equation (100) as the "implicit" form. It can be seen that in the "explicit" form each temperature T_i^{n+1} may be solved for "explicitly" knowing the initial temperature field T_i^n. In the "implicit" form the solution of T_i^{n+1} is linked to temperatures T_{i+1}^{n+1} and T_{i-1}^{n+1} thus resulting in the simultaneous solution of i_{max} equations and the solution of T_i^{n+1} is determined "implicitly". In the explicit form the temperature T_i^{n+1} becomes

$$T_i^{n+1} = \frac{(\Delta X)^2}{k} \frac{\sum_j q_i'''(T_j^{n+1})}{M} + \frac{T_{i+1}^n}{M} + \left(1 - \frac{2}{M}\right) T_i^n + \frac{T_{i-1}^n}{M} \qquad (101)$$

where the Fourier Modulus, M, is introduced and defined as:

$$M = \frac{(\Delta X)^2}{\frac{k}{\rho c} \Delta t} \qquad (102)$$

In order not to violate the second law of thermodynamics the quantity $\left(1 - \frac{2}{M}\right)$ must not become negative. Thus a stability criteria

$$M > 2$$

must be maintained. (Actually the stability criteria for the exposed surface is more stringent than that given above.) For a given spatial increment the stability criteria dictates the maximum time increment allowable for each calculation step made. In contrast, the implicit scheme has no stability criteria that must be satisfied. Therefore, though more demanding mathematically, the implicit form of the finite difference equation allows for larger time increments per calculation, at least from the standpoint of stability considerations.

Both the "implicit" and "explicit" forms are subject to truncation error. This arises from the approximations made in equations (96) and (97) in which the first few terms of the Taylor series are utilized to approximate the function $T(X, t)$. Furthermore, the energy absorbed term, $\sum_j q_i'''(T_j^{n+1})$, requires the new

temperature field be known before numerical integration is performed in its evaluation. For this matter, an iteration on $\sum_j q_i'''(T_j^{n+1})$ should solve the dilemma. However, both truncation error and the determination of the energy absorbed term can be handled by the technique that follows.

At the beginning of a computation, a temperature field is presumed known; T_i^n. Using this temperature field the energy absorbed terms are computed for each position. With the field, $\sum_j q_i'''(T_j^n)$, determined the new temperature field, $\hat{T}_i^{n+1}$ is computed after a time increment Δt. The new temperature field is not accepted at this point since it is not known whether the time increment, Δt, chosen for the computation is excessive in terms of truncation error and variance of $\sum_j q_i'''(T_j^n)$ over the increment. Now, using the $\sum_j q_i'''(T_j^n)$ a temperature field $T_i^{\frac{2n+1}{2}}$ is computed for a time increment $\Delta t/2$ and a new energy absorbed field, $\sum_j q_i'''(T_j^{\frac{2n+1}{2}})$ is computed. Using $\sum_j q_i'''(T_j^{\frac{2n+1}{2}})$ the temperature field, T_j^{n+1}, is computed for an additional time increment $\Delta t/2$. Now $\hat{T}_i^{n+1}$ is compared with T_i^{n+1} and if the comparison agrees to within a prescribed accuracy, the temperature field, T_i^{n+1}, is considered acceptable and the time is advanced by the increment Δt and the computation proceeds. If, however, the temperature fields do not agree, the time increment is halved again and the procedure is repeated until agreement is achieved. The entire process is shown diagramatically in Figure 62.

Boundary Conditions

Though equation (100) is valid for all interior points, the boundaries must account for the inputs and losses from and to the environment. To apply such things as aerodynamic heating to a finite incremented glazing, nodal points are chosen as shown in Figure 63.

The glazing is divided into 10 parts. Nine full parts are used for the interior and 2 one-half parts for the surfaces forming 11 nodal points with a nodal point on each surface. It is assumed that each element is isothermal within itself and temperatures are a step function being discontinuous at the dividing lines. Nodal point 1 is on the surface exposed to outside while nodal point 11 is on the surface exposed to the cabin.

The exposed surface boundary condition is expressed in the following heat balance.

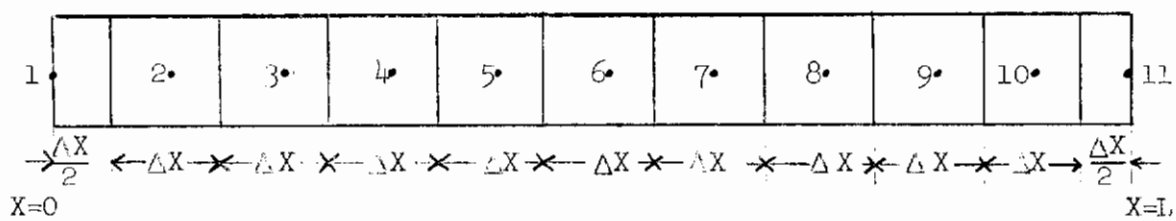

Figure 63 NODAL POINTS

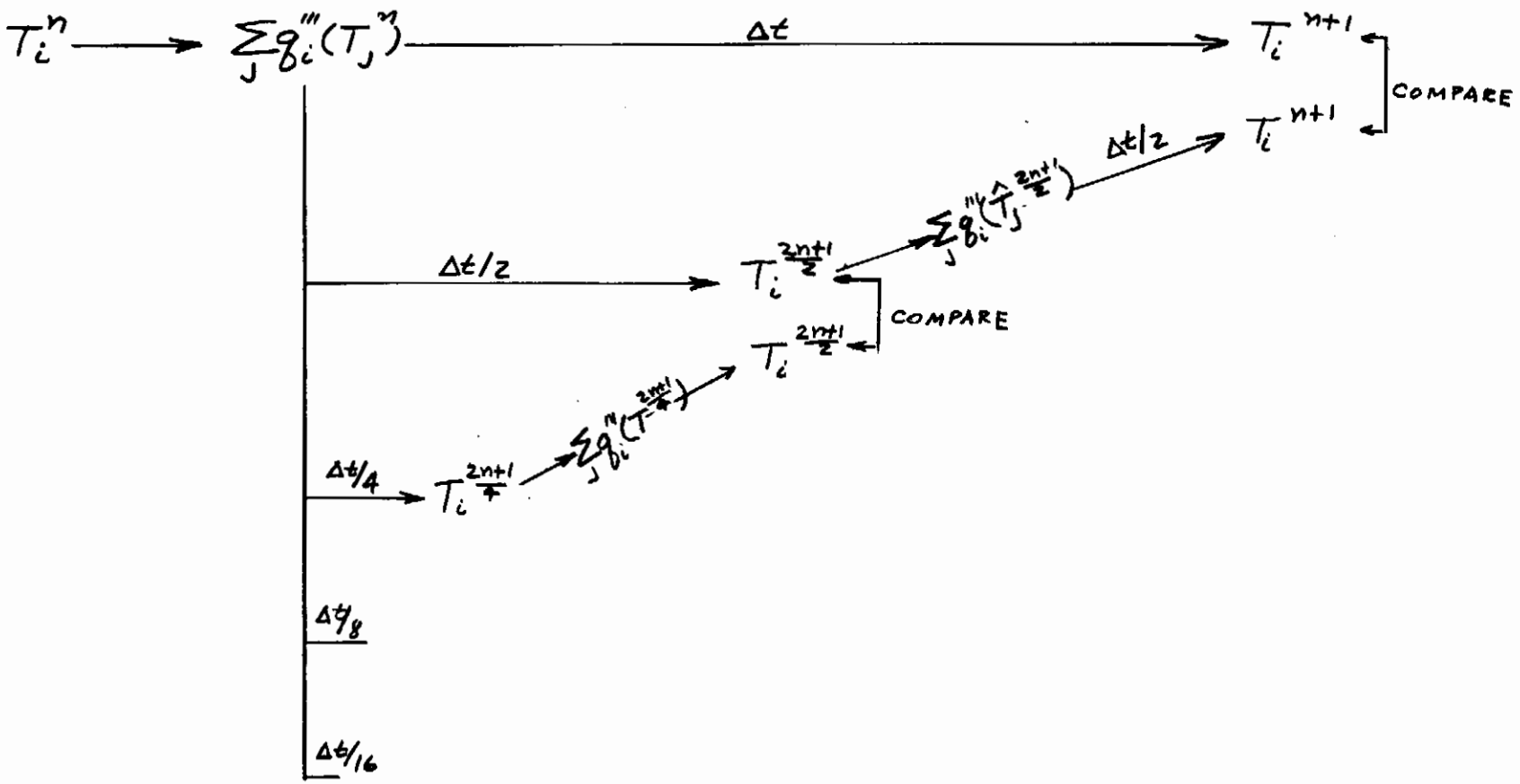

Figure 62 CONVERGENCE SCHEMATIC

$$\rho c \frac{\Delta X}{2} \frac{\partial T_1}{\partial t} \quad \text{.... storage rate}$$

$$= \frac{\Delta X}{2} \sum_j q_i''' (\hat{T}_j^{n+1}) \quad \text{.... absorbed by radiation in the transparent portion of the spectrum}$$

$$+ q_1'' \quad \text{.... convective input}$$

$$+ (1 - \alpha_{Hm}) W_{Hm} \quad \text{.... absorbed by radiation in the opaque portion of the spectrum}$$

$$- \epsilon_m W_{Bm}(T_1) \quad \text{.... emitted by radiation in the opaque portion of the spectrum}$$

$$- k \frac{\partial T}{\partial X} \quad \text{.... conducted into the plate} \qquad (103)$$

Assuming that a diffuse radiation source exists external to the glazing and that it has a temperature of T_H and a greybody emissivity of ϵ_g, the radiative input to the sheet in the opaque portion of the spectrum which is absorbed at the surface is:

$$W_{Hm} = [1 - p_m(T_H)] \epsilon_g \sigma T_H^4 \qquad (104)$$

where $p_m(T_H)$ = percent of blackbody energy at temperature T_H below the cut-off wavelength λ_m

σ = Stefan-Boltzman constant

Similarly, the opaque portion of emitted energy not handled in the $\sum_j q_i''' (\hat{T}_j^{n+1})$ term is determined from

$$W_{Bm}(T_1) = [1 - p_m(T_1)] \sigma T_1^4 \qquad (105)$$

However, this term may be linearized to the form

$$W_{Bm}(T_1) = \{[1 - p_m(T_1^n)] \sigma (T_1^n)^3\} T_1^{n+1} \qquad (106)$$

Reducing equation (103) to implicit finite difference form yields:

$$\rho c \frac{\Delta X}{2} \frac{T_1^{n+1} - T_1^n}{\Delta t} = \frac{\Delta X}{2} \sum_j q_1''' (\hat{T}_j^{n+1}) + q_1'' + (1 - \alpha_{Hm}) [1 - p_m(T_H)] \epsilon_g \sigma T_H^4$$

$$- \epsilon_m [1 - p_m(T_1^n)] \sigma (T_1^n)^3 T_1^{n+1} - \frac{k}{\Delta X} (T_1^{n+1} - T_2^{n+1}) \qquad (107)$$

This is the expression for the exposed boundary.

The boundary condition for the interior surface is expressed in the following heat balance:

$$\rho c \frac{\Delta X}{2} \frac{\partial T_{11}}{\partial t} \quad \text{.... storage rate}$$

$$= \frac{\Delta X}{2} \sum_j q'''_{11}(\hat{T}_j^{n+1}) \quad \text{.... absorbed by radiation in the transparent portion of the spectrum}$$

$$- h_c(T_{11}^{n+1} - T_c) \quad \text{.... convection loss to the cabin}$$

$$- \epsilon_m W_{Bm}(T_{11}) \quad \text{.... emitted by radiation in the opaque portion of the spectrum}$$

$$+ k \frac{\partial T_{11}}{\partial X} \quad \text{.... conducted from the glazing} \qquad (108)$$

Reducing equation (108) to implicit finite difference form and linearizing in a similar manner as before, the interior surface boundary condition becomes:

$$\rho c \frac{\Delta X}{2} \frac{T_{11}^{n+1} - T_{11}^{n}}{\Delta t} = \frac{\Delta X}{2} \sum_j q'''_{11}(\hat{T}_j^{n+1}) - h_c (T_{11}^{n+1} - T_c)$$

$$- \epsilon_m [1 - p_m(T_{11})] \sigma (T_{11}^{n})^3 T_{11}^{n+1} + \frac{k}{\Delta X} (T_{10}^{n+1} - T_{11}^{n+1}) \qquad (109)$$

Convective and Radiative Input

It is clear that equations (100), (107) and (109) comprise the set of simultaneous equations to be solved for the nodal point temperatures shown in Figure 63. The remaining part of the problem to be defined is the convective and radiative input at the exposed surface. These inputs are a function of the mission under consideration. Three cases considered are:

1. Hypersonic Re-entry
2. Supersonic Flight
3. Circular Earth Orbit

For hypersonic re-entry, convective input is assumed to be expressed by a percentage of stagnation point heat transfer rate. The stagnation point heat transfer rate for a six-inch radius nose can be determined by: (Reference 10)

$$q''_{Hyp} = 3.042 \eta \sqrt{\rho} \left(\frac{V}{1000}\right)^{3.25} \left(1 - \frac{H_{wall}}{H_{stag}}\right) \left[\text{watts/cm}^2\right] \qquad (110)$$

where ρ = free stream density (lb/ft^3)
V = free stream velocity (fps)
η = ratio of local to stagnation point heat transfer rate
H = enthalpy

It is assumed that $\eta = 0.10$. Radiative input is considered to be from a normal shock layer of a thickness equal to the stand-off distance at the stagnation point. Graybody emissivities for shock heated air at densities and temperatures behind the normal shock are taken from curve fits of the data of Kivel & Bailey. Thus, T_H and ϵ_g used in equation (104) are defined.

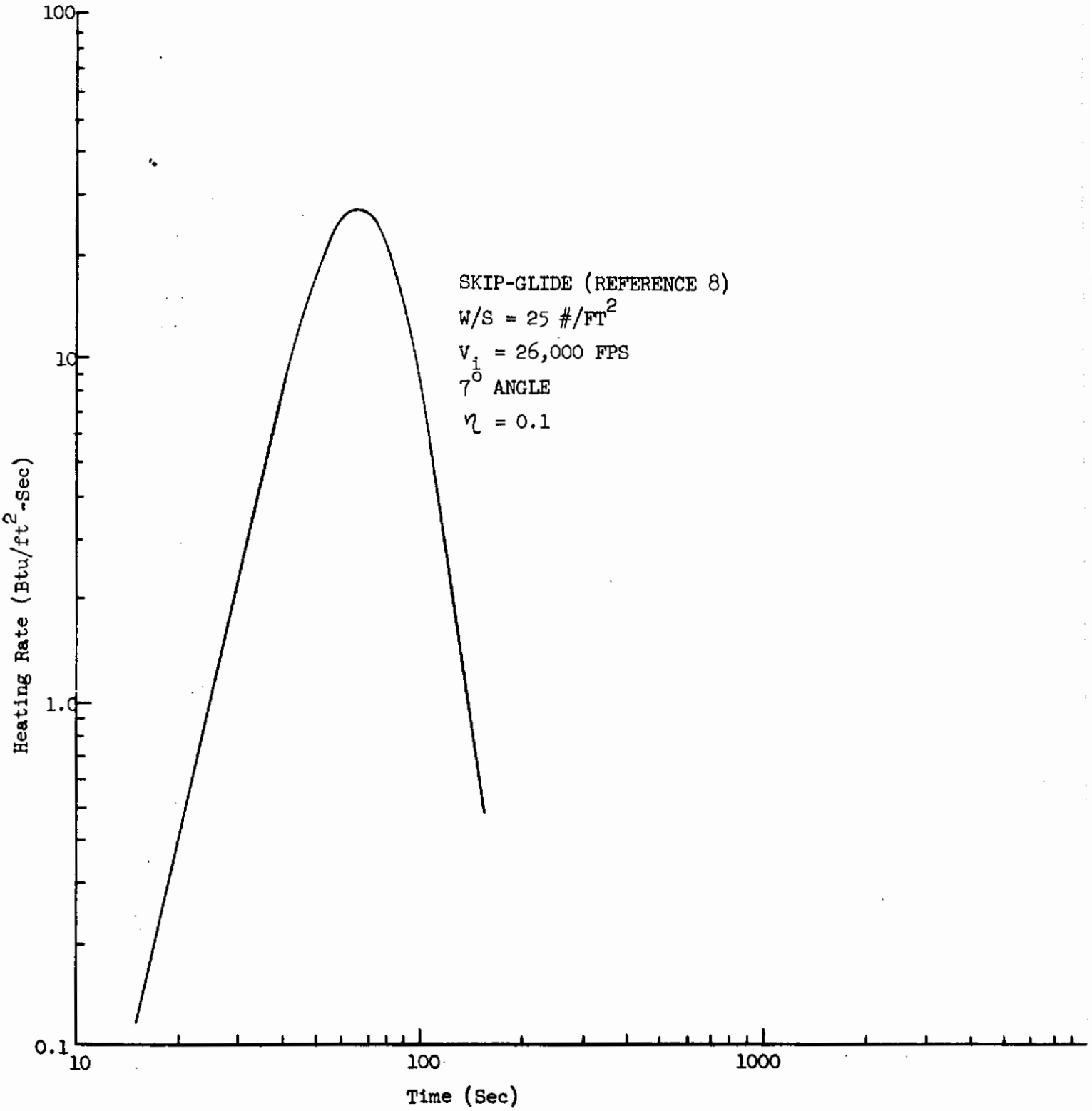

Figure 64 HYPERSONIC HEATING RATE

For supersonic flight, the convective input of a flat plate at zero angle of attack is used. Accordingly, the correlations based upon free stream conditions used are: (Reference 28)

$$N_{st} = 0.016\, N_{Re}^{-0.145} \tag{111}$$

and

$$\frac{h}{h_i} = 0.961\, N_{Ma}^{-0.24} \left(\frac{T_s}{T_a}\right)^{-0.34} \tag{112}$$

where

N_{St} = Stanton Number = $\dfrac{h_i}{\rho_a C_p V}$

N_{Re} = Reynolds Number = $\dfrac{VL}{\nu}$

N_{Ma} = Mach number

T_s & T_a = surface and ambient temperatures, respectively

h & h_i = are the local and incompressible heat transfer coefficients, respectively

ρ_a = free stream density

C_p = specific heat at constant free stream pressure

V = free stream velocity

L = distance from the leading edge

ν = kinematic viscosity at free stream conditions

Once the local heat transfer coefficient is determined the convective heat transfer rate is computed by: (Reference 28)

$$q''_{cst} = h\,(T_{Wo} - T_s) \tag{113}$$

where

$$T_{Wo} = T_a(1 + 0.178\, N_{Ma}^2)$$

(the adiabatic wall temperature for a turbulent boundary layer)

No radiative input is considered for the supersonic flight case.

For circular earth orbit the convective input is based upon stagnation point heat transfer in free molecular flow and may be expressed as: (Reference 10):

$$q''_{orb} = 2.271 \times 10^{-5}\, \rho V^3 \quad (\text{watt/cm}^2) \tag{114}$$

where the density, ρ, is taken as free stream density (lb/ft^3) and the velocity, V, is taken as free stream velocity (10^3 fps). For a 200-mile circular orbit the convective input is a constant:

$$q''_{orb} = 7.409 \times 10^{-4} \quad (\text{watt/cm}^2) \tag{115}$$

Radiative input is considered as emanating from the sun whose form factor is taken as: (Reference 29)

$$F = \frac{\text{solar constant}}{\sigma T_{sun}^4} = 1.882 \times 10^{-5} \qquad (116)$$

where the sun's temperature is assumed to be 6000°K.

Computer Program

A computer program was written to solve the single glaze problem on the IBM 7090. It can be divided into five sections:

1. Data input and program control
2. Integration and storage of ϕ and $\hat{P}$ (See figure 59)
3. Integration of $\Sigma_j q_i'''(T_j^{n+1})$
4. Simultaneous solution of temperature matrix
5. Supporting functions and subroutines

In the data input section all the necessary data such as physical dimensions, thermal and optical properties, blackbody radiation tables, trajectory tables, and time increment instructions and program control are read into the machine.

Once the data are read into the machine, the program proceeds to compute the ϕ and P integrals numerically. These functions are integrated over intervals of the angle α and depend on the absorption coefficient, γ_λ, nodal point, and wavelength band. Thus, providing the absorption coefficient does not change (which only occurs when temperatures affect such a change) the integrated values are computed once and stored for future use. However, when the temperature field changes sufficiently to affect the absorption coefficient, the integrals for the nodal points affected are recomputed and stored.

The energy-absorbed integration is a temperature-field dependent quantity which requires repeated computations to check convergence of the iteration and truncation effects. This section of the program essentially handles the radiant interchange within the material. Before passing through this section of the program the $\Sigma_j q_i'''(\hat{T}_j^{n+1})$ field is computed for each nodal point. These are successively computed at each nodal point calling out of storage the ϕ and $\hat{P}$ functions previously computed and in turn storing each of its values for use in the temperature field computations.

The section of the program dealing with the simultaneous solution of the temperature matrix is divided into two parts:

a. the computation of matrix coefficients, and

b. the solutions of the matrix unknowns.

In computing the matrix coefficients, trajectory information read in as data are used for the boundary equations. The energy-absorbed field is called for and all information on material properties, time increments, etc. are utilized. Once the coefficient matrix is computed the program proceeds to the solution of the matrix

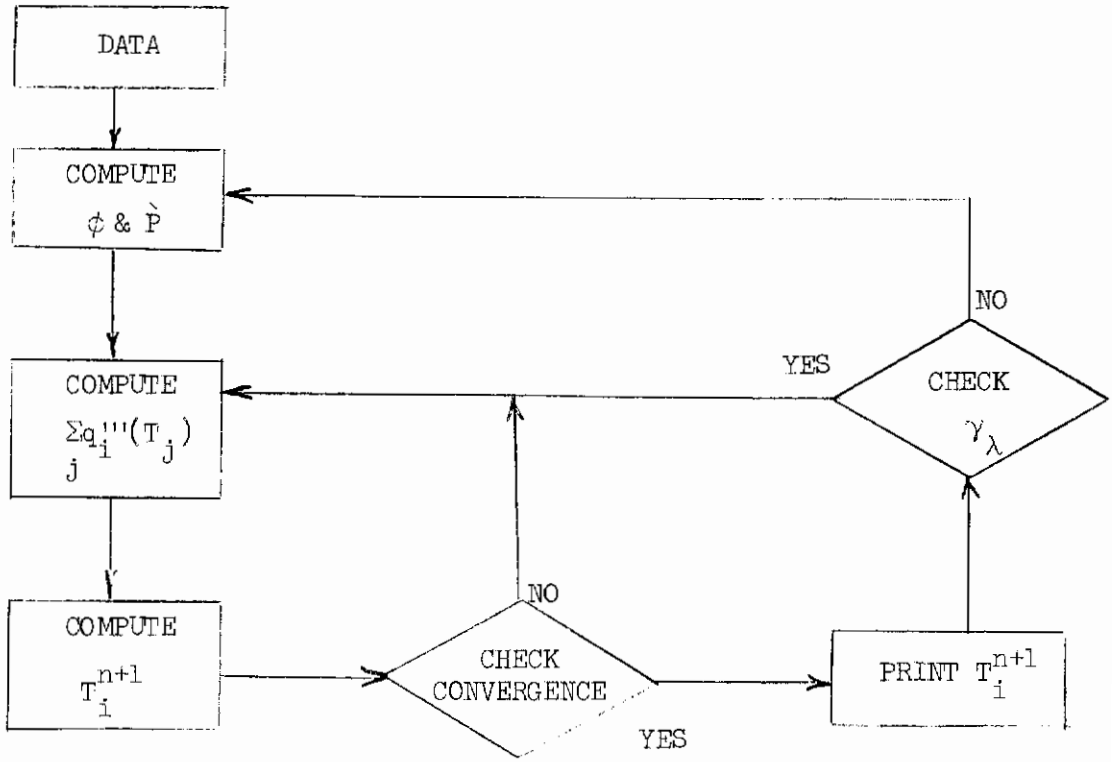

Figure 65 OVERALL COMPUTER PROGRAM SCHEMATIC

for the new temperature field. With the temperature field computed, the convergence subroutine is called for which decided either to accept the temperature field or to instruct the machine to recompute the temperature field until a desired accuracy is achieved. Once this is accomplished the temperature and energy absorbed fields are written out, and the time is stepped to the accepted value, and the next computation is begun.

The final section of the program deck is the supporting functions and subroutines used throughout the program. The functions essentially are interpolations within properties, blackbody radiation, and trajectory tables read in as data. The convergence subroutine controls the computations and acceptance of temperatures computed.

Security Classification

DOCUMENT CONTROL DATA - R&D

(Security classification of title, body of abstract and indexing annotation must be entered when the overall report is classified)

1. ORIGINATING ACTIVITY (Corporate author) MRD Division General American Transportation Corp. Niles, Illinois	2a. REPORT SECURITY CLASSIFICATION Unclassified 2b. GROUP

3. REPORT TITLE
Window Systems for Advanced Vehicles

4. DESCRIPTIVE NOTES (Type of report and inclusive dates)
Preliminary Draft of Final Technical Report — June 62 to October 63, April 64 to December 64

5. AUTHOR(S) (Last name, first name, initial)
Lis, S. J.
Barile, R. G.
Engholm, G.

6. REPORT DATE	7a. TOTAL NO. OF PAGES	7b. NO. OF REFS
December 1964	128	29

8a. CONTRACT OR GRANT NO.	9a. ORIGINATOR'S REPORT NUMBER(S)
AF 33(657)-9138 b. PROJECT NO. 1368 c. 136802 Task No. d.	N/A 9b. OTHER REPORT NO(S) (Any other numbers that may be assigned this report) N/A

10. AVAILABILITY/LIMITATION NOTICES
Not Releasable to OTS

11. SUPPLEMENTARY NOTES	12. SPONSORING MILITARY ACTIVITY
N/A	Structures Division Design Concepts - FDTS AFFDL - Wright-Patterson AFB, Ohio

13. ABSTRACT
A basic investigation to describe the heat transfer and temperature distribution in semi-transparent window materials subjected to simultaneous convective and radiative heat input. The mechanism of heat transfer within the window is treated by separated conductive and radiative modes. Results derived from IBM 7090 Digital Computer Programs are presented for single glaze windows subjected to a hypersonic skip glide trajectory, a supersonic flight and a circular earth orbit. The conditions where radiative interchange is important are studied. Initial results considering the effects of a thin transparent film on a single glazing are presented.

DD FORM 1 JAN 64 1473

Security Classification